



Photoplethysmogram Analysis and Applications: An Integrative Review

Junyung Park¹, Hyeon Seok Seok¹, Sang-Su Kim¹ and Hangsik Shin^{2*}

¹ Department of Biomedical Engineering, Chonnam National University, Yeosu, South Korea, ² Department of Convergence Medicine, University of Ulsan College of Medicine, Asan Medical Center, Seoul, South Korea

OPEN ACCESS

Edited by:

Bingmei M. Fu,
City College of New York (CUNY),
United States

Reviewed by:

Jie Wei,
City College of New York (CUNY),
United States

Min Wu,

University of Maryland, College Park,
United States

***Correspondence:**

Hangsik Shin
hangsik.shin@gmail.com

Specialty section:

This article was submitted to

Vascular Physiology,
a section of the journal
Frontiers in Physiology

Received: 03 November 2021

Accepted: 21 December 2021

Published: 01 March 2022

Citation:

Park J, Seok HS, Kim S-S and
Shin H (2022) Photoplethysmogram
Analysis and Applications: An
Integrative Review.
Front. Physiol. 12:808451.
doi: 10.3389/fphys.2021.808451

Beyond its use in a clinical environment, photoplethysmogram (PPG) is increasingly used for measuring the physiological state of an individual in daily life. This review aims to examine existing research on photoplethysmogram concerning its generation mechanisms, measurement principles, clinical applications, noise definition, pre-processing techniques, feature detection techniques, and post-processing techniques for photoplethysmogram processing, especially from an engineering point of view. We performed an extensive search with the PubMed, Google Scholar, Institute of Electrical and Electronics Engineers (IEEE), ScienceDirect, and Web of Science databases. Exclusion conditions did not include the year of publication, but articles not published in English were excluded. Based on 118 articles, we identified four main topics of enabling PPG: (A) PPG waveform, (B) PPG features and clinical applications including basic features based on the original PPG waveform, combined features of PPG, and derivative features of PPG, (C) PPG noise including motion artifact baseline wandering and hypoperfusion, and (D) PPG signal processing including PPG preprocessing, PPG peak detection, and signal quality index. The application field of photoplethysmogram has been extending from the clinical to the mobile environment. Although there is no standardized pre-processing pipeline for PPG signal processing, as PPG data are acquired and accumulated in various ways, the recently proposed machine learning-based method is expected to offer a promising solution.

Keywords: bio-signal processing, motion artifacts, photoplethysmography, physiological signal, signal quality assessment, noise reduction, physiological measurement

INTRODUCTION

Photoplethysmography (PPG) is a non-invasive method for measuring blood volume changes in a microvascular bed of the skin based on optical properties, such as absorption, scattering, and transmission properties of human body composition under a specific light wavelength (Challoner, 1979). PPG is a compound word that consists of “photo,” meaning light; “plethysmo,” meaning volume; and “graphy,” meaning recording (Alnaeb et al., 2007). In 1937, Hertzman found that the amount of light detected by back scattering after irradiating light to the skin was significantly changed according to cardiac activity. He suggested that PPG was a technique for measuring blood volume changes in a specific area irradiated with light (Hertzman, 1937, 1938). PPG records the amount of light transmitted or reflected by the change in concentration of substances in the blood and the optical path according to pulsation, which can be explained by the Beer–Lambert law that defines the attenuation of light intensity by the extinction coefficient, concentration, and optical path length of a medium when light passes through it (Beer, 1851). The Beer–Lambert law, as



光电体积描记图分析及其应用综述

朴俊容、玄锡锡、尚素基满杭植新*

†韩国丽水全南国立大学生物医学工程系、韩国首尔牙山医学中心蔚山大学医学院融合医学系

除了其在临床环境中的使用之外，光电容积描记图（PPG）越来越多地用于测量个体日常生活中的生理状态。本文从工程角度对光电容积图的产生机理、测量原理、临床应用、噪声定义、预处理技术、特征检测技术和后处理技术等方面进行了综述。我们对PubMed、Google Scholar、电气和电子工程师协会（IEEE）、ScienceDirect 和Web of Science 数据库进行了广泛的检索。排除条件不包括发表年份，但排除非英文发表的文章。基于118篇文章，我们确定了实现PPG的四个主要主题：(A) PPG波形，(B) PPG特征和临床应用，包括基于原始PPG波形的基本特征、PPG的组合特征和PPG的衍生特征，(C) PPG噪声，包括运动伪影基线漂移和灌注不足，以及(D) PPG信号处理，包括PPG预处理、PPG峰值检测，和信号质量指数。光电容积脉搏波的应用领域已从临床扩展到移动的环境。虽然PPG信号处理没有标准化的预处理流水线，但由于PPG数据以各种方式获取和积累，因此最近提出的基于机器学习的方法有望提供有前途的解决方案。

OPEN ACCESS

编辑:

冰梅傅，纽约城市学院 (CUNY)，

美国

复核人:

魏杰，纽约城市学院 (CUNY)
吴锐，马里兰州大学帕克分校，

美国

美国

* 通信:

申亨植

hangsik.shin@gmail.com

保留字: 生物信号处理, 运动伪影, 光电容积脉搏波, 生理信号, 信号质量评估, 降噪, 生理测量

专业部分:
本文提交给

血管生理学,
杂志的一部分
Frontiers in Physiology

收到日期: 2021年1月03日
接受日期: 2021年12月21日

发布时间: 2022年3月1日

引文:
Park J, Seok HS, Kim S-S and Shin H (2022) 光电容积描记图

分析与应用:

综合审查。

前面生理学12: 808451。

doi: 10.3389/fphys.2021.808451

介绍

光电体积描记术（PPG）是一种非侵入性方法，用于基于光学特性（例如，人体成分在特定光波长下的吸收、散射和透射特性）测量皮肤微血管床中的血容量变化（Challoner，1979）。PPG是一个复合词，由“photo”（光）、“plethysmo”（体积）和“graphy”（记录）组成（Alnaeb等人，2007年）。1937年，Hertzman发现，在将光照射到皮肤后，通过后向散射检测到的光量根据心脏活动而显著变化。他认为PPG是一种测量光照射特定区域血容量变化的技术（Hertzman，1937, 1938）。PPG记录通过血液中物质的浓度变化和根据脉动的光路透射或反射的光量，这可以通过Beer - Lambert 定律来解释，该定律定义了当光穿过介质时介质的消光系数、浓度和光路长度对光强度的衰减（Beer，1851）。Beer - Lambert 定律

shown in $I = I_0 e^{-\varepsilon lc}$, defines that the transmitted light intensity (I) through a medium will decrease exponentially in irradiated light intensity (I_0) in relation to the absorption coefficient (ε), optical path length (l), and concentration of the medium (c). The exponent part of the Beer–Lambert law is defined as absorbance (A), which can be expressed as $A = -\varepsilon lc$. The Beer–Lambert law is used in various PPG applications that include calculating oxygen saturation (Nitzan et al., 2014) and developing multi-layer light–skin interaction models (Liu et al., 2016a). A recent study, based on modified Beer–Lambert law, measured PPG depending on skin depth by applying different extinction coefficients according to characteristics of the microvascular bed of the skin (Baker et al., 2014; Liu et al., 2016a). **Figure 1** shows skin structure, optical path, and light intensity change represented by the Beer–Lambert law in photoplethysmogram measurement. Light irradiated into the skin will pass through skin structures, such as tissues, veins, and arteries; then, finally it is detected by a photodetector. The amount of light absorbed or scattered during this process may vary depending on the composition of the skin structure. In **Figure 1**, the total absorbance throughout skin layers is equal to the total sum of the absorbances of the k layers ($A_k = -\varepsilon_k c_k l_k$), where ε , c , and l are the extinction coefficient, concentration, and optical path length, respectively, and the amount of light that is finally transmitted can be expressed as $I = I_0 e^{\sum A_k}$. In this case, the total absorbance depends on the skin structure.

Unlike transmissive-mode PPG that has a straight optical pathway, reflective-mode PPG requires a more complex physical model, because the optical path between the emitter and the photodetector is curved and has a nonlinear pathway. Rubynok and Kyriacou assumed that the optical path between the emitter and the photodetector has multiple “canoe” shapes and modeled the absorbance of the Beer–Lambert law $A_{pi\lambda}$ as $A_{pi\lambda} = -\log(I_{Dpi\lambda}/I_{Epi\lambda}) = \mu_\lambda l_{pi\lambda} = \sum_{j=0}^{m_\lambda} \mu_{sj\lambda} l_{pisj\lambda}$ through the banana-shaped mean light pathway representing each “canoe” shape (Rubynok and Kyriacou, 2010), where, $I_{Dpi\lambda}$ and $I_{Epi\lambda}$ are the radiation and detection light intensity, respectively, in the banana-shaped light pathway, μ_λ is the absorption coefficient for the whole optical pathway in the scattering sample, $l_{pi\lambda}$ is the mean optical pathway corresponding to the pi fraction of the transmitted light power in the vascular tissue, m is the matter segments along the mean light pathway with different absorption coefficients, $\mu_{sj\lambda}$ is the total absorption coefficient tilde within the scattering matter segment sj , and $l_{pisj\lambda}$ is a part of the mean light pathway within the scattering matter segment sj . The total absorption coefficient $\mu_{sj\lambda}$ can be further extended by absorptivities and concentrations of the absorbing components present in the light pathway segment sj : $\mu_{sj\lambda} = \sum_{k=0}^{n_{sj}} \varepsilon_{k\lambda} c_{ksj}$, where n_{sj} is the number of light-absorbing components in the j , $\varepsilon_{k\lambda}$ is the Beer–Lambert law absorptivity of the absorbing component k at wavelength λ , and c_{ksj} is the concentration of the light absorbing component k in the light pathway segment j . In addition, the extinction coefficient of the reflective mode can be modeled as $\Delta A = \log(\Delta I_0/\Delta I) = \varepsilon \Delta cl \cdot DPF$ through the differential path length factor (DPF) based on the Modified Beer–Lambert Law (MBLL),

where $DPF(\lambda) \approx \frac{1}{2}(3\mu'_s(\lambda)/\mu_a(\lambda))^{1/2}$ and $\mu_a(\lambda)$ and $\mu'_s(\lambda)$ are the absorption coefficient and reduced scattering coefficient, respectively (Pintaviroo et al., 2021).

The volume of blood volume in the measurement site, arterial diameter, hemoglobin concentration, and hemoglobin direction according to the cardiac cycle are also major factors that affect the detected light intensity (De Trafford and Lafferty, 1984; Kamal et al., 1989; Lindberg and Oberg, 1993). For example, during the diastolic phase, blood volume, arterial diameter, and hemoglobin concentration in the measurement site are minimized. Thus, absorbance is minimized, while the amount of light detected by the photodetector is maximized. Conversely, in the systolic phase, the light intensity detected by the photodetector becomes minimum (Ding and Zhang, 2015; Ding et al., 2017).

Photoplethysmography (PPG) can be measured using light sources of various wavelengths. In general, when the wavelength of light increases, the depth of penetration also increases (Spigulis et al., 2007a,b; Ruggiero et al., 2016). For example, it is known that wavelengths of 470, 570, and 660 nm or more can reach the epidermis with capillaries, dermis with arterioles, and arteries of subcutaneous tissues, respectively (Liu et al., 2015, 2016a,b, 2018). Major blood vessels and arteries with strong pulsation are mainly located in the skin dermis or subcutaneous tissue. Thus, light with a red wavelength of 640–660 nm and infrared wavelength of 880–940 nm is mainly used for PPG measurement (Jones, 1987). PPG is mainly obtained at the extremities of the human body, such as fingers, toes, and earlobes that are advantageous for measuring changes in blood volume, because the vascular bed is shallow and widely spread (Stern, 1974; Allen and Murray, 2002; Millasseau et al., 2006). PPG can also be obtained from the forehead, esophagus, and nose (Barnes et al., 1977; Kyriacou et al., 2002; Choi et al., 2018).

A PPG device is composed of a light-emitting diode (LED) that emits light, and a photodetector that detects the emitted light. The device can be divided into transmissive type and reflective type according to the position of the LED and photodetector. **Figure 2** shows configurations for a photoplethysmogram measurement device. For the transmissive type, the photodetector is located on the opposite side of the LED, with skin tissues in between. For the reflective type, the photodetector is located next to the LED. Since the transmissive type measures attenuated light intensity after the light passes through skin tissues, it is mainly used for measuring PPG in the distal part of the body, where skin tissues, such as those of fingers, toes, and earlobes, are thin. The transmission-type PPG sensor shows more stable PPG measurement performance than the reflective type (Li et al., 2018). On the other hand, since the reflective type measures scattered light intensity after light irradiates the skin tissue, the measured light intensity is relatively smaller than that of the transmissive type, and the quality of the signal may be degraded. However, it has the advantage of being able to measure PPG not only in the distal part of the body but also in parts of the body, such as the forehead, wrist, carotid artery, and esophagus, where light transmission is difficult (Venema et al., 2012; Wannenburg and Malekian, 2015). The PPG measurement system has the basic hardware structure of an LED to irradiate light, and a photo

如 $I = I_e$ 所示，定义了通过介质的透射光强度 (I) 将相对于介质的吸收系数 (ε)、光程长度 (l) 和浓度 (c) 以指数方式减小照射光强度 (I)。比尔-朗伯定律的指数部分定义为吸光度 (A)，可以表示为 $A = -\varepsilon cl$ 。Beer - Lambert 定律用于各种PPG 应用，包括计算氧饱和度 (Nitzan 等人, 2014) 和开发多层光-皮肤相互作用模型 (Liu 等人, 2016 年a)。最近的一项研究基于修正的Beer - Lambert 定律，通过根据皮肤的微血管床的特性应用不同的消光系数来测量取决于皮肤深度的PPG (Baker 等人, 2014 年; Liu 等人, 2016 年a)。图1示出了光体积描记图测量中由比尔-朗伯定律表示的皮肤结构、光路和光强度变化。照射到皮肤中的光将穿过皮肤结构，例如组织、静脉和动脉；然后，最终由光电探测器检测。在此过程中吸收或散射的光的量可以根据皮肤结构的组成而变化。在图1中，整个皮肤层的总吸收率等于k层的消光系数的总和 ($A = \sum \varepsilon_k l$)，其中 ε 、 c 和 l 分别是消光系数、浓度和光程长度，并且最终透射的光量可以表示为 $I = I_e$

$\sum \varepsilon_k l$.在这种情况下，总吸光度

取决于皮肤结构。

与具有直光路的透射模式PPG 不同，反射模式PPG 需要更复杂的物理模型，因为发射器和光电检测器之间的光路是弯曲的并且具有非线性路径。Rubynok 和Kyriacou 假设发射器和光电探测器之间的光路具有多个“独木舟”形状，并将Beer - Lambert 定律A的吸光度建模为 $A = -\log(I/I_e) = \mu l$

μl 通过代表每个“独木舟”形状的香蕉形平均光路 (Rubynok 和 Kyriacou , 2010)，其中， I 和 I_e 分别是香蕉形光路中的辐射和检测光强度， μ 是散射样本中整个光路的吸收系数， l 是对应于血管组织中透射光功率的 p_i 分数的平均光路， m 是沿平均光路沿着具有不同吸收系数的物质段， μ 是散射物质段 s_j 内的总吸收系数 $\tilde{\mu}$ ，并且 I_s 是散射物质段 s_j 内的平均光路的一部分。总吸收系数 μ 可以通过存在于光路径段 S_j 中的吸收组分的吸收率和浓度进一步扩展：

$\sum \varepsilon_k c_k$ ，其中 n_{is} 是在 j 中的光吸收组分的数量， ε 是吸收组分 k 在波长 λ 处的比尔-朗伯定律吸收率，并且 c 是光路径段 j 中的光吸收组分 k 的浓度。另外，反射模的消光系数可通过微分光程因子 (DPF) 表示为 $A = \log(1/I/I_e) = \varepsilon cl \cdot DPF$ 基于修正的比尔-朗伯定律 (MBLL) ，

其中 $DPF(\lambda) = (3\mu(\lambda)/\mu(\lambda))$ ， $\mu(\lambda)$ 和 $\mu(\lambda)$ 分别是吸收系数和约化散射系数 (Pintavirooj 等人, 2021 年)。

测量部位的血容量、动脉直径、血红蛋白浓度和根据心动周期的血红蛋白方向也是影响检测到的光强度的主要因素 (De特拉福德和Lafford , 1984 ; Kamal 等人, 1989 年; Lindberg 和Oberg , 1993 年)。例如，在舒张期，测量部位的血容量、动脉直径和血红蛋白浓度被最小化。因此，吸光度被最小化，而由光电检测器检测到的光量被最大化。相反，在收缩期，由光电探测器检测到的光强度变得最小 (Ding and Zhang , 2015 ; Ding 等人, 2017 年)。

可以使用各种波长的光源来测量光电体积描记术 (PPG)。通常，当光的波长增加时，穿透深度也增加 (Spigulis 等人, 2007 a, B; Ruggiero 等人, 2016 年)。例如，已知470、570 和660 nm或更大的波长可以分别到达具有毛细血管的表皮、具有小动脉的真皮和皮下组织的动脉 (Liu 等人, 2015, 2016 a, B, 2018)。搏动较强的主要血管和动脉主要位于皮肤真皮或皮下组织。因此，具有640 - 660 nm的红色波长和880 - 940 nm的红外波长的光主要用于PPG 测量 (Jones , 1987)。PPG 主要在人体的四肢处获得，例如手指、脚趾和耳垂，其有利于测量血容量的变化，因为血管床较浅且分布广泛 (Stern , 1974; 艾伦和Murray , 2002 ; Millasseau 等人, 2006 年)。PPG 也可以从前额、食道和鼻子获得 (巴恩斯等人, 1977; Kyriacou 等人, 2002 ; Choi 等人, 2018 年)。

PPG 装置由发射光的发光二极管 (LED) 和检测所发射的光的光电检测器组成。根据发光二极管和光电探测器的位置，该装置可分为透射式和反射式。图2示出了光电体积描记图测量设备的配置。对于透射型，光电探测器位于LED的相对侧，皮肤组织位于其间。对于反射型，光电探测器位于LED旁边。由于透射型测量光穿过皮肤组织后衰减的光强度，因此其主要用于测量身体远端部分中的PPG，其中皮肤组织 (诸如手指、脚趾和耳垂的皮肤组织) 较薄。透射型PPG 传感器显示出比反射型更稳定的PPG 测量性能 (Li 等人, 2018 年)。另一方面，由于反射型测量在光照射皮肤组织之后的散射光强度，所以测量的光强度相对小于透射型的测量的光强度，并且信号的质量可能劣化。然而，其具有不仅能够测量身体的远端部分中的PPG 而且能够测量身体的部分中的PPG 的优点，所述身体的部分诸如前额、手腕、颈动脉和食道，其中光传输是困难的 (Venema 等人, 2012 年; Wannenburg 和Malekian , 2015 年)。PPG 测量系统具有用于照射光的LED的基本硬件结构，以及用于照射光的照片的基本硬件结构。

detector to measure the amount of transmitted light; in addition, it includes an emitter driver to drive the LED, a filter to remove noise and enhance the quality of the obtained signal, an analog-to-digital converter, and a microprocessor. Due to its low cost and a simple hardware structure characteristic, PPG has been used in various applications.

In a clinical environment, PPG is typically used for measuring blood oxygen saturation (pulse oximetry), peripheral vascular tone, and changes in peripheral blood flow according to the respiratory cycle. Blood oxygen saturation is calculated as the ratio of the concentration of oxyhemoglobin to total hemoglobin in the blood. Traditionally, both infrared wavelength (~ 880 nm) and red wavelength (~ 660 nm) are used for measuring oxygen saturation, because deoxyhemoglobin absorbs more red wavelength, while oxygenated hemoglobin absorbs more infrared wavelength (Zijlstra et al., 1991; Webster, 1997; Sinex, 1999).

Perfusion index measured with PPG is defined as the ratio of pulsatile component to non-pulsatile component of PPG. It indicates the contraction of peripheral vascular smooth muscle. It is used for peripheral vascular tone evaluation related to hypertension and coronary artery diseases (Shelley et al., 1997; Hummler et al., 2006; Landsverk et al., 2008; Mowafi et al., 2008, 2009). The Pleth variability index indicates the fluctuation of perfusion index, which is known to have an inverse relationship with blood flow in blood vessels (Cannesson et al., 2008b; Zimmermann et al., 2010). Changes in blood flow in peripheral blood vessels according to the respiratory cycle can be measured to monitor patients with respiratory distress or heart failure; this technique is also used to evaluate the intrathoracic pressure–cardiac function correlation (Cannesson et al., 2005; Monnet et al., 2005). PPG is also used in arterial blood pressure estimation, heart function evaluation, and pain assessment studies. Using PPG, arterial blood pressure can be estimated by hemodynamic modeling (Chen et al., 2000; Poon and Zhang, 2005). It can also be estimated using a linear or nonlinear regression model based on pulse transit time (PTT) derived by PPG (Fung et al., 2004; Muehlsteff et al., 2006; Baek et al., 2009; Wong et al., 2009; Mase et al., 2011; Ma, 2014; Mousavi et al., 2019). In pain assessment research using PPG, the surgical Pleth index (SPI; GE Healthcare, Chicago, IL, United States) has been calculated through the amplitude and heart beat interval of PPG for intraoperative pain evaluation (Ahonen et al., 2007; Struys et al., 2007; Kallio et al., 2008). Another study has shown that the amplitude variation, area, triangulated area, width, ascending slope, and descending slope of PPG are significantly correlated with pain (Yang et al., 2018; Seok et al., 2019). PPG measured with a mobile device can be used to evaluate the exercise state, sleep state, and stress index of a user through various approaches based on pulse rate and respiratory rate analysis or waveform analysis (Choi et al., 2011; Lin et al., 2011; Madhav et al., 2011; Karlen et al., 2013; Parak and Korhonen, 2014; Temko, 2017; Zangróniz et al., 2018; Saganowski et al., 2020). Compared with other hemodynamic analysis devices, PPG is an inexpensive and noninvasive technique with higher mobility. It is also an easy technique for attaching electrodes and measuring signals. Thus, its use in the clinical and mobile fields is increasing. However, PPG is easily affected by various external factors, such as the body

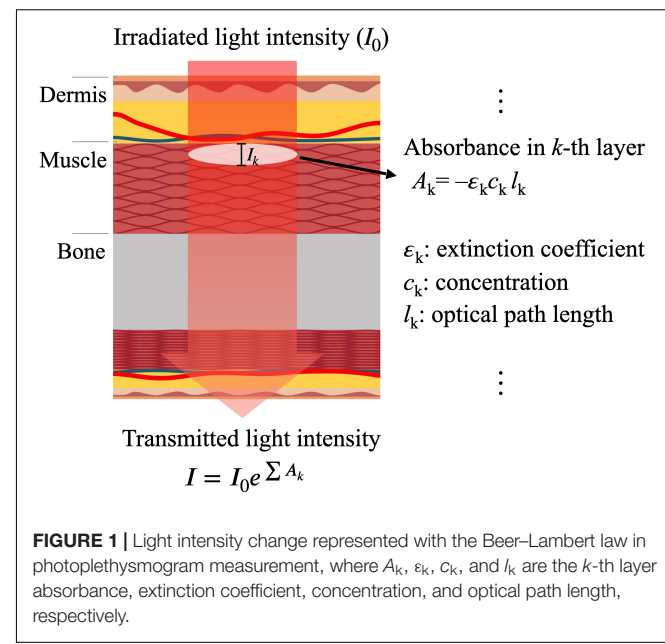


FIGURE 1 | Light intensity change represented with the Beer–Lambert law in photoplethysmogram measurement, where A_k , ϵ_k , c_k , and l_k are the k -th layer absorbance, extinction coefficient, concentration, and optical path length, respectively.

temperature of the measurement site (Senay et al., 1963; Bohusch et al., 1994), intensity of ambient light in the experimental space (Kim et al., 2015), and individual differences, such as skin type (Adler et al., 1998; Spigulis et al., 2007a; Fallow et al., 2013); therefore, additional research on advanced signal processing techniques is needed to obtain a robust PPG waveform.

The purpose of this study was to examine PPG from an engineering viewpoint through the previous research and literature, and review the current status and vision of PPG, including its measurement principle and mechanism, waveform characteristics, representative noise, pre-processing technology, feature extraction technology, and post-processing technology. Reviewing the results of the research performed to date on the above contents is expected to contribute to the application of PPG, which, with the recent growth of mobile healthcare for daily health care or clinical environment, is increasingly being utilized.

METHODS

Search Strategy

A review of the literature was conducted using the following five databases: PubMed, Institute of Electrical and Electronics Engineers (IEEE), Google Scholar, ScienceDirect, and Web of Science. Search terms *photoplethysmogram*, *review*, *motion artifacts (MA)*, *preprocessing*, *signal processing*, *noise reduction*, *derivative*, *feature*, *feature detection*, *peak*, *peak detection*, *noise*, *waveform*, *signal quality*, and *perfusion* were combined.

Inclusion Criteria

To be eligible for inclusion in this review, the primary requirement was that an article needed to focus on signal characteristics, waveform analysis, noise reduction, peak detection, waveform reconstruction, or quality assessment of

它包括一个用于测量透射光量的发射器驱动器、一个用于去除噪声并提高所获得信号质量的滤波器、一个模数转换器和一个微处理器。由于其低成本和简单的硬件结构特性，PPG 已被用于各种应用中。

在临床环境中，PPG 通常用于测量血氧饱和度（脉搏血氧测定法）、外周血管张力以及根据呼吸周期的外周血流变化。血氧饱和度计算为血液中氧合血红蛋白浓度与总血红蛋白浓度的比值。传统上，红外波长 (λ 880 nm) 和红色波长 (λ 660 nm) 都用于测量氧饱和度，因为脱氧血红蛋白吸收更多的红色波长，而氧合血红蛋白吸收更多的红外波长 (Zijlstra 等人, 1991; 韦伯斯特, 1997; Sinex, 1999)。

用PPG 测量的灌注指数被定义为PPG 的脉动分量与非脉动分量的比率。表明外周血管平滑肌收缩。其用于与高血压和冠状动脉疾病相关的外周血管张力评估 (Shelley 等人, 1997; Hummler 等人, 2006; Landsverk 等人, 2008 年; Mowlett 等人, 2008 年, 2009 年)。Pleth 变异性指数指示灌注指数的波动，已知灌注指数与血管中的血流具有反比关系 (Cannesson 等人, 2008 b; Zimmermann 等人, 2010 年)。根据呼吸周期，可以测量外周血管中的血流变化，以监测呼吸窘迫或心力衰竭患者；该技术还用于评估胸内压-心脏功能相关性 (Cannesson 等人, 2005; Monnet 等人, 2005 年)。PPG 还用于动脉血压估计、心脏功能评估和疼痛评估研究。使用PPG，可以通过血液动力学建模来估计动脉血压 (Chen 等人, 2000; Poon and Zhang, 2005)。它也可以使用基于由PPG 导出的脉搏传导时间 (PTT) 的线性或非线性回归模型来估计 (Fung 等人, 2004; Muehlsteff 等人, 2006; Baek 等人, 2009; Wong 等人, 2009; Mase 等人, 2011; Ma, 2014; Mousavi 等人, 2019 年)。在使用PPG 的疼痛评估研究中，已经通过PPG 的幅度和心跳间隔计算了手术Pleth 指数 (SPI; GE Healthcare, 芝加哥, IL, 美国)，用于术中疼痛评估 (Ahonen 等人, 2007; Struys 等人, 2007; Kallio 等人, 2008 年)。另一项研究表明，

PPG 的幅度变化、面积、三角形面积、宽度、上升斜率和下降斜率与疼痛显著相关 (Yang 等人, 2018; Seok 等人, 2019 年)。利用移动终端测量的PPG 可以用于通过基于脉搏率和呼吸率分析或波形分析的各种方法来评估用户的锻炼状态、睡眠状态和压力指数 (Choi 等人, 2011; Lin 等人, 2011; Madhav 等人, 2011; Karlen 等人, 2013; Parak 和 Korhonen, 2014; Temko, 2017; Zangróniz 等人, 2018; Saganowski 等人, 2020 年)。与其他血流动力学分析设备相比，PPG 是一种廉价、无创的技术，具有更高的机动性。它也是一种连接电极和测量信号的简单技术。因此，其在临床和移动的领域的使用正在增加。但是PPG 很容易受到各种外界因素的影响，比如身体

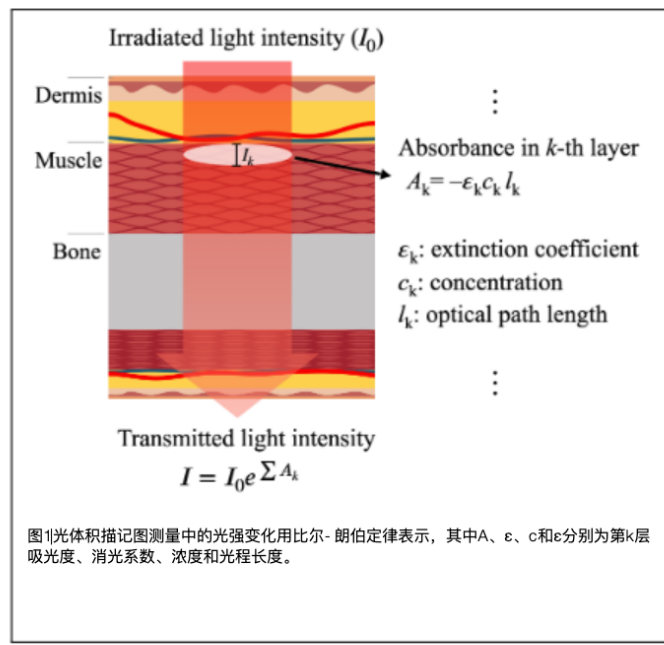


图1光体积描记图测量中的光强变化用比尔-朗伯定律表示，其中A、 ϵ 、c和 ε 分别为第k层吸光度、消光系数、浓度和光程长度。

测量部位的温度 (Senay 等人, 1963; Bohusch 等人, 1994)、实验空间中的环境光强度 (Kim 等人, 2015) 和个体差异，例如皮肤类型 (Adler et al., 1998; Spigulis 等人, 2007 a; Fallow 等人, 2013)；因此，需要对高级信号处理技术进行额外的研究以获得稳健的PPG 波形。

本研究的目的是通过以往的研究和文献，从工程的角度来审视 PPG，并回顾了PPG 的现状和愿景，包括其测量原理和机制，波形特征，代表性噪声，预处理技术，特征提取技术，后处理技术。回顾迄今为止对上述内容进行的研究的结果，预计将有助于PPG 的应用，随着近来移动的医疗保健在日常医疗保健或临床环境中的增长，PPG 的应用越来越多。

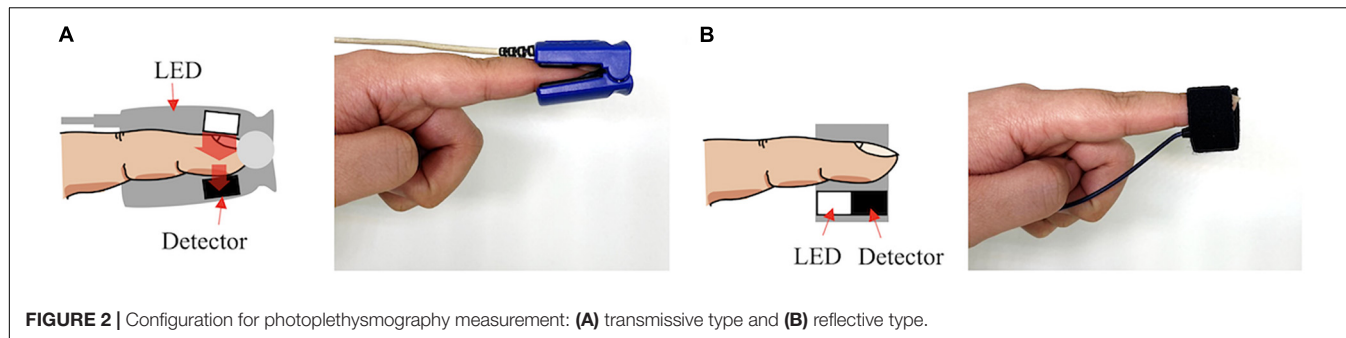
方法

搜索策略

使用以下五个数据库进行文献综述：PubMed、电气和电子工程师协会 (IEEE)、Google Scholar、ScienceDirect 和 Web of Science。结合检索词光电容积描记图、回顾、运动伪影 (MA)、预处理、信号处理、降噪、导数、特征、特征检测、峰值、峰值检测、噪声、波形、信号质量和灌注。

入选标准

要符合纳入本综述的条件，主要要求是文章需要关注信号特征、波形分析、降噪、峰值检测、波形重建或



PPG. If possible, the literature review was focused on recently published articles or articles with a high number of citations, but reports were not excluded because of their year of publication. However, review articles and original articles not published in English were excluded.

Review Process

The searched articles were reviewed, and detailed subcategories were organized according to the characteristics and processing procedures of PPG. In this process, the authors selected appropriate articles focusing on subcategories, and detailed technological items were listed through in-depth review. In discussion, all the authors presented the details and trends of subcategories and drew conclusions based on common trends.

RESULTS

Photoplethysmogram Waveform

Figure 3 shows that PPG waveform is obtained from the amount of light absorption by inverting the light intensity recorded with a photodetector after the light is transmitted through or reflected from human tissue. In general, the PPG waveform is divided into a pulsatile component and a non-pulsatile component (Lee et al., 2011a). The pulsatile component, known as the alternating current (AC) component, is related to changes in blood volume in the artery. It is synchronized with the cardiac cycle and is related to vasodilation, vasomotor, and vascular tones (Nitzan et al., 2006; Shelley et al., 2006, 2014; Allen, 2007; Shelley, 2007; Reisner et al., 2008). It can be used to detect ventricular tachycardia and ventricular fibrillation (Alian and Shelley, 2014). The non-pulsatile component, known as the direct current (DC) component, refers to the remaining components excluding the pulsatile component of the PPG waveform (Challoner, 1979; Nilsson et al., 2003a,b). Non-pulsatile components are affected by biological characteristics, such as tissue composition and basic blood volume of the measurement site, as well as external factors, such as ambient light and measurement device specifications. It has been reported that respiration, vasomotor activity, Traube-Hering-Mayer wave, and thermoregulation can also affect the non-pulsatile component (Hertzman and Dillon, 1940; Hertzman and Roth, 1942; Senay et al., 1963; Allen and Murray, 2000a,b). The amplitude of the PPG waveform has an arbitrary unit, because the physical characteristics, such as oxygen-carrying

capacity, bone size, skin color, blood vessel distribution, cardiac output, vascular stiffness, and vascular compliance, differ from person to person (Zhang et al., 2001; Krishnaswamy and Baranowski, 2004; Valencell, 2015). Its measurement depends on experimental environment, such as ambient light (Li et al., 2014; Xu et al., 2017).

The PPG waveform changes according to cardiac activity. It may also change because of respiration, autonomic nervous system activity, arterial activity, and venous activity (McKay et al., 2014; Pimentel et al., 2015; Bentham et al., 2018; Lakshmanan et al., 2018; Yuan et al., 2018). The PPG waveform includes cardiac activity and lung activity by frequency analysis. Shin and Min reported that most of the energy of the waveform is contained up to the 3rd harmonics (Shin and Min, 2017). The PPG waveform has a rising curve according to increase in capillary blood volume by cardiac contraction, and a descending

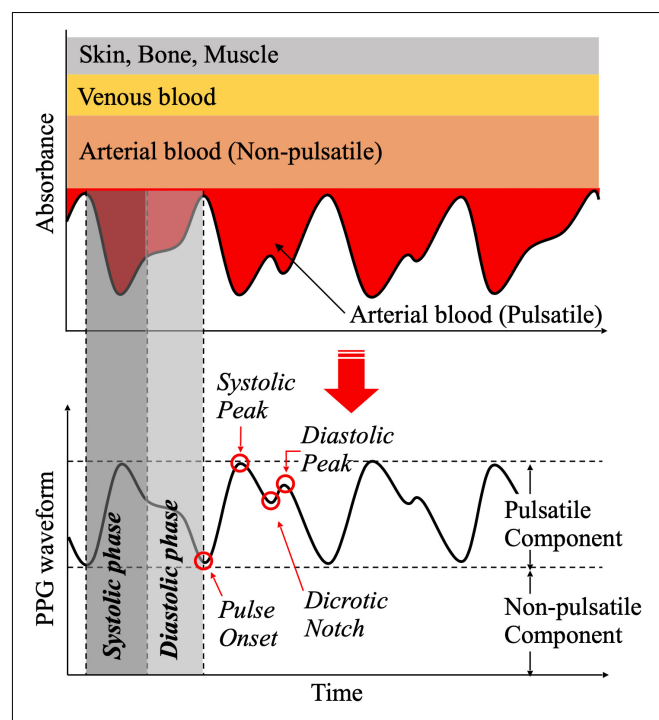
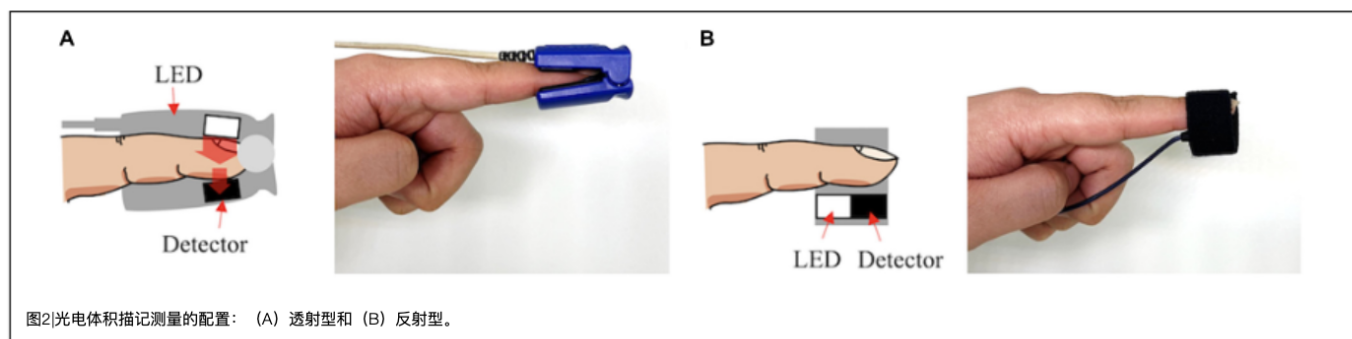


FIGURE 3 | Principle of photoplethysmogram generation and waveform features.



PPG。如果可能，文献综述重点关注最近发表的文章或引用次数较多的文章，但不会因发表年份而排除报告。但是，未以英文发表的综述文章和原创文章被排除在外。

例如携氧能力、骨骼尺寸、皮肤颜色、血管分布、心输出量、血管硬度和血管顺应性，因人而异 (Zhang 等人, 2001; Krishnaswamy 和Baranoski , 2004; Valencell , 2015)。其测量取决于实验环境，例如环境光 (Li等人, 2014 年; Xu等人, 2017 年)。

审查进程

对检索到的文献进行了综述，并根据PPG的特点和处理过程组织了详细的子类别。在此过程中，作者选择了适当的文章，重点放在子类别，并通过深入审查列出详细的技术项目。在讨论中，所有作者都介绍了子类别的详细信息和趋势，并根据共同趋势得出结论。

PPG 波形根据心脏活动而变化。

它也可能因为呼吸、自主神经系统活动、动脉活动和静脉活动而改变 (McKay 等人, 2014; Pimentel 等人, 2015; Bentham 等人, 2018; Lakshmanan 等人, 2018 年; Yuan 等人, 2018 年)。PPG 波形通过频率分析包括心脏活动和肺活动。Shin 和Min报告称，波形的大部分能量包含在三次谐波中 (Shin 和Min, 2017)。PPG 波形具有根据由心脏收缩引起的毛细血管血容量的增加的上升曲线和根据由心脏收缩引起的毛细血管血容量的增加的下降曲线。

结果

光电容积描记图波形

图3示出了PPG 波形是通过在光透射通过人体组织或从人体组织反射之后反转用光电检测器记录的光强度而从光吸收量获得的。通常，PPG 波形被分为脉动分量和非脉动分量 (Lee 等人, 2011年a)。脉动分量，称为交流 (AC) 分量，与动脉中的血容量变化有关。它与心动周期同步并且与血管舒张、血管收缩和血管紧张度有关

(Nitzan 等人, 2006; Shelley 等人, 2006, 2014; 艾伦, 2007; 雪莱, 2007; Reisner 等人, 2008 年)。可用于检测室性心动过速和室颤 (Alian 和 Shelley , 2014)。被称为直流 (DC) 分量的非脉动分量是指除了PPG 波形的脉动分量之外的其余分量 (Challoner , 1979; Nilsson 等人, 2003 a, B)。非脉动成分受生物学特性 (如测量部位的组织成分和基础血容量) 以及外部因素 (如环境光和测量器械规格) 的影响。据报道，呼吸、血管活性、Traube - Hering - Mayer 波和体温调节也可以影响非脉动分量 (Hertzman 和Dillon, 1940; Hertzman 和Roth , 1942; Senay 等人, 1963; 艾伦和默里, 2000 a, B)。PPG 波形的幅度具有任意单位，因为物理特性

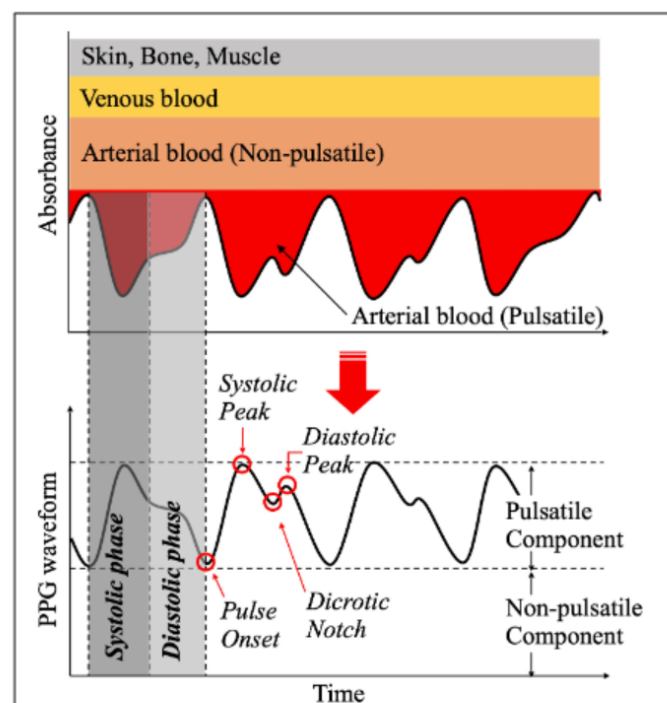


图3|光电容积脉搏波产生原理及波形特征。

curve according to decrease in capillary blood volume by cardiac dilation. It is repeated according to cardiac activity. At that time, rising curve is defined as the systolic phase of the PPG waveform, while descending curve is defined as the diastolic phase of the PPG waveform. **Figure 3** shows the PPG waveform of one pulsation and various feature points. Pulse onset is defined as the point where pulsation begins at the point where blood volume is lowest before the systolic phase. Systolic peak is defined at the point where blood volume is maximized. Transient rising and falling of the PPG waveform during diastole occur when blood volume in capillaries temporarily increases again because of the occurrence of a pressure gradient in the opposite direction to the blood flow, just before the aortic valve closes (Dahlgren et al., 1991; He et al., 1995). At this time, recessed point is defined as a dicrotic notch, and the point at which the first derivative of the waveform is closest to zero after the systolic peak is defined as a diastolic peak (Millasseau et al., 2002). PPG waveform can change because of body composition, physiological status, and external stimuli. A previous study reported that it is difficult to use the absolute value of PPG amplitude for comparison, because it can change according to the characteristics of body tissues and individual characteristics, such as race, skin color, fingernail color, and finger size (Alian and Shelley, 2014). Moreover, PPG baseline is affected by respiration, vascular compliance, vascular tone, pain, and drug use (Nitzan et al., 2000; Shelley et al., 2006; Shelley, 2007). The amplitude of the systolic peak, a representative characteristic of the PPG waveform, has been reported to have a significant correlation with microvascular expansion, and is in proportion to the cardiac output (Dorlas and Nijboer, 1985; Murray and Foster, 1996). In addition, results from studies related to anesthesia, sympathetic activation, and use of vasoconstrictors related to autonomic nervous system activity have confirmed that when the peripheral vasculature is dilated, the amplitude of the systolic peak is increased, while when vasculature is constricted, it is decreased (Korhonen and Yli-Hankala, 2009). Dicrotic notch changes with vascular tone and vascular compliance. It has been found that the location of notch occurrence is advanced at a high vascular tone (Shi et al., 2009). In addition, it has been reported that the time difference

between diastolic peak and systole peak decreases with aging (Yousef et al., 2012).

Photoplethysmogram Features and Clinical Applications

Basic Features Based on the Original Photoplethysmogram Waveform

Figure 4 shows the basic features obtained directly from the PPG waveform. Such PPG features are frequently used clinically (see **Table 1**). Systolic amplitude refers to the maximum amplitude of the PPG systolic phase. This is a feature related to the pulsatile component of blood volume (Asada et al., 2003). Systolic amplitude is highly correlated to stroke volume (Murray and Foster, 1996). It is directly proportional to the vasodilatation of the local body site where PPG is measured (Dorlas and Nijboer, 1985). A pulse width related index, PW₅₀, refers to the pulse width between points corresponding to 50% of the PPG systolic peak amplitude, and shows a high correlation with systemic vascular resistance (Awad et al., 2007). Regarding pulse area, this is a feature that is calculated as the total area of the PPG waveform; it changes according to surgical skin incision (Seitsonen et al., 2005). Inflection point area ratio is calculated as the area ratio between the systolic and diastolic sections based on the dicrotic notch, and is correlated with total peripheral resistance (Wang et al., 2009). Pulse-to-pulse interval is obtained from the time interval between the characteristic points of two adjacent pulses of PPG. Pulse onset, systolic peak, and maximum value of derivative PPG are mainly used to measure pulse-to-pulse intervals. Pulse-to-pulse interval refers to one cycle of cardiac activity (Linder et al., 2006; Fu et al., 2008; Jubadi and Sahak, 2009; Gil et al., 2010). By calculating the pulse width ratio at different systolic amplitudes, the characteristic of an individual's cardiovascular system by exercise could be determined (Poon et al., 2004). Pulse rate variability obtained through the pulse-to-pulse interval of PPG shows high correlation with the traditional heart rate variability obtained through electrocardiogram, and has been introduced as a surrogate method for measuring electrocardiogram-based heart rate variability under resting conditions (Lu et al., 2008).

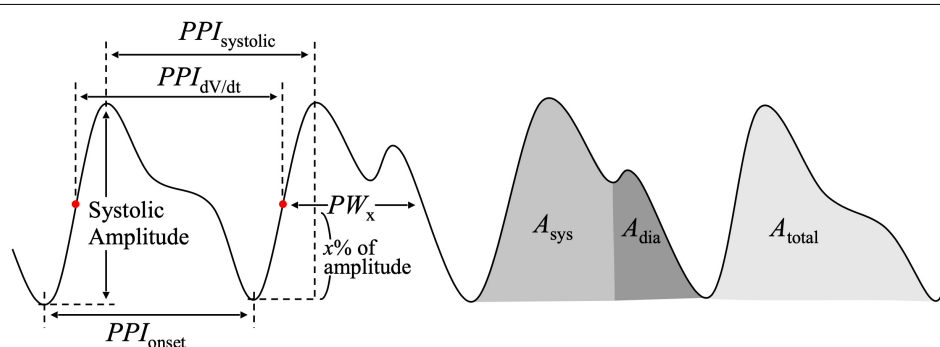


FIGURE 4 | Features of the photoplethysmogram waveform. PPI_{systolic} , interval between systolic peaks of adjacent pulse; $PPI_{dV/dt}$, interval between maximum dV/dt of adjacent pulse; PPI_{onset} , interval between pulse onsets of adjacent pulse; PW_x , pulse width at $x\%$ of systolic amplitude; A_{sys} , systolic area; A_{dia} , diastolic area; A_{total} , total pulse area.

根据心脏扩张引起的毛细血管血容量减少而绘制的曲线。根据心脏活动重复。此时，上升曲线被定义为PPG波形的收缩期，而下降曲线被定义为PPG波形的舒张期。图3示出了一次脉动和各种特征点的PPG波形。脉搏开始定义为在收缩期之前血容量最低的点处开始搏动的点。收缩压峰值定义为血容量最大化的点。当毛细血管中的液体体积由于在主动脉瓣关闭之前在与血流相反的方向上出现压力梯度而暂时再次增加时，在主动脉瓣关闭期间PPG波形的瞬时上升和下降发生（Dahlgren等人，1991；He等人，1995年）。此时，凹点被定义为重搏切迹，并且在收缩峰之后波形的一阶导数最接近于零的点被定义为舒张峰（Millasceau等人，2002年）。PPG波形可能会因身体成分、生理状态和外部刺激而发生变化。之前的一项研究报告称，很难使用PPG幅度的绝对值进行比较，因为它会根据身体组织的特征和个体特征（如种族、肤色、指甲颜色和手指大小）而变化（Alian和Shelley，2014）。此外，PPG基线受呼吸、血管顺应性、血管张力、疼痛和药物使用的影响（Nitzan等人，2000；Shelley等人，2006；Shelley，2007）。据报道，收缩期峰值的幅度（PPG波形的代表性特征）与微血管扩张具有显著相关性，并且与心输出量成比例（Dorlas和Nijboer，1985；Murray和Foster，1996）。此外，与麻醉、交感神经激活和自主神经系统活动相关的血管收缩剂使用相关的研究结果证实，当外周血管扩张时，收缩峰的幅度增加，而当血管收缩时，收缩峰的幅度降低（Korhonen和YliHankala，2009）。Dicotic切迹随血管张力和血管顺应性而变化。已经发现，切迹出现的位置在高血管张力下提前（Shi等人，2009年）。此外

已经报道舒张峰和收缩峰之间的时间差随着年龄的增长而减小（Yousef等人，2012年）。

光电容积描记图的特点及临床应用

基于原始光电容积脉搏波波形的基本特征

图4示出了直接从PPG波形获得的基本特征。这种PPG特征在临幊上经常使用（见表1）。收缩期振幅是指PPG收缩期的最大振幅。这是与血容量的脉动分量相关的特征（Asada等人，2003年）。收缩压振幅与每搏输出量高度相关（Murray和Foster，1996）。它与测量PPG的局部身体部位的血管舒张成正比（Dorlas和Nijboer，1985）。脉宽相关指数PW是指对应于50%的PPG收缩期峰值幅度的点之间的脉宽，并且显示出与全身血管阻力的高度相关性（Awad等人，2007年）。关于脉搏面积，这是被计算为PPG波形的总面积的特征；其根据手术皮肤切口而变化（Seitsonen等人，2005年）。拐点面积比计算为基于重搏切迹的收缩和舒张部分之间的面积比，并且与总外周阻力相关（Wang等人，2009年）。脉冲-脉冲间隔由PPG的两个相邻脉冲的特征点之间的时间间隔获得。脉冲起始、收缩期峰值和导数PPG的最大值主要用于测量脉冲到脉冲间隔。脉冲间隔是指心脏活动的一个周期（Linder等人，2006；Fu等人，2008；Jubadi和Sahak，2009；Gil等人，2010年）。通过计算不同收缩幅度下的脉宽比，可以确定个体心血管系统的运动特征（Poon等人，2004年）。通过PPG的脉搏到脉搏间隔获得的脉搏率变异性显示出与通过心电图获得的传统心率变异性的高度相关性，并且已经被引入作为用于测量静息条件下基于心电图的心率变异性替代方法（Lu等人，2008年）。

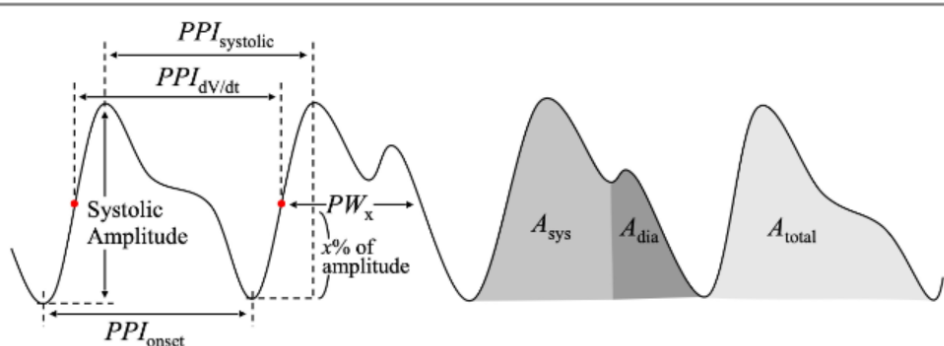


图4|光电容积描记图波形的特征。PPI，收缩期，相邻脉搏收缩峰之间的间隔；PPI_{dV/dt}，相邻脉搏最大dV/dt之间的间隔；PPI_{onset}，相邻脉搏脉冲开始之间的间隔；PW，收缩幅度x%时的脉宽；A，收缩面积；A_{sys}，舒张面积；A_{total}，总脉搏面积。

TABLE 1 | Summary of photoplethysmogram (PPG) features and clinical relationship.

Feature type	Definition	Description	Clinical use
Basic	Systolic amplitude	<ul style="list-style-type: none"> • Maximum amplitude of the PPG systolic phase. 	<ul style="list-style-type: none"> • Pulsatile component of blood volume (Asada et al., 2003; Chua and Heneghan, 2006) • Stroke volume (Murray and Foster, 1996) • Local vasodilatation (Dorlas and Nijboer, 1985) • Systemic vascular resistance (Awad et al., 2007; Lee et al., 2011c)
	Pulse width	<ul style="list-style-type: none"> • The width of pulse. It usually represented as a time interval between the x% of the maximum systolic amplitude of PPG. 	<ul style="list-style-type: none"> • Surgical skin incision (Seitsonen et al., 2005) • Total peripheral resistance (Wang et al., 2009)
	Pulse Area	<ul style="list-style-type: none"> • The total area of the PPG in a pulsation. • The area of the systolic section, or the area of the diastolic section, divided based on the dicrotic notch. 	
	Pulse-to-pulse interval	<ul style="list-style-type: none"> • The time interval between the maximum systolic amplitudes of two adjacent pulsations of PPG. • The time interval between the pulse onsets of two adjacent pulsations of PPG. • Time interval between the points of maximum derivative of two adjacent pulsations of PPG. 	<ul style="list-style-type: none"> • Cardiac cycle (Linder et al., 2006; Fu et al., 2008; Jubadi and Sahak, 2009; Gil et al., 2010) • The systolic amplitude and pulse interval ratio reflect the individual's cardiovascular system characteristics (Poon et al., 2004) • Heart (or Pulse) rate variability (Lu et al., 2008) • Peripheral perfusion (Lima and Bakker, 2006; Hasanin et al., 2017; Chu et al., 2018)
Combined	Perfusion index	<ul style="list-style-type: none"> • The ratio of the amplitude of the pulsatile component to the non-pulsatile component of PPG. 	<ul style="list-style-type: none"> • Arterial stiffness (Millasseau et al., 2002, 2003; Yousef et al., 2012))
	Large artery stiffness index	<ul style="list-style-type: none"> • Index calculated by dividing the subject's height by the time interval between the systolic peak and the diastolic peak. 	<ul style="list-style-type: none"> • Arterial stiffness (Takazawa et al., 1998; Brillante et al., 2008; Rubins et al., 2008)
	PPG augmentation index	<ul style="list-style-type: none"> • The ratio of the systolic peak amplitude to the diastolic peak amplitude of a PPG. • The ratio of the difference between the systolic peak amplitude and diastolic peak amplitude to the diastolic peak amplitude of a PPG. 	
Derivative	Pulse transit time	<ul style="list-style-type: none"> • Time difference between the specific features of PPGs measured at two different body sites. • Time interval between the pulse onset and the first zero-crossing of the derivative PPG. 	<ul style="list-style-type: none"> • Cuffless blood pressure (Foo et al., 2006; Liu et al., 2018)
	1st	<p>Crest time</p> <p>ΔT</p>	<ul style="list-style-type: none"> • Longer in vascular disease or hypertension patients (Hertzman, 1937; Dillon and Hertzman, 1941) • Time taken for the blood ejected from the heart to pass to the peripheral blood vessel (Alty et al., 2007)
	2nd	b/a	<ul style="list-style-type: none"> • Proportional to the stiffness of blood vessels, and increases with age (Takazawa, 1993; Imanaga et al., 1998; Baek et al., 2007) • Inversely related to lead poisoning (Aiba et al., 1999) • Proportional to the Framingham risk score (Otsuka et al., 2006) • Vascular stiffness, and decreases with age (Takazawa, 1993; Baek et al., 2007) • Identifying hypertensive patients (Simek et al., 2005) • Inversely proportional to vascular stiffness, and decreases with age (Takazawa, 1993; Baek et al., 2007) • Evaluation of vasoactive agents (Takazawa, 1993; Baek et al., 2007) • Inversely proportional to vascular stiffness, and decreases with age (Takazawa, 1993; Baek et al., 2007)
	c/a		
Derivative	d/a	<ul style="list-style-type: none"> • Ratio of the amplitude of the late systolic re-decreasing peak to the amplitude of the early systolic positive peak of SDPTG. 	
	e/a	<ul style="list-style-type: none"> • Ratio of the amplitude of the late systolic re-increasing peak to the amplitude of the early systolic positive peak of SDPTG. 	
		<ul style="list-style-type: none"> • Ratio of the amplitude of the early diastolic positive peak to the amplitude of the early systolic positive peak of SDPTG. 	

(Continued)

表1|光电容积描记图 (PPG) 特征和临床关系总结。

特征类型	定义	描述	临床使用
基本	同步振幅	· PPG收缩期的最大幅度。	· 血液体积的脉动分量 (Asada等人, 2003年; Chua和Heneghan, 2006年)
	脉冲宽度	· 脉冲宽度。它通常表示为PPG最大收缩幅度的x%之间的时间间隔。	· 每搏输出量 (Murray 和Foster , 1996) · 局部血管舒张 (Dorlas 和Nijboer , 1985) · 全身血管阻力 (Awad等人, 2007年; Lee等人, 2011年c)
	脉冲面积	· 脉动中PPG的总面积。 · 根据重搏切迹划分的收缩期截面面积或舒张期截面面积。	· 手术皮肤切口 (Seitsonen 等人, (2005年) · 总外周阻力 (Wang等人, (2009年)
	脉间 间隔	· PPG的两个相邻脉动的最大收缩幅度之间的时间间隔。 · PPG的两个相邻脉动的脉冲开始之间的时间间隔。 · PPG的两个相邻脉动的最大导数点之间的时间间隔。	· 心动周期 (Linder 等人, 2006; Fu等人, 2008; Jubadi 和Sahak, 2009; Gil等人, (2010年) · 收缩幅度和脉冲间隔比反映了个体的心血管系统特征 (Poon等人, (2004年第10期)
组合	灌注指数	· PPG的脉动分量与非脉动分量的幅度的比率。	· 心脏 (或脉搏) 率变异性 (Lu等人, (2008年) · 外周灌注 (Lima 和Bakker , 2006; Hasanin 等人, 2017; Chu等人, 2018年)
	大动脉 刚度指数	· 通过受试者身高除以收缩峰和舒张峰之间的时间间隔计算的指数。	· 动脉僵硬 (Miliasseau 等人, 2002, 2003 ; Yousef 等人, (2012年))
	PPG增强 指数	· PPG的收缩期峰值幅度与舒张期峰值幅度的比值。 · 收缩期峰值振幅与舒张期峰值振幅之差与PPG舒张期峰值振幅之比。	· 动脉僵硬 (Takazawa 等人, 1998; Brillante 等人, 2008; Rubins 等人, (2008年)
	脉搏传导时间	· 在两个不同身体部位处测量的PPG的特定特征之间的时间差。	· 无袖带血压 (Foo等人, 2006 ; Liu等人, 2018年)
衍生物	1st 波峰时间	· 脉搏开始与导数PPG的第一个过零点之间的时间间隔。	· 在血管疾病或高血压患者中更长 (Hertzman , 1937; Dillon 和Hertzman , 1941)
	ΔT	· 在PPG导数的正值到负值中进行的第一和第二过零点之间的时间差。	· 血液从心脏喷射到外周血管所花费的时间 (Altı 等人, (2007年)
	2nd b/a	· SDPTG的早期收缩负峰的振幅与早期收缩正峰的振幅的比率。	· 与血管的硬度成比例, 并随着年龄的增长而增加 (Takazawa , 1993; Imanga 等人, 1998; Baek 等人, (2007年) · 与铅中毒有关的炎症 (Aiba 等人, (1999年) · 与脆性风险评分成比例 (Otsuka et al., (2006年)
	c/a	· SDPTG的收缩晚期再增加峰的振幅与收缩早期正峰的振幅的比率。	· 识别高血压患者 (Simek 等人, (2005年) · 肌张力与血管僵硬度成比例, 并随年龄增长而降低 (Takazawa , 1993; Baek 等人, (2007年)
	d/a	· SDPTG的收缩晚期再降低峰的振幅与收缩早期正峰的振幅的比率。	· 肌张力与血管僵硬度成比例, 并随年龄增长而降低 (Takazawa , 1993; Baek 等人, (2007年)
	e/a	· SDPTG的舒张早期正峰的振幅与收缩早期正峰的振幅的比率。	· 血管活性剂的评价 (Takazawa , 1993; Baek 等人, (2007年) · 肌张力与血管僵硬度成比例, 并随年龄增长而降低 (Takazawa , 1993; Baek 等人, (2007年)

(续)

TABLE 1 | (Continued)

Feature type	Definition	Description	Clinical use
(b-c-d-e)/a		• Ratio of the amplitude of all of the late systolic re-increasing peaks, the late systolic re-decreasing peak, and the early diastolic positive peak subtracted from the early systolic negative peak, to the amplitude of the early systolic positive peak of SDPTG.	• Vascular aging assessment (Takazawa, 1993; Baek et al., 2007) • Atherosclerosis assessment (Takazawa, 1993; Baek et al., 2007)
(b-e)/a		• Ratio of the amplitude of the early diastolic positive peak subtracted from the early systolic negative peak, to the amplitude of the early systolic positive peak of SDPTG.	• Substitute indicator when c and d waveforms of indicator (b-c-d-e)/a are not identified (Takazawa, 1993; Baek et al., 2007)
(b-c-d)/a		• Ratio of the amplitude of all of the late systolic re-increasing peaks and the late systolic re-decreasing peak subtracted from the early systolic negative peak, to the amplitude of the early systolic positive peak of SDPTG.	• Increases with chilly sensation (Ushiroyama, 2005)

PPG, photoplethysmogram; SDPTG, second derivative PPG.

However, it was reported that PRV could be differ from HRV under dynamic conditions, such as exercise or mental stress conditions (Schäfer and Vagedes, 2013; Mejía-Mejía et al., 2020).

Combined Features of Photoplethysmogram

Features that combine several characteristic points of PPG include perfusion index, large artery stiffness index, PPG augmentation index, and PTT. Perfusion index is calculated as the ratio of the pulsatile component to the non-pulsatile component of the PPG. It is used as an index to evaluate peripheral perfusion (Lima and Bakker, 2006; Hasanin et al., 2017; Chu et al., 2018). Aortic stiffness index is calculated by dividing the height of a subject by the time interval of the maximum amplitude of the systolic and diastolic peaks. It represents the stiffness of an artery (Millasseau et al., 2002, 2003; Yousef et al., 2012)). PPG augmentation index is used as a feature for the stiffness of arterial vessels; it is calculated as the ratio of the amplitude of the systolic peak to the amplitude of the diastolic peak (Takazawa et al., 1998; Brillante et al., 2008) or by dividing the difference between the amplitude of the systolic and diastolic peaks by the amplitude of the systolic peak (Rubins et al., 2008). PTT is obtained through the time difference between specific feature points of PPGs measured in two different body sites. It is used as a feature to estimate blood pressure (Foo et al., 2006; Liu et al., 2018). **Table 1** describes the common features.

Derivative Features of Photoplethysmogram

Since the 1970s, studies have shown that the differential waveform of PPG has physiological significance. After Takazawa et al. (1998) showed a correlation between the second derivative PPG and aging, PPG derivative studies began to receive full-scale attention. **Figure 5** shows a PPG waveform, derivative PPG, and second derivative PPG. Derivative and second derivative PPGs are advantageous for representing spatiotemporal variations of PPG with respect to peak position, inflection point, number of peaks, ascending slope, and descending slope. They can be used as an alternative method to detect dicrotic and diastolic peaks that are difficult to detect in original PPG waveforms. The first-order derivative waveform of PPG is also called velocity

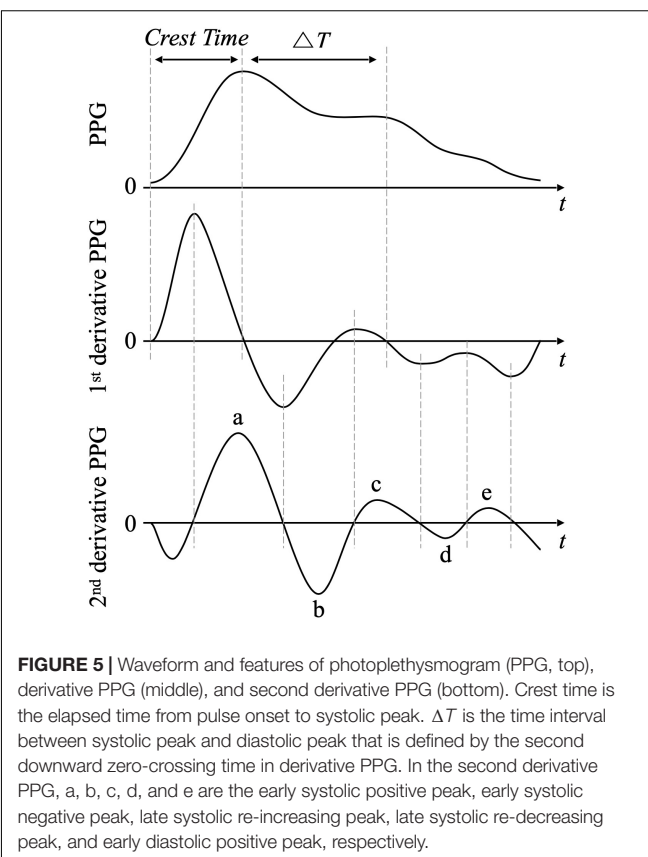


FIGURE 5 | Waveform and features of photoplethysmogram (PPG, top), derivative PPG (middle), and second derivative PPG (bottom). Crest time is the elapsed time from pulse onset to systolic peak. ΔT is the time interval between systolic peak and diastolic peak that is defined by the second downward zero-crossing time in derivative PPG. In the second derivative PPG, a, b, c, d, and e are the early systolic positive peak, early systolic negative peak, late systolic re-increasing peak, late systolic re-decreasing peak, and early diastolic positive peak, respectively.

plethysmography (VPG). The first derivative waveform of PPG can be used to extract crest time, the time taken to contract from the pulse onset of the original signal to the systolic peak, or time interval ΔT from the systolic peak to the diastolic peak. Crest time can be defined as the time taken from the start point of the VPG waveform to the following zero-crossing. Hertzman (1937) and Dillon and Hertzman (1941) proposed that crest time could be longer in patients with vascular disease or hypertension than

表1(续)

特征类型	定义	描述	临床使用
(b- c- d- e) / a		·所有收缩晚期再增加峰、收缩晚期再减少峰和从收缩早期负峰减去舒张早期正峰的振幅与SDPTG的收缩早期正峰的振幅的比率。	•血管老化评估 (Takazawa , 1993; Baek等人, (2007年)) •动脉粥样硬化评估 (Takazawa , 1993; Baek等, (2007年))
(b- e)/ a		·从收缩早期负峰减去舒张早期正峰的振幅与SDPTG的收缩早期正峰的振幅的比率。	• Substitute indicator when c and d waveforms of指标 (b- c- d- e) / a未确定 (Takazawa , 1993年; Baek等人, (2007年))
(b- c- d) / a		·所有收缩晚期再增加峰的振幅与收缩晚期再增加峰的振幅的比率 再减峰减去收缩早期负峰, 得到SDPTG收缩早期正峰的振幅。	• 增加冷冰冰的感觉 (Ushiroyama , 2005)

PPG, 光电容积描记图; SDPTG, 二阶导数PPG。

然而, 据报道, 在动态条件下, 如运动或精神压力条件下, PRV可能与HRV不同 (Schäfer 和Vagedes , 2013 ; Mejía - Mejía 等人, 2020 年)。

光电容积描记图的组合特征

联合收割机的几个特征点的PPG包括灌注指数, 大动脉硬度指数, PPG增强指数, 和PTT。灌注指数计算为PPG的脉动分量与非脉动分量的比率。它被用作评价外周灌注的指标 (Lima 和Bakker , 2006 ; Hasanin 等人, 2017 ; Chu等人, 2018 年)。通过将受试者的身高除以收缩峰和舒张峰的最大幅度的时间间隔来计算主动脉僵硬指数。它代表动脉的硬度 (Millasseau 等人, 2002, 2003 ; Yousef 等人, 2012)。PPG增强指数被用作动脉血管硬度的特征;其被计算为收缩峰的幅度与舒张峰的幅度的比率 (Takazawa 等人, 1998 ; Brillante 等人, 2008) 或通过将收缩峰和舒张峰的幅度之间的差除以收缩峰的幅度 (Rubins 等人, 2008 年)。PTT通过在两个不同身体部位测量的PPG的特定特征点之间的时间差获得。它被用作估计血压的特征 (Foo 等人, 2006 ; Liu等人, 2018 年)。表I描述了共同特征。

光电容积脉搏波的导数特征

自20世纪70年代以来, 研究表明PPG的微分波形具有生理意义。在Takazawa 等人 (1998) 证明二阶导数PPG与衰老之间的相关性后, PPG导数研究开始受到全面关注。图5示出了PPG波形、导数PPG和二阶导数PPG。导数和二阶导数PPG对于表示PPG关于峰值位置、拐点、峰值数量、上升斜率和下降斜率的时空变化是有利的。它们可以用作检测在原始PPG波形中难以检测的重搏峰和舒张峰的替代方法。PPG的一阶导数波形也称为速度

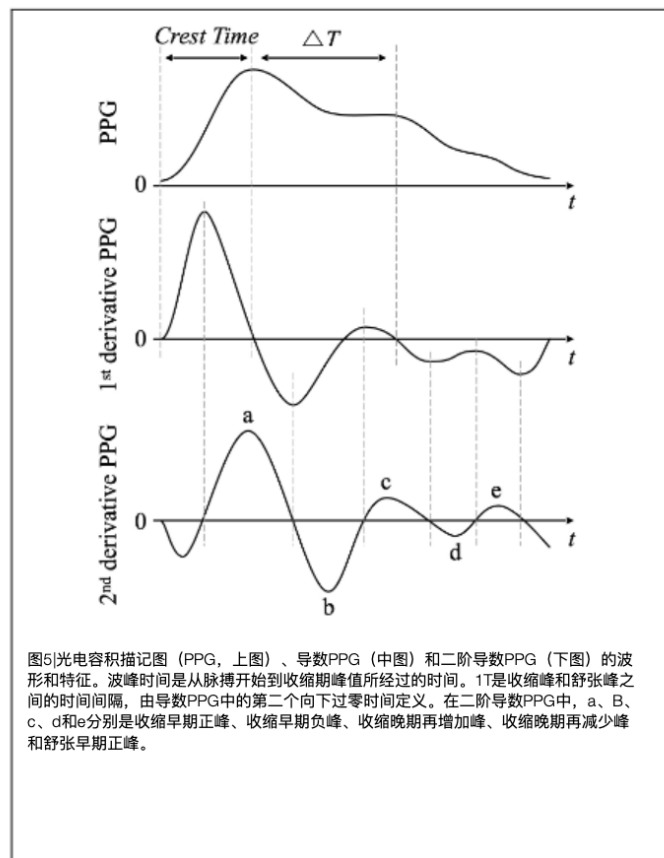


图5|光电容积描记图 (PPG, 上图)、导数PPG (中图) 和二阶导数PPG (下图) 的波形和特征。波峰时间是从脉搏开始到收缩期峰值所经过的时间。1T是收缩峰和舒张峰之间的时间间隔, 由导数PPG中的第二个向下过零时间定义。在二阶导数PPG中, a、B、c、d和e分别是收缩早期正峰、收缩早期负峰、收缩晚期再增加峰、收缩晚期再减少峰和舒张早期正峰。

体积描记法 (VPG)。PPG的一阶导数波形可以用于提取波峰时间, 从原始信号的脉搏开始到收缩峰收缩所花费的时间, 或者从收缩峰到舒张峰的时间间隔1T。波峰时间可以定义为从VPG波形的起始点到下一个过零点所花费的时间。Hertzman (1937) 和Dillon和Hertzman (1941) 提出, 血管疾病或高血压患者的波峰时间可能长于

in a normal group. Alty et al. (2007) reported that among the features extracted from the first derivative PPG, ΔT , defined as the time difference between the first and second zero-crossing points proceeding in the positive to negative value in the VPG waveform and crest time shows high accuracy for predicting cardiovascular disease. They showed that ΔT is related to the time it takes for blood ejected from the heart to pass to peripheral blood vessels, and that it can classify cardiovascular diseases with an accuracy of 87.5% using a support vector machine. The second-order derivative PPG waveform is also called the second derivative of photoplethysmogram (SDPTG), second derivative of the digital volume pulse (SDDVP), and acceleration plethysmogram (APG). Takazawa et al. (1998) defined the peaks and valleys of the second-order differentiated PPG waveform as a , b , c , d , and e , as shown in **Figure 5**. They showed that combined indices, such as b/a , c/a , d/a , and e/a , had a significant correlation with aging.

Other Clinical Applications

In addition, studies for predicting various parameters or diagnosing diseases have been conducted using PPG. In addition to basic heart rate estimation, PPG is used for blood pressure estimation (Poon and Zhang, 2005; Muehlsteff et al., 2006; He et al., 2014; Nabeel et al., 2017; Wang et al., 2018; El Hajj and Kyriacou, 2020), vascular aging assessment (Takazawa et al., 1998; Bortolotto et al., 2000; Millasseau et al., 2003; Baek et al., 2007; Jubadi and Sahak, 2009; Wang et al., 2009; Yousef et al., 2012; Dall'Olio et al., 2020; Korkalainen et al., 2020), arterial fibrillation prediction (Poh et al., 2018; Kwon et al., 2019; Aschbacher et al., 2020; Cheng et al., 2020; Pereira et al., 2020), diabetes prediction (Shan et al., 2016; Tang et al., 2017; Poh et al., 2018; Eerikäinen et al., 2019; Guo et al., 2019; Kwon et al., 2019; Proesmans et al., 2019; Yang et al., 2019; Aschbacher et al., 2020; Cheng et al., 2020; Pereira et al., 2020), peripheral vascular disease assessment (Allen and Murray, 1993; Alnaeb et al., 2007; Bentham et al., 2018; Allen et al., 2021), surgical and postoperative pain assessment (Ahonen et al., 2007; Struys et al., 2007; Kallio et al., 2008; Hasanin et al., 2017; Yang et al., 2018; Seok et al., 2019), heterogeneous bio-signal (e.g., ECG) reconstruction (Zhu et al., 2021), hemodynamic parameter estimation such as cardiac output (McCombie et al., 2005; Wang et al., 2009; Wang et al., 2010, 2014; Lee et al., 2013) or stroke volume (Liu et al., 2020a,b), sleep monitoring including apnea and hypopnea detection (Behar et al., 2014; Uçar et al., 2015; Park and Choi, 2019; Hilmisson et al., 2020; Lazazzera et al., 2020), and emotional recognition (Rakshit et al., 2016; Ayata et al., 2018; Goshvarpour and Goshvarpour, 2018, 2020; Lee et al., 2019).

Photoplethysmogram Noise

The results of our literature research related to PPG noise reduction are summarized. Representative noises that affect PPG analysis results include MAs related to body movement and sensor attachment, baseline change due to respiration and body movement, and hypoperfusion due to decreased peripheral perfusion. **Figure 6** describes these representative photoplethysmogram distortions. Each noise is described in the following subsections.

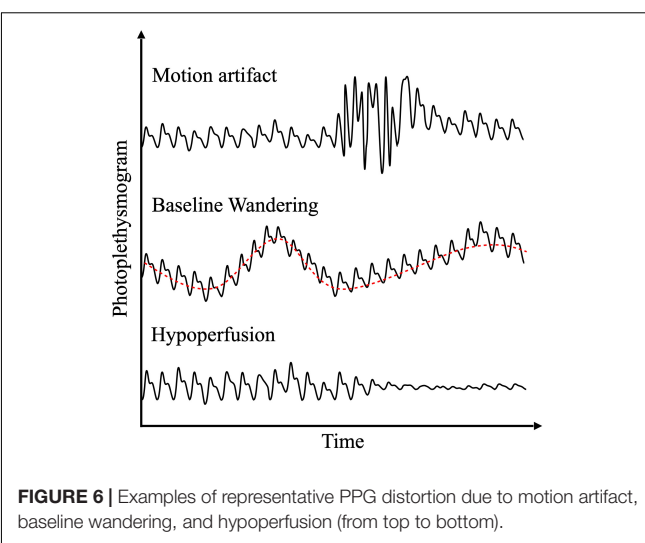


FIGURE 6 | Examples of representative PPG distortion due to motion artifact, baseline wandering, and hypoperfusion (from top to bottom).

Motion Artifact

Motion artifact, which is mainly caused by body motions, such as hand movement, walking, and running, is a critical noise when measuring PPG. Depending on probe type and light source, PPG measurement may be more sensitive to MA; it has been reported that red and green wavelengths are more robust to MA (Matsumura et al., 2020). In addition, depending on measuring sites, it was shown that MA in ear PPG is less than in finger or forehead PPG (Selvaraj et al., 2011). Since MA is known to have a frequency range of 0.01–10 Hz, the major component of PPG can be distorted by overlapping with the main frequency band (0.5–5 Hz) of PPG (Bagha and Shaw, 2011; Rojano and Isaza, 2016; Lee et al., 2020). Such distortion makes it difficult to detect important features during analysis, and that causes false diagnosis. Therefore, an MA must be removed or corrected prior to analysis. In MA removal using a frequency domain filter, a high-pass filter is mainly used. Joseph et al. reported that a high-pass filter with a cut-off frequency of 0.15 Hz does not change pulse shape, while maintaining an ideal ratio of the pulsatile and non-pulsatile components of PPG (Joseph et al., 2014). In addition, a study by Allen and Murray comparing the performance of a total of 90 filters by combining 9 filter types and 10 filter orders found the fourth-order Chebyshev type II filter to have the best performance in improving PPG signal quality (Allen and Murray, 2004). However, since the frequency domain filter alone has limitations in removing MA according to various motion intensities and motion types, studies on removal of MAs are being conducted using algorithms based on filters, accelerometers, and multiple wavelengths. The MA reduction method by independent component analysis (ICA) is a method of removing only the MA component by extracting independent components corresponding to PPG and MA from PPG containing MAs, assuming that PPG and MA are random vectors. Kim and Yoo (2006) qualitatively confirmed that the PPG and MA components can be separated by ICA. Lee et al. (2020) proposed a method to reduce MA by applying ICA to the multi-channel PPG obtained with a multi-wavelength light

在一个正常的组。Alty等人（2007）报告称，在从一阶导数PPG提取的特征中， $1T$ （定义为VPG波形中从正值到负值的第一个和第二个过零点之间的时间差）和波峰时间显示出预测心血管疾病的高准确性。他们表明， $1T$ 与血液从心脏喷射到外周血管所需的时间有关，并且使用支持向量机可以对心血管疾病进行分类，准确率为87.5%。二阶导数PPG波形也称为光电容积描记图的二阶导数（SDPTG）、数字容积脉搏的二阶导数（SDDVP）和加速度容积描记图（APG）。Takazawa等人（1998）将二阶微分PPG波形的峰和谷定义为a、B、c、d和e，如图5所示。他们发现，综合指数，如 b/a 、 c/a 、 d/a 和 e/a ，与衰老有显著的相关性。

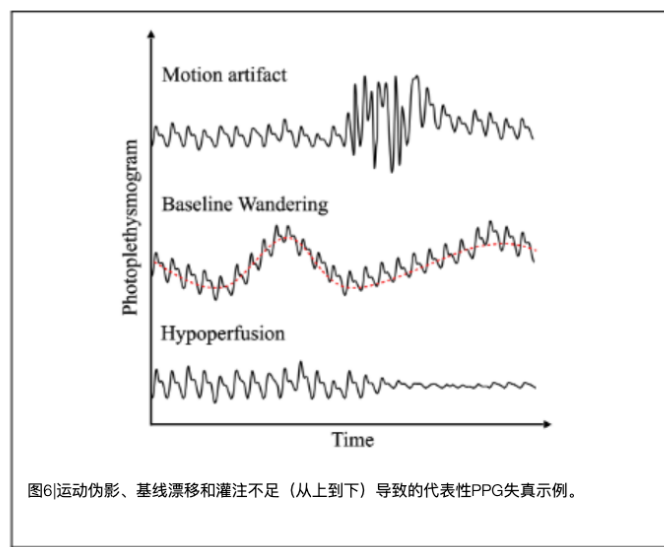


图6运动伪影、基线漂移和灌注不足（从上到下）导致的代表性PPG失真示例。

其他临床应用

此外，已经使用PPG进行了用于预测各种参数或诊断疾病的研究。除了基本心率估计之外，PPG还用于血压估计（Poon 和 Zhang，2005；Muehlsteff 等人，2006；He 等人，2014；Nabeel 等人，2017；Wang 等人，2018；El Hajj 和 Kyriacou，2020），血管老化评估（Takazawa 等人，1998；Bortolotto 等人，2000；Millasseau 等人，2003；Baek 等人，2007；Jubadi 和 Sahak，2009；Wang 等人，2009；Yousef 等人，2012；Dall'Olio 等人，2020；Korkalainen 等人，2020）、动脉纤颤预测（Poh 等人，2018；Kwon 等人，2019；Aschbacher 等人，2020 年；Cheng 等人，2020；佩雷拉等人，2020）、糖尿病预测（Shan 等人，2016 年；Tang 等人，2017；Poh 等人，2018；Eerikäinen 等人，2019；Guo 等人，2019；Kwon 等人，2019；Proesmans 等人，2019 年；Yang 等人，2019；Aschbacher 等人，2020 年；Cheng 等人，2020；佩雷拉等人，2020）、外周血管疾病评估（艾伦和默里，1993；Alnaeb 等人，2007；Bentham 等人，2018；艾伦等人，2021）、手术和术后疼痛评估（Ahonen 等人，2007；Struys 等人，2007；Kallio 等人，2008；Hasanin 等人，2017；Yang 等人，2018；Seok 等人，2019）、异质生物信号（例如，ECG）重建（Zhu 等人，2021）、血液动力学参数估计，例如心输出量（McCombie 等人，2005；Wang 等人，2009；Wang 等人，2010, 2014；Lee 等人，2013）或每搏输出量（Liu 等人，2020 a, B），包括呼吸暂停和呼吸不足检测的睡眠监测（Behar 等人，2014；Uçar 等人，2015；Park 和 Choi，2019；Hilmisson 等人，2020；Lazazzera 等人，2020）和情感识别（Rakshit et al., 2016；Ayata 等人，2018；Goshvarpour 和 Goshvarpour，2018, 2020；Lee 等人，2019 年）。

光电体积描记图噪声

我们的文献研究的结果与PPG降噪进行了总结。影响PPG分析结果的代表性噪声包括与身体运动和传感器连接相关的MA、由于呼吸和身体运动引起的基线变化以及由于外周灌注减少引起的灌注不足。图6描述了这些代表性的光电体积描记图失真。每种噪声在以下小节中描述。

运动伪影

运动伪影是PPG测量时的一种重要噪声，主要由手部运动、步行和跑步等身体运动引起。根据探头类型和光源，PPG测量可能对MA更敏感；据报道，红色和绿色波长对MA更稳健（Matsumura 等人，2020 年）。此外，根据测量部位，已经表明耳朵PPG中的MA小于手指或前额PPG中的MA（Selvaraj 等人，2011年）。由于已知MA具有0.01 - 10 Hz的频率范围，因此PPG的主要分量可能会因与PPG的主频带（0.5 - 5 Hz）重叠而失真（Bagha 和 Shaw，2011；Rojano 和 Isaza，2016；Lee 等人，2020 年）。这种失真使得在分析期间难以检测重要特征，并且导致错误诊断。因此，必须在分析前删除或纠正MA。在使用频域滤波器的MA去除中，主要使用高通滤波器。Joseph 等人报道了具有0.15Hz 截止频率的高通滤波器不改变脉冲形状，同时保持PPG的脉动和非脉动分量的理想比率（Joseph 等人，2014 年）。此外，艾伦和 Murray 的一项研究通过组合9种滤波器类型和10种滤波器阶数比较了总共90 种滤波器的性能，发现四阶Chebyshev I型滤波器在改善PPG信号质量方面具有最佳性能（艾伦和 Murray，2004）。然而，由于单独的频域滤波器在根据各种运动强度和运动类型去除MA方面具有局限性，因此正在使用基于滤波器、加速度计和多波长的算法来进行关于去除MA的研究。基于独立分量分析（伊卡）的MA减少方法是通过从包含MA的PPG中提取与PPG和MA相对应的独立分量来仅去除MA分量的方法，假设PPG和MA是随机向量。Kim 和 Yoo（2006）定性证实，PPG 和 MA 组分可通过伊卡分离。Lee 等人（2020）提出了一种通过将伊卡应用于利用多波长光获得的多通道PPG 来减少MA的方法。

source. In their study, the MA included in PPG during walking, fast walking, and running was reduced by ICA. PPG peak was then detected. The position of the detected PPG peak was 99, 96.2, and 82.0%, consistent with the QRS position of the ECG in walking, fast walking, and running, respectively. In MA removal using adaptive noise cancelation (ANC), the accelerometer and PPG are measured simultaneously. The damaged part of the PPG is found and removed by the motion detected by the accelerometer (Widrow et al., 1975). Foo and Wilson (2006) used ANC to remove the MA generated from light motion, while Poh et al. (2010) used ANC to remove the MA generated from walking and running. In addition, Han et al. (2007) proposed a method of removing MA by simultaneously measuring PPG and acceleration, and applying a two-dimensional active noise cancelation algorithm. This algorithm can reduce the signal distortion rate from 52.3 to 3.53 at a frequency of 1–2.5 Hz using the 4th-order normalized least mean square (NLMS) adaptive filter. Seyedtabaii and Seyedtabaii (2008) proposed that adaptive filtering based on the Kalman filter may be effectively used for MA reduction. A study by Reddy et al. (2008) reduced the normalized root mean squared error by 35 dB after eliminating MA components in a frequency domain by cycle-by-cycle Fourier series analysis for each pulse in PPG. Patterson and Yang (2011) showed that MA for vertical finger movement and rotational movement could be removed through stationary wavelet transform. The error with HR and HRV obtained from ECG can be reduced (Joseph et al., 2014).

Baseline Wandering

The baseline of the pulsatile component of PPG and AC amplitude of PPG can be changed by various factors, such as respiration, sympathetic nervous system activities, and thermoregulation (Allen, 2007). The change in PPG baseline interferes with the analysis of the AC component of PPG. Therefore, to accurately analyze the AC component of PPG, Timimi et al. (2017) proposed a method of directly removing the change in baseline and a method of removing the change in baseline by subtraction from the measured signal based on estimation of the change in baseline. Jang et al. (2014) reported that high-pass filtering (HPF) is frequently performed in the method of directly removing the baseline. The frequency component of the AC of PPG is a component related to pulsation. This is normally higher than 0.5 Hz (30 bpm) in a healthy person. However, the respiratory component that causes baseline change has a frequency range of 0.15–0.5 Hz. HPF is performed to remove baseline movement located in the low-frequency range without damaging the AC component, based on the frequency range difference of signals. HPF is simpler and more convenient to perform than the method of baseline removal based on direct estimation. However, when the frequency component of PPG AC is lower than the cut-off frequency band of HPF, this method may cause signal distortion. As a method of indirectly estimating and removing the baseline, interpolation methods, such as linear interpolation and cubic spline interpolation, can be used for baseline estimation. A method combining wavelet and least mean square (LMS) adaptive filter can also be used (Wang et al., 2003). The linear interpolation method can simply

estimate the baseline with a low-order polynomial. However, linear interpolation has the disadvantage that it is not very precise and the interpolant is not differentiable. Cubic spline interpolation can compensate for this discontinuity of signal by estimating the change in baseline through a cubic polynomial. In baseline removal using the interpolation technique, baseline wander is removed by subtracting the estimated baseline from PPG. In the method of removing baseline variation by combining wavelet transformation and LMS adaptive filter, the baseline component extracted by wavelet transformation is applied to the LMS adaptive filter to remove the baseline component. Then, the PPG from which the baseline is removed is obtained through inverse wavelet transform. Considering that PPG has non-stationary characteristics, wavelet-based baseline estimation may be appropriate. However, since both wavelet and adaptive filtering must be performed, its computational complexity may be high compared to other methods. In addition, due to the transition band of the filter, such method is unsuitable for cases with short signals.

Hypoperfusion

Hypovolemia, hypothermia, vasoconstriction, and decreased cardiac output or mean arterial pressure may weaken changes of blood volume in blood vessels, called poor perfusion or low perfusion (Alnaeb et al., 2007). Hypoperfusion becomes more pronounced toward the peripheries of the body. It affects the pulsatile component of PPG, thus weakening amplitude change (Kyriacou et al., 2002). To improve the low perfusion waveform, Foo and Wilson applied a non-causal Wiener filter with a 0.1- to 15-Hz pass band (Foo and Wilson, 2006); they showed that the heart rate error estimated from low-perfusion PPG could be reduced to less than 5.12%. Shafique et al. (2012) proposed a method to improve low perfusion by simultaneously measuring PPG using a transmission-type and a reflection-type measuring device, and reconstructing the PPG using a summing amplifier. The reconstituted PPG showed higher sensitivity than single-mode PPG in PPG measurement in a low perfusion state that was forcibly generated using the cuff. Oxygen saturation measurement also showed lower failure rate than commercial products.

In addition to the movement, respiration, and low perfusion of a subject, there are numerous factors that can distort the PPG waveform. Typical examples include ambient light, temperature of the measuring site, skin pigmentation in the measurement body site, alignment of light source and photodetector, method of attaching the sensor to the skin, contact pressure between the sensor and the skin, and posture of a subject (Reynolds et al., 1991; Adler et al., 1998; Teng and Zhang, 2006; Zhang and Zhang, 2006; Lee et al., 2011b; Kim et al., 2016). Ambient noise reduction is mainly attempted through hardware improvement. Kim et al. (2016) developed a PPG readout chip equipped with a technique that can remove the effect of ambient light through a charge redistribution method after cross-sampling PPG mixed with ambient light with complementary metal-oxide-semiconductor (CMOS) process. Cold site temperature causes vasoconstriction of the measurement site and reduces perfusion, thereby degrading the quality of the measured signal

源头在他们的研究中，伊卡降低了步行、快走和跑步期间PPG中的MA。然后检测PPG峰值。检测到的PPG峰值的位置分别为99%、96.2%和82.0%，与步行、快速步行和跑步时ECG的QRS位置一致。在使用自适应噪声消除(ANC)的MA去除中，同时测量加速度计和PPG。PPG的受损部分通过加速度计检测到的运动被发现并移除(Widrow等人，1975年)。Foo和Wilson(2006年)使用ANC来消除由轻微运动产生的MA，而Poh等人(2010年)使用ANC来消除由步行和跑步产生的MA。此外，Han等人(2007)提出了一种通过同时测量PPG和加速度并应用二维主动噪声消除算法来消除MA的方法。该算法在1-2频率下可将信号失真率从52.3降低到3.53。5Hz，使用4阶归一化最小均方(NLMS)自适应滤波器。

Seyedtabaii 和Seyedtabaii (2008)提出，基于卡尔曼滤波器的自适应滤波可以有效地用于MA减少。Reddy等人(2008)的一项研究通过逐周期傅立叶级数分析PPG中的每个脉冲，在频域中消除MA分量后，将归一化均方根误差降低了35 dB。Patterson 和Yang (2011)表明，垂直手指运动和旋转运动的MA可以通过平稳小波变换去除。可以减少从ECG获得的HR和HRV的误差(Joseph等人，2014年)。

线性插值法可以简单地用低阶多项式估计基线。然而，线性插值的缺点是它不是很精确，插值是不可微的。三次样条插值可以通过三次多项式估计基线的变化来补偿信号的这种不连续性。在使用插值技术的基线去除中，通过从PPG中减去估计的基线来去除基线漂移。在小波变换与LMS自适应滤波器相结合的基线变化去除方法中，将小波变换提取的基线分量应用于LMS自适应滤波器，去除基线分量。然后，通过小波逆变换获得去除基线的PPG。考虑到PPG具有非平稳特性，基于小波的基线估计可能是合适的。然而，由于必须执行小波和自适应滤波，因此与其他方法相比，其计算复杂度可能较高。此外，由于滤波器的过渡带，这种方法不适用于短信号的情况。

基线漂移

PPG的脉动分量和PPG的AC振幅的基线可通过各种因素改变，例如呼吸、交感神经系统活动和体温调节(艾伦，2007)。PPG基线的变化干扰PPG的AC分量的分析。因此，为了准确地分析PPG的AC分量，Timimi等人(2017)提出了直接去除基线变化的方法和通过基于基线变化的估计从测量信号中减去去除基线变化的方法。

Jang等人(2014)报告称，在直接去除基线的方法中经常进行高通滤波(HPF)。PPG的AC的频率分量是与脉动相关的分量。在健康人中，这通常高于0.5 Hz(30 bpm)。然而，引起基线变化的呼吸成分的频率范围为0.15-0.5 Hz。基于信号的频率范围差异，执行HPF以去除位于低频范围内的基线移动而不损坏AC分量。HPF法比直接估计基线的方法简单、方便。然而，当PPG AC的频率分量低于HPF的截止频带时，该方法可能导致信号失真。作为一种间接估计和去除基线的方法，可以使用诸如线性插值和三次样条插值的插值方法来进行基线估计。也可以使用组合小波和最小均方(LMS)自适应滤波器的方法(Wang et al. (2003年)

低灌注

血容量不足、体温过低、血管收缩和心输出量或平均动脉压降低可能会减弱血管中血容量的变化，称为灌注不良或低灌注(Alnaeb et al., 2007年)。灌注不足在身体周围变得更加明显。它影响PPG的脉动分量，从而减弱幅度变化(Kyriacou等人，2002年)。为了改善低灌注波形，Foo和Wilson应用了通常为0.1-15 Hz的非因果维纳滤波器(Foo和Wilson，2006)；他们表明，根据低灌注PPG估计的心率误差可降低至5.12%以下。Shafique等人(2012)提出了一种通过使用透射型和反射型测量设备同时测量PPG并使用求和放大器重建PPG来改善低灌注的方法。在使用袖带强制生成的低灌注状态下，重构PPG在PPG测量中显示出比单模PPG更高的灵敏度。氧饱和度测量也显示出比商业产品更低的故障率。

除了受试者的运动、呼吸和低灌注之外，还有许多因素可以使PPG波形失真。典型的例子包括环境光、测量部位的温度、测量身体部位中的皮肤色素沉着、光源和光电检测器的对准、将传感器附接到皮肤的方法、传感器和皮肤之间的接触压力以及受试者的姿势(Reynolds等人，1991；Adler等人，1998；Teng和Zhang，2006；Zhang和Zhang，2006；Lee等人，2011 b；Kim等人，2016年)。环境噪声的降低主要是通过硬件改进来尝试的。Kim等人(2016)开发了一种PPG读出芯片，该芯片配备了一种技术，该技术可以在利用互补金属氧化物半导体(CMOS)工艺对PPG与环境光混合进行交叉采样后，通过电荷重新分布方法消除环境光的影响。冷部位温度导致测量部位的血管收缩并减少灌注，从而降低测量信号的质量。

(Khan et al., 2016). Massage or warming is known to be effective for increasing blood flow or perfusion, and improvement of signal quality through this method has also been reported (Bohusch et al., 1994; Foo, 2007; Freckmann et al., 2012). It is known through several studies that the signal-to-noise ratio of PPG measured according to skin color or pigmentation shows a significant difference (Fallow et al., 2013; Yan et al., 2017; Sañudo et al., 2019). Yan et al. (2017) suggested multi-wavelength measurement to be effective as a method to reduce deviation by skin type. In addition, Fallow et al. (2013) reported that high-resolution PPG can be obtained for various skin types with green wavelength under resting conditions, and green or blue wavelength under exercise conditions. When measuring PPG, probe pressure causes change in PPG waveform and could affect analysis result (Dresher and Mendelson, 2006b; Liu et al., 2015). A method of adjusting the contact force by optimizing the housing design of the PPG probe (Dresher and Mendelson, 2006a) or using a measuring platform with a built-in force regulator in the probe (Sim et al., 2018) has been proposed as a method to improve non-uniform contact force.

Photoplethysmogram Signal Processing

Photoplethysmogram Preprocessing

Table 2 summarizes the pre-processing techniques of PPG. Because of the simplicity of its waveform, PPG has a relatively simple pre-processing process. Our literature search found that most PPG pre-processing was dependent on frequency filtering to remove high-frequency or low-frequency noise. In frequency filtering, the lower bound of the passband in most studies is about 0.5 Hz (Sukor et al., 2011; Papini et al., 2018; Canac et al., 2019; Pradhan et al., 2019) to remove the DC component below 0.1 Hz and respiratory component in the 0.1–0.5 Hz band while obtaining only the AC component of PPG. The upper bound of the bandpass filter is usually determined considering that the main frequency components of PPG are included within the fourth harmonics in the frequency domain. The upper bound of the frequency filter at 10 Hz as the position of the fourth harmonics is often used when heart rate is 150 bpm (2.5 Hz). Thus, in the general case, the low pass filter that has a 10-Hz cutoff frequency can include most PPG frequencies (Papini et al., 2018; Canac et al., 2019; Liu et al., 2020a,b). The Butterworth, Chebychev I, and finite impulse response (FIR) filters are mainly used for frequency filtering. PPG pre-processing is also performed by decomposing the waveform into several frequency components, removing noise for each component, and then recombining them. A representative of these methods is the method based on empirical mode decomposition (EMD) or wavelet decomposition. With the EMD-based method, the noise component is removed by excluding the intrinsic mode function (IMF) based on a specific frequency after obtaining the IMF of PPG and then recombining it. Lu et al. (2008) removed low-frequency noise and the trend of PPG by recombining only IMF with a dominant frequency > 0.5 Hz. Similarly, in a study using a wavelet transform, noise is removed by obtaining a sub-band signal through wavelet decomposition and combining specific sub-bands. Vadrevu and Manikandan (2018) showed

that low-frequency and high-frequency noise of PPG can be effectively removed in the preprocessing step to detect the peak by recombining the sub-band signal after applying the stationary wavelet transform. Shin et al. (2010) used the discrete cosine transform to remove noise outside the 0.5- to 10-Hz band, and found that it can be used for PPG pre-processing with sparse frequency characteristics. Selvaraj et al. (2011) showed that a high-order polynomial can be used to handle non-stationary dynamics. In addition to noise reduction, pre-processing is also performed for signal enhancement purposes. Kim et al. (2019) proposed an amplitude regularization technique using an envelope curve to reduce the fluctuation of PPG amplitude. Canac et al. (2019) used a moving differentiation filter to sharpen PPG upslope and eliminate high-frequency noise.

Photoplethysmogram Peak Detection

Peak detection is essential for analyzing PPG. Detection methods based on zero-crossing, local maxima or minima (LCM), adaptive threshold, and machine learning have been proposed. Zero-crossing is a method that can find the point where the sign of the slope changes, in the same way as a quasi-periodic signal peak detection method. However, since the zero-crossing-based method is highly likely to erroneously detect peaks due to tiny fluctuations of signals, various filtering methods must be applied in the peak detection method based on zero-crossing to simplify the PPG waveform. To detect PPG peaks using the zero-crossing method, Canac et al. (2019) used a 0.5- to 10-Hz 4th order Butterworth filter and a moving difference filter for the detection of pulsating wave peaks, while Kavsaoglu et al. (2016) segmented the PPG signal and divided it by the sign of each slope. In addition, a method for detecting peaks through zero-crossing after wavelet or Hilbert transform of the PPG signal has been reported (Scholkmann et al., 2012; Ferro et al., 2015). Ferro et al. (2015) detected onsets and systolic peaks of a pulse wave with low complexity and low computation cost; however, their study was validated with only a small number of study subjects ($N = 10$) in a noise-free environment. Vadrevu and Manikandan (2018) decomposed the PPG component through wavelet decomposition and then detected systolic and onset peaks, without by knowledge rule-based post-processing. This approach showed over 99% of sensitivity and predictivity on the total number of 116,255 beats taken from three PPG databases; however, it has relatively high complexity from the use of wavelet decomposition. Also, it is hard to apply for real-time application because of being designed for a non-causal system. One of the most frequently used PPG peak detection methods is a method based on LCM detection. LCM is a method of finding the maximum or minimum value within a specific region based on a pre-defined threshold. In LCM peak detection, peaks are detected by repeated window sliding and peak detection. The detection threshold can have a fixed value or an adaptive value. Lu et al. (2008) determined the threshold at a certain ratio of the maximum PPG value. Xu et al. (2008) set the threshold based on pulse height and detected peaks by comparing the heights of candidate peaks within a 2-s window. The LCM method requires appropriate window size selection. It has the disadvantage that if there are large-scale baseline changes due to

(Khan 等人, 2016 年)。已知按摩或加温对于增加血流或灌注是有效的, 并且也已经报道了通过该方法改善信号质量 (Bohusch 等人, 1994; Foo, 2007; Freckmann 等人, 2012 年)。通过几项研究已知, 根据皮肤颜色或色素沉着测量的PPG 的信噪比显示出显著差异 (Fallow 等人, 2013; Yan 等人, 2017; Sañudo 等人, 2019 年)。Yan 等人 (2017) 建议多波长测量是一种有效的方法, 可以减少皮肤类型的偏差。此外, Fallow 等人 (2013) 报告称, 在静息条件下使用绿色波长, 在运动条件下使用绿色或蓝色波长, 可以获得各种皮肤类型的高分辨率PPG。测量PPG 时, 探头压力会导致 PPG 波形变化, 并可能影响分析结果 (德雷舍和Mendelson , 2006 b; Liu等人, 2015 年)。通过优化PPG 探头的外壳设计 (德雷舍和Mendelson , 2006 a) 或使用探头内置力调节器的测量平台 (Sim 等人, 2018) 已经被提出作为改善非均匀接触力的方法。

Vadrevu 和Manikandan (2018) 表明, 在预处理步骤中可以有效去除PPG 的低频和高频噪声, 以通过在应用平稳小波变换后重组子带信号来检测峰值。Shin 等人 (2010) 使用离散余弦变换去除0.5 - 10 Hz频带外的噪声, 并发现其可用于具有稀疏频率特性的PPG 预处理。Selvaraj 等人 (2011年) 表明, 高阶多项式可用于处理非平稳动态。除了降噪之外, 还执行预处理以用于信号增强目的。Kim 等人 (2019) 提出了一种使用包络曲线的振幅正则化技术, 以减少PPG 振幅的波动。Canac 等人 (2019) 使用移动微分滤波器来锐化PPG 上斜率并消除高频噪声。

光电体积描记信号处理

光电体积描记图预处理

表2总结了PPG 的预处理技术。由于其波形的简单性, PPG 具有相对简单的预处理过程。我们的文献检索发现, 大多数PPG 预处理依赖于频率滤波来去除高频或低频噪声。在频率滤波中, 大多数研究中通带的下限约为0.5 Hz (Sukor 等人, 2011; Papini 等人, 2018; Canac 等人, 2019; Pradhan 等人, 2019) 以去除0.1 Hz以下的DC 分量和0.1- 0.5 Hz频带中的呼吸分量, 同时仅获得PPG 的AC分量。带通滤波器的上限通常是考虑到PPG 的主要频率分量被包括在频域中的四次谐波内而确定的。当心率为150 bpm (2.5 Hz) 时, 通常使用频率滤波器在10 Hz处的上限作为四次谐波的位置。因此, 在一般情况下, 具有10- Hz截止频率的低通滤波器可以包括大多数PPG 频率 (Papini 等人, 2018; Canac 等人, 2019 年; Liu等人, 2020 a, B)。巴特沃思、切比雪夫和有限脉冲响应 (FIR) 滤波器主要用于频率滤波。PPG 预处理还通过将波形分解成若干频率分量、去除每个分量的噪声并且然后将它们重新组合来执行。这些方法的代表是基于经验模式分解 (EMD) 或小波分解的方法。对于基于EMD的方法, 在获得PPG 的固有模态函数 (IMF) 之后, 通过基于特定频率排除固有模态函数 (IMF) 并且然后将其重组来去除噪声分量。Lu 等人 (2008) 通过仅重组具有> 0.5 Hz的主频率的IMF来去除低频噪声和PPG 的趋势。类似地, 在使用小波变换的研究中, 通过小波分解获得子带信号并组合特定子带来去除噪声

光电体积描记图峰值检测

峰值检测对于分析PPG 是必不可少的。基于过零、局部最大值或最小值 (LCM) 、自适应阈值和机器学习的检测方法已经被提出。过零是一种可以找到斜率的符号改变的点的方法, 以与准周期信号峰值检测方法相同的方式。然而, 由于基于过零的方法很可能由于信号的微小波动而错误地检测峰值, 因此必须在基于过零的峰值检测方法中应用各种滤波方法以简化PPG 波形。为了使用过零方法检测PPG 峰值, Canac 等人 (2019) 使用0.5 至10 Hz的4 阶巴特沃思滤波器和移动差分滤波器来检测脉动波峰, 而Kavsaoglu Moglu 等人 (2016) 对PPG 信号进行分段, 并将其除以每个斜率的符号。此外, 已经报道了一种用于在PPG 信号的小波变换或希尔伯特变换之后通过过零来检测峰值的方法 (Scholkmann 等人, 2012; Ferro 等人, 2015 年)。Ferro 等人 (2015) 以低复杂度和低计算成本检测脉搏波的起始和收缩峰;然而, 他们的研究仅在无噪声环境中用少量研究受试者 ($N = 10$) 进行了验证。Vadrevu 和Manikandan

(2018) 通过小波分解对PPG 分量进行分解, 然后检测收缩期和发作峰, 而不进行基于知识规则的后处理。该方法对取自三个PPG 数据库的116, 255 次搏动的总数显示出超过99 %的灵敏度和预测性;然而, 由于使用小波分解, 其具有相对较高的复杂性。此外, 由于它是为非因果系统设计的, 因此很难应用于实时应用。最常用的PPG 峰值检测方法之一是基于LCM 检测的方法。LCM 是一种基于预定义阈值在特定区域内找到最大值或最小值的方法。在LCM 峰值检测中, 通过重复的窗口滑动和峰值检测来检测峰值。检测阈值可以具有固定值或自适应值。Lu 等人 (2008) 在最大PPG 值的一定比例下确定阈值。Xu 等人 (2008) 通过比较2秒窗口内候选峰的高度, 基于脉冲高度和检测到的峰设置阈值。LCM 方法需要选择适当的窗口大小。它的缺点是, 如果由于气候变化而造成大规模的基线变化,

TABLE 2 | Summary of preprocessing methods for PPG.

Preprocessing method	Details	Purpose
Frequency filtering	<p>Bandpass filter</p> <ul style="list-style-type: none"> - 1st order Butterworth [(0.5 – 5) Hz] (Sukor et al., 2011) - 2nd order Butterworth [(0.2 – 10) Hz] (Liu et al., 2020b) - 3rd order Butterworth [(0.4 – 10) Hz] (Papini et al., 2018) - 4th order Butterworth [(0.5 – 50) Hz] (Pradhan et al., 2019) - 4th Chebychev I [(0.5 – 16) Hz] (Ferro et al., 2015) - 4th order Butterworth [(0.5 – 10) Hz] (Canac et al., 2019) - 64th order FIR [(0.1 – 10) Hz] (Selvaraj et al., 2011) - Discrete cosine transform filtering [(0.5 – 10) Hz] (Shin et al., 2010) <p>High pass filter</p> <ul style="list-style-type: none"> - 4th order Butterworth, cut-off: 0.01 Hz (Fischer et al., 2017) <p>Low pass filter</p> <ul style="list-style-type: none"> - 2nd order Butterworth, cut-off 10 Hz (Liu et al., 2020a) - 4th order Butterworth, cut-off 15 Hz (Fischer et al., 2017) 	Reduction for high-frequency noise, baseline movement reduction
Empirical mode decomposition	Waveform reconstruction using intrinsic mode functions whose dominant frequency is > 0.5 Hz (Lu et al., 2008)	Reduction for low-frequency (<0.5 Hz) noise and baseline noise reduction
Wavelet transform	Signal reconstruction using specific sub-bands after stationary wavelet transform (Vadrevu and Manikandan, 2018)	Suppression of background artifacts and noises
Independent component analysis	Reducing motion artifact using frequency domain independent component analysis based on red and infrared signal (Krishnan et al., 2008)	Motion artifacts reduction
Moving difference filter	Calculating the difference with the sample after a window size of a moving window (Canac et al., 2019)	Enhancing upslope of the photoplethysmogram
Curve fitting	<p>Amplitude normalization</p> <ul style="list-style-type: none"> - Amplitude compensation curve (Kim et al., 2019) - Detrending - 32nd-order polynomial fitting (Selvaraj et al., 2011) 	Eliminating non-stationary dynamics

respiration or other various causes, accurate detection becomes difficult. Shin et al. (2009) proposed an adaptive threshold PPG peak detection method based on a dynamic threshold that tracks the signal amplitude and finds peaks at the maximum amplitude outside the refractory period. Adaptive threshold is known to overcome the shortcoming of the LCM method that is vulnerable to baseline noise, such as baseline fluctuations due to respiration, with better detection performance than the LCM method for detecting the peaks of PPG signals. Scholkmann et al. (2012) proposed a method of estimating the local maxima by obtaining a scalogram of wavelet transformation and then rescaling it. In this method, the local maxima scalogram was first calculated and rescaled. Peaks were then detected by row-wise summation and column-wise standard deviation. The proposed method has high robustness against high-frequency and low-frequency noise, and has a potential to be used for detection of various signal peaks. Recently, there have been attempts to apply deep learning to PPG peak detection. Orjuela-Cañón et al. (2013) proposed a PPG peak detection method based on a self-organized map. Although the PPG peak detection method using machine learning has not yet been confirmed to have stable performance, performance improvement is expected in the future through continuous development. The PPG peak detection methods mentioned above

can detect peaks with high accuracy in PPG signals without noise. However, their PPG peak detection performance may be greatly degraded because of MAs, baseline wandering, and low perfusion. In addition, in the case of systolic peak, there is the possibility of erroneous detection due to interference of the dicrotic and diastolic peaks. Therefore, noise removal through proper signal pre-processing and restoration of distorted signals remains important for PPG utilization. **Table 3** briefly summarizes the PPG peak detection techniques.

Photoplethysmogram Waveform Reconstruction

Photoplethysmography (PPG) waveform reconstruction is mainly performed to restore the damage to PPG caused by noise, such as MAs. If distortion of PPG is not severe with preservation of the main components of the waveform, PPG can be decomposed into wavelet components through discrete wavelet transform, and noise can be removed for each component to restore PPG (Tang et al., 2016). In addition to the reconstruction method in the time–frequency domain using discrete wavelet transform, a method of reconstructing PPG using eigen-decomposition has also been proposed (Salehizadeh et al., 2014). In this method, after eigen-decomposition is performed to extract the eigen components of PPG, PPG is restored only

表2| PPG预处理方法总结。

预处理方法	细节	目的
频率过滤	带通滤波器 - 一阶巴特沃思[(0.5 - 5) Hz] (Sukor等人, (2011年) - 二阶巴特沃思[(0.2 - 10) Hz] (Liu等人, (2020年b) - 三阶巴特沃思[(0.4 - 10) Hz] (Papini等人, 2018年) - 四阶巴特沃思[(0.5 - 50) Hz] (Pradhan等人, 2019年度) - 第四Chebychev I [(0.5 - 16) Hz] (Ferro等人, (2015年) - 四阶巴特沃思[(0.5 - 10) Hz] (Canac等人, 2019年度) - 64阶FIR [(0.1 - 10) Hz] (Selvaraj等人, (2011年) - 离散余弦变换滤波[(0.5 - 10) Hz] (Shin等人, 2010) 高通滤波器 - 四阶巴特沃思, 截止: 0.01 Hz (Fischer等人, 2017) 低通滤波器 - 二阶巴特沃思, 截止频率10 Hz (Liu等人, (2020年a) - 四阶巴特沃思, 截止15 Hz (Fischer等人, (2017年))	复位术 高频噪声, 基线移动 减少
经验模态分解	使用主频> 0.5 Hz的固有模式函数进行波形重建 (Lu等人, (2008年))	复位术
小波变换	在平稳小波变换后使用特定子带进行信号重建 (Vadrevu 和Manikandan , 2018)	低频 (<0.5 Hz) 噪声和基线噪声 减少
独立组件分析	使用基于红色和红外信号的频域独立分量分析来减少运动伪影 (Krishnan等人, (2008年))	背景抑制 伪影和噪声 运动伪影减少
移动差分滤波器	在移动窗口的窗口大小之后计算与样本的差异 (Canac等人, 2019)	加强上坡的容积图
曲线拟合	幅度归一化 - 振幅补偿曲线 (Kim等人, 2019年度) 去趋势 - 32阶多项式拟合 (Selvaraj等人, (2011年))	消除非平稳动力学

呼吸或其他各种原因，准确检测变得困难。Shin 等人 (2009) 提出了一种基于动态阈值的自适应阈值PPG 峰值检测方法，该方法跟踪信号幅度并在不应期外的最大幅度处找到峰值。已知自适应阈值克服了LCM方法易受基线噪声（诸如由于呼吸引起的基线波动）影响的缺点，具有比用于检测PPG 信号的峰值的LCM方法更好的检测性能。Scholkemann et al. (2012) 提出了一种通过获得小波变换的尺度图然后对其进行尺度变换来估计局部极大值的方法。然后通过行求和和列标准差检测峰。该方法对高频和低频噪声具有很强的鲁棒性，可用于各种信号峰值的检测。最近，有人尝试将深度学习应用于PPG 峰值检测。Orjuela - Cañón 等人 (2013) 提出了一种基于自组织图的PPG 峰值检测方法。虽然使用机器学习的PPG 峰值检测方法尚未被确认具有稳定的性能，但通过不断开发，未来有望实现性能提升

上述PPG 峰值检测方法可以在没有噪声的情况下以高精度检测PPG 信号中的峰值。然而，由于MA、基线漂移和低灌注，它们的PPG 峰值检测性能可能大大降低。此外，在收缩峰的情况下，由于重搏峰和舒张峰的干扰，存在错误检测的可能性。因此，通过适当的信号预处理和失真信号的恢复来去除噪声对于PPG 利用仍然是重要的。表3简要总结了PPG 峰值检测技术。

光电容积图波形重建

光电容积描记 (PPG) 波形重建主要用于恢复由噪声（如MA）对PPG 造成的损害。如果PPG 的失真在保留波形的主要分量的情况下不严重，则PPG 可以通过离散小波变换被分解成小波分量，并且可以针对每个分量去除噪声以恢复PPG (Tang 等人, 2016 年)。除了使用离散小波变换的时频域中的重建方法之外，还提出了使用本征分解重建PPG 的方法 (Salehizadeh 等人, 2014 年)。在该方法中，在进行特征分解以提取PPG 的特征分量之后，仅恢复PPG

TABLE 3 | Overview of studies on peak detection of PPG.

Study	Subjects (age)	Recording time (minute)	Experimental condition (default is resting)	Device used	Sensor position	Peak type	Results
Canac et al., 2019	108 patients (30–64)	n.s.	Supine	Multi-Dop X (Compumedics DWL, Singen, Germany)	Head	Onset	Acc: 99.5%
Kavsaoglu et al., 2016	20 healthy adults (18–41)	1	Sitting	SDPPG_V2.0 (APMKorea, Daejeon, Korea)	n.s.	Systolic	Acc: 100%
Ferro et al., 2015	10 healthy adults (19.3 ± 1.4)	5	Supine	In-house device	n.s.	Onset, systolic	Acc: 95% (onset) Acc: 100% (systolic)
Vadrevu and Manikandan, 2018	20 healthy adults (18–35)	10–15	Sitting	In-house sensor	Finger	Onset, systolic	Acc: 99.3% (onset) Acc: 99.3% (systolic)
Lu et al., 2008	10 healthy adults (26 ± 7.5)	20	Upright, supine	MP506 (Medtronic, MN, United States)	n.s.	Onset	Obtaining pulse rate variability highly correlated with heart rate variability
Shin et al., 2009	18 healthy adults (17–30)	5	Supine (respiratory control), Sitting (spontaneous breathing)	PPG 100C (Biopac, CA, United States)	Finger	Onset, systolic	Acc: 98.9% (onset) Acc: 98.2% (systolic)
Scholkmann et al., 2012	n.s.	3.5	n.s.	Functional near-infrared spectroscopy MCP-II (n.s.)	Prefrontal cortex	Systolic	Acc: 100%
Orjuela-Cañón et al., 2013	7 healthy adults (19.3 ± 1.5)	5	Supine	n.s.	n.s.	Onset, systolic	Acc: 100% (onset, systolic)

Acc, accuracy; n.s., not specified.

with the main components from which the noise components are removed. When most of the waveform information is lost because of severe distortion of PPG, detecting the damaged part and estimating the waveform of the corresponding part to restore it using a machine learning technique, such as recurrent neural network, have been reported (Tarvirdizadeh et al., 2018; Roy et al., 2019). In addition to restoring distorted parts, reconstruction of the PPG waveform can be performed to enhance the waveform. To equalize PPG amplitude fluctuations when severe fluctuations in the PPG baseline or amplitude occur, Kim et al. (2019) proposed a method of compensating the PPG amplitude using an amplitude compensation curve generated from the envelope of the PPG waveform. **Figure 7** shows an example of PPG waveform reconstruction.

Signal Quality Index

Feature-Based Signal Quality Assessment

Signal quality index (SQI) is generally used to evaluate signal quality, such as signal-to-noise ratio. It is applied before signal analysis to evaluate the usability of a signal (see **Figure 8**). Pulse quality index refers to the quality of pulses constituting the signal,

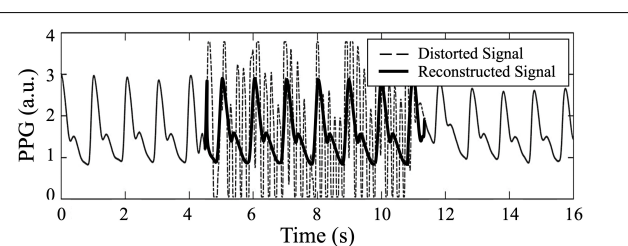


FIGURE 7 | Example of PPG waveform reconstruction. Dashed line is distorted PPG, while bold line is reconstructed PPG.

and is used to evaluate the quality of the pulse waveform as part of the SQI. Waveform quality is the most important factor in deriving accurate analysis results. A signal of low quality increases the false alarm, as well as probability of occurrence of an analysis error, which can lead to clinical misdiagnosis. For example, if part of the waveform is lost when calculating heart rate, an error may occur in peak detection, resulting in change in heart rate.

Such a case may also occur in a patient-monitoring device that monitors the physiological signals of a patient in real

表3| PPG峰值检测研究综述。

研究	受试者 (年龄)	记录 time (分钟)	实验 条件 (默认值为 休息)	被用于的设备	传感器 位置	峰型	成果
Canac 等人, 2019	108例 (30- 64)	n.s.	仰卧	Multi - Dop X (Compumedics DWL, Singen, 德国)	Head	发作	加速度: 99.5%
高加索人 吃吧2016	20名健康成人 (18- 41)	1	坐	SDPPG_V2.0 (APM Korea , 韩国大田)	n.s.	收缩	访问: 100%
Ferro 等人, 2015	10名健康成人 (19.3± 1.4)	5	仰卧	内部设备	n.s.	收缩压发作	加速度: 95% (发病) 访问: 100% (收缩压)
瓦德雷武和 马尼坎丹, 2018	20名健康成人 (18- 35)	10- 15	坐	内部传感器	手指	收缩压发作	访问: 99.3% (发病) 访问: 99.3% (SYSTELIC)
李 et al., 2008	10名健康成人 (26± 7.5)	20	直立、仰卧MP506	(Medtronic , 美国明尼苏达州)	n.s.	发作	获取脉冲 心率变异性 高度 相关 心率 变异性
Shin等人, 2009	18名健康成人 (17- 30)	5	仰卧 (呼吸 控制), 坐 (自发) 呼吸)	PPG 100 C (Biopac , 美国加利福尼亚州)	手指	收缩压发作	加速度: 98.9% (发病) 加速度: 98.2% (收缩压)
朔尔克曼 例如, 2012	n.s.	3.5	n.s.	功能 近红外 光谱 MCP- II (n.s.)	前额叶 皮层	收缩	访问: 100%
Orjuela - Canon 等, 2013	7名健康成人 (19.3± 1.5)	5	仰卧	n.s.	n.s.	收缩压发作	访问: 100% (发作, 收缩期)

Accc, 准确度; n.s., 未具体说明。

其中噪声分量被去除。当大多数波形信息由于PPG的严重失真而丢失时, 已经报道了检测受损部分并估计对应部分的波形以使用机器学习技术(诸如递归神经网络)来恢复它(Tarvirdizadeh 等人, 2018; Roy 等人, 2019年)。除了恢复失真部分之外, 还可以执行PPG波形的重建以增强波形。为了在PPG基线或振幅发生严重波动时均衡PPG振幅波动, Kim等人(2019)提出了一种使用根据PPG波形包络生成的振幅补偿曲线补偿PPG振幅的方法。图7示出了PPG波形重建的示例。

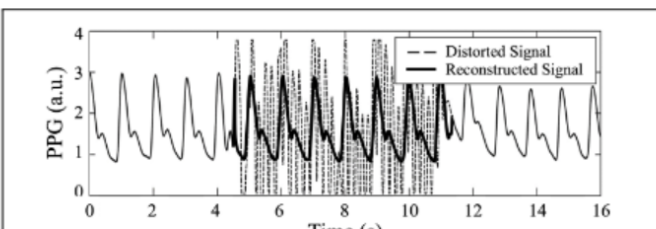


图7| PPG波形重建示例。虚线是失真PPG, 而粗线是重建PPG。

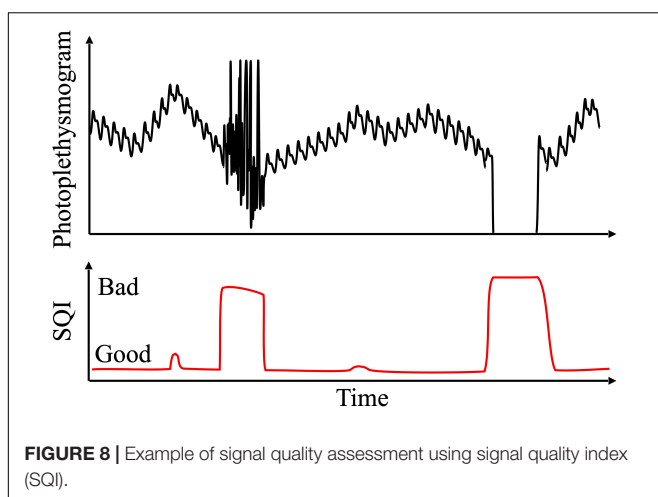
信号质量指数

基于频谱分析的信号质量评估

信号质量指数(SQI)通常用于评价信号质量, 如信噪比。它在信号分析之前应用, 以评估信号的可用性(见图8)。脉冲质量指数是指构成信号的脉冲的质量,

并且用于评估作为SQI的一部分的脉搏波形的质量。波形质量是获得准确分析结果的最重要因素。低质量的信号增加了假警报, 以及发生分析错误的可能性, 这可能导致临床误诊。例如, 如果在计算心率时波形的一部分丢失, 则在峰值检测中可能出现错误, 导致心率变化。

这种情况也可能发生在真实的监测患者的生理信号的患者监测设备中



time. Patient monitoring alerts medical staff when vital signs, such as HR, deteriorate. As in the previous case, false alarms may occur because of deterioration of waveform quality caused by movement or sensor attachment condition, although the condition of a patient is normal. These false alarms cause noise stress to medical staff and can interfere with their accurate and immediate response. In addition, because of recent increase in the use of PPG in the field of mobile healthcare, there is an increasing demand to improve its usability in the mobile environment. However, PPG is very vulnerable to MAs. It may suffer from signal quality degradation due to various factors, such as low perfusion or ambient light. Therefore, it is very important to distinguish between analyzable and non-analyzable sections of the measured PPG signals. To improve the accuracy of analysis results, SQI evaluation of PPG is becoming more important, especially in the mobile environment.

Table 4 summarizes previous studies on signal quality assessment. Among methods for evaluating SQI, the rule-based method can determine the availability of a signal by sequentially determining various parameter values, such as amplitude, beat interval, and feature value, describing the PPG waveform based on specific thresholds. Fischer et al. (2017) evaluated signal quality using thresholds for amplitude, rise time, pulse-to-pulse interval, number of diastolic peaks, and waveforms of a pulsation. Sukor et al. (2011) similarly proposed a method for evaluating SQI by applying a decision tree to amplitude, beat interval, waveform width, ensemble mean of all beats, and Euclidean distance; the quality of PPG was distinguished into three grades and was evaluated with an accuracy of $83 \pm 11\%$ and sensitivity of $89 \pm 10\%$ compared to the expert-labeled gold standard.

Orphanidou et al. (2014) evaluated the quality of PPG signal in two grades using heart rate, PPI interval and ratio, and template matching, resulting in sensitivity and specificity of more than 90%. Skewness and kurtosis are also frequently used features for signal quality evaluation. Krishnan et al. (2008) evaluated signal quality based on skewness and kurtosis. Selvaraj et al. (2011) evaluated signal quality in two grades through kurtosis and Shannon entropy. Elgendi (2016) classified PPG into three grades (excellent, acceptable, and unfit), and

compared the performance of SQI evaluation indices, such as perfusion index, kurtosis, skewness, relative power, non-stationarity, zero-crossing, and entropy. Kurtosis and skewness are statistical measures for quantifying the characteristics of a normal distribution. Morphologically, “How sharp is the shape?” and “In which direction and by how much is the shape skewed?” can be quantified. From this morphological point of view, the kurtosis and skewness of the PPG pulse can comprehensively reflect the amplitude or position of the PPG shape, such as pulse width, systolic peak, diastolic peak, and dicrotic notch. In addition, since the kurtosis or skewness of the PPG pulse can be clearly distinguished from motion noise, this can be an effective means of distinguishing the PPG waveform from noise. On the other hand, kurtosis and skewness may be inefficient to detect the distortion caused by amplitude or pulse width in an abnormal range, because they are determined by relative shape, not by absolute value. The ratio of AC component to DC component of PPG is called perfusion index (PI), and it has been used in several studies to evaluate signal quality (Hartmut Gehring et al., 2002; Cannesson et al., 2008a). PI is useful in detecting waveform degradation by low perfusion, because it is known to reflect vasomotor tone that may affect the pulsatile absorption component; moreover, it is a direct indicator of low perfusion by itself.

Song et al. (2019) proposed PQR as a method for evaluating signal quality through high-frequency noise effect (P), baseline effect (Q), and MA effect (R). In the PQR method, a PQI score called rSQI is calculated by adding each score of P, Q, and R, where P is the ratio before and after applying the low pass filter, Q is the ratio before and after applying the baseline removal filter, and R is calculated by the computation of extreme point dispersion. In a study that evaluates SQI based on a template, the template for a normal-quality waveform is generated and compared with the input waveform to evaluate the quality. Orphanidou et al. (2014) proposed a method for evaluating waveform quality using HR, RR interval range, ratio of the maximum RR interval to the minimum RR interval, and result of adaptive template matching for ensemble average waveform of the whole pulsatile waveform. Li and Clifford (2012) normalized the length between the template and each pulse signal by dynamic time warping when matching the template. In their study, the template was created by ensemble-averaging pulsation waves within the first 30 s. Papini et al. (2018) used a template created by applying dynamic time warping barycenter averaging to PPG measured for an hour in template-based signal quality evaluation. Unlike existing methods, this template generation method does not require an alignment process for ensemble averaging. Thus, it offers more robust performance. Karlen et al. (2012) proposed a technique to evaluate signal quality in the range of 0–100 by calculating the cross correlation between successive beats and inputting a normalized cross-correlation coefficient to a nonlinear scaling function; this algorithm showed reasonable performance, but because it is based on exponential operation, it requires high computing power. In addition to the SQI evaluation method based on shape characteristics or templates of PPG or rule-based, studies on the SQI evaluation of PPG using machine learning have been actively conducted in recent years.

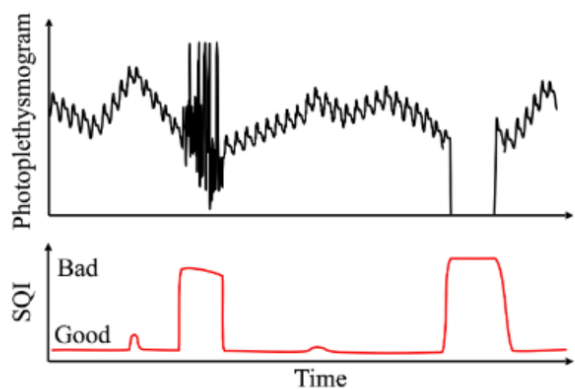


图8|使用信号质量指数（SQI）进行信号质量评估的示例。

时间当生命体征（如HR）恶化时，患者监测会提醒医务人员。如前所述，尽管患者的状况是正常的，但由于移动或传感器附接条件引起的波形质量劣化，可能会发生误报警。这些假警报会对医务人员造成噪音压力，并可能干扰他们准确和即时的反应。此外，由于PPG在移动的医疗保健领域中的使用的最近增加，因此存在对改善其在移动的环境中的可用性的增加的需求。然而，PPG非常容易受到MA的影响。由于各种因素，例如低灌注或环境光，它可能会遭受信号质量下降。因此，区分所测量的PPG信号的可分析部分和不可分析部分是非常重要的。为了提高分析结果的准确性，PPG的SQI评估变得越来越重要，特别是在移动的环境中。

表4总结了先前关于信号质量评估的研究。在用于评估SQI的方法中，基于规则的方法可以通过基于特定阈值顺序地确定描述PPG波形的各种参数值（诸如幅度、搏动间隔和特征值）来确定信号的可用性。Fischer等人（2017）使用振幅阈值、上升时间、脉搏间期、舒张峰数量和脉动波形评价了信号质量。Sukor等人（2011）类似地提出了一种通过将决策树应用于振幅、搏动间隔、波形宽度、所有搏动的总体平均值和欧几里得距离来评价SQI的方法；PPG质量被区分为三个等级，与专家标记的金标准相比，其准确度为 $83 \pm 11\%$ ，灵敏度为 $89 \pm 10\%$ 。

Orphanidou等人（2014）使用心率、PPI间期和比值以及模板匹配在两个等级中评价了PPG信号的质量，灵敏度和特异性均超过90%。偏度和峰度也是用于信号质量评估的常用特征。Krishnan等人（2008）基于偏度和峰度评估信号质量。Selvaraj等人（2011年）通过峰度和香农熵在两个等级中评估信号质量。

Elgendi（2016）将PPG分为3个等级（极好、可接受和不合格）

比较了灌注指数、峰度、偏度、相对功率、非平稳性、过零和熵等SQI评价指标的性能。峰度和偏度是用于量化正态分布特征的统计度量。从形态学上讲，“形状有多尖锐？”以及“形状向哪个方向倾斜以及倾斜了多少？”可以量化。从这一形态学角度看，PPG脉搏的峰度和偏度可以综合反映PPG形态的幅度或位置，如脉宽、收缩期峰值、舒张期峰值、重搏切迹等。另外，由于PPG脉冲的峰度或偏斜度能够与运动噪声清楚地区分开，因此这能够是区分PPG波形与噪声的有效手段。另一方面，峰度和偏度对于检测异常范围内由幅度或脉宽引起的失真可能是低效的，因为它们是由相对形状而不是绝对值确定的。PPG的AC分量与DC分量的比率被称为灌注指数（PI），并且其已经在若干研究中用于评估信号质量（Hartmut Gehring等人，2002；Cannesson等人，2008a）。PI可用于检测低灌注引起的波形退化，因为已知PI可反映可能影响脉动吸收成分的血管紧张度；此外，PI本身也是低灌注的直接指标。

Song等人（2019）提出PQR作为通过高频噪声效应（P）、基线效应（Q）和MA效应（R）评估信号质量的方法。在PQR方法中，通过将P、Q和R的每个分数相加来计算称为rSQI的PQI分数，其中P是应用低通滤波器之前和之后的比率，Q是应用基线去除滤波器之前和之后的比率，并且R通过极值点离散度的计算来计算。在基于模板评估SQI的研究中，生成正常质量波形的模板并与输入波形进行比较以评估质量。Orphanidou等人（2014）提出了一种使用HR、RR间期范围、最大RR间期与最小RR间期的比值以及整个脉动波形的总体平均波形的自适应模板匹配结果来评估波形质量的方法。Li和Clifford（2012）在匹配模板时通过动态时间扭曲来归一化模板与每个脉冲信号之间的长度。在他们的研究中，模板是通过在前30秒内对脉动波进行整体平均来创建的。Papini等人（2018）在基于模板的信号质量评价中使用了通过将动态时间规整重心平均值应用于测量一小时的PPG而创建的模板。与现有方法不同，该模板生成方法不需要用于系统平均的对准过程。因此，它提供了更强大的性能。Karlen等人（2012）提出了一种通过计算连续搏动之间的互相关并将归一化互相关系数输入到非线性缩放函数来评估0–100范围内的信号质量的技术；该算法表现出合理的性能，但由于它基于指数运算，因此需要高计算能力。除了基于PPG的形状特征或模板或基于规则的SQI评价方法之外，近年来还积极进行了使用机器学习的PPG的SQI评价的研究。

TABLE 4 | Overview of studies on PPG signal quality assessment.

Study	Number of subjects (age)	Recording time (minute)	Experimental condition (default is resting)	Device used	Sensor position	Classification grades	Results
Fischer et al., 2017	69 unspecified (>18)	30	n.s.	n.s.	n.s.	2	PPV: 98.6% Sen: 99.5% Acc: 98.4% Spe: 91.6% F1 score: 99.1%
Sukor et al., 2011	13 healthy adults (28 ± 4)	1	Sitting (movement)	n.s.	Finger	3	Sen: 89 ± 10% Acc: 83 ± 11% Spe: 77 ± 19%
Selvaraj et al., 2011	24 healthy adults (n.s.)	5–20	Supine (involuntary movement, 10 subjects), sitting (voluntary finger movement, 14 subjects)	MLT1020 (ADI Instruments, CO, United States), PPG 100 (Biopac, CA, United States)	Finger, ear, forehead	2	In involuntary movement, Acc: 99.0% (ear) Acc: 94.8% (finger) Acc: 93.3% (forehead) In voluntary movement (finger), Sen: 85.0% Spe: 99.4%
Elgendi, 2016	40 healthy adults (34.7 ± 6.6)	80 s	Exercise (movement)	Salus APG (Kashima Mediabind Co., Osaka, Japan)	Finger	3	F1 score Excellent: 86% Acceptable: 87.2% Unfit: 79.1%
Orphanidou et al., 2014	19 healthy adults (n.s.)	5	n.s.	EQ-02 Life Monitor (Hidalgo, Swavesey, United Kingdom), Wrist Ox2 3150 (Nonin Medical Inc., Plymouth, MN, United States)	Finger	2	Sen: 91% Spe: 95%
Li and Clifford, 2012	104 patients from MIMIC II database (n.s.)	n.s.	n.s.	n.s.	n.s.	3	Acc: 88.1% (training) Acc: 91.8% (testing)
Papini et al., 2018	16 healthy adults, 16 arrhythmia patients (n.s.)	Overnight or 24 h	Supine	n.s.	Finger	2	PPV: 97% (healthy) PPV: 95% (arrhythmia)
Karlen et al., 2012	Unspecified patients from Capnibase and Complex System Laboratory database (1–74)	2–8	n.s.	n.s.	n.s.	0–100	PPV: 99.2% Sen: 96.2%
Liu et al., 2020b	10 healthy adults (23.5 ± 1.7)	3	n.s.	CS2000 (medis, Ilmenau, Germany)	Neck (carotid artery)	3	In grade 'high', Sen: 81% Spe: 90% In grade 'low', Sen: 84% Spe: 93%
Liu et al., 2020a	14 healthy adults (22.7 ± 2.1)	3	n.s.	CS2000 (medis, Ilmenau, Germany)	Neck (carotid artery)	3	Acc: 89.5% (VGG-19) Acc: 92.5% (ResNet-50)
Naeini et al., 2019	n.s. (n.s.)	5 days	Ordinary life	E4 (Empatica, MA, United States), PulseOn (pulseon, Espoo, Finland)	Wrist	2	In grade 'unreliable', PPV: 76.74% Sen: 83.54% In grade 'reliable', PPV: 88.50% Sen: 83.33%
Pradhan et al., 2019	26 healthy adults (approx. 65)	24 h	Ordinary life	E4 (Empatica, MA, United States)	Wrist	5	Acc: 74.5%

PPV, positive predictive value; Sen, sensitivity; Acc, accuracy; Spe, specificity; n.s., not specified.

表4| PPG信号质量评估研究综述。

研究	数量 受试者 (年龄)	记录 时间 (分钟)	实验 条件 (默认值为 休息)	被用于的设备	传感器 位置	分类 成绩	成果
Fischer等人, 2017	69例未指明 (> 18)	30	n.s.	n.s.	n.s.	2	PV: 98.6% 阅读: 99.5% 加速度: 98.4% Spe: 91.6% F1评分: 99.1%
Sukor等人, 2011	13名健康成人 (28± 4)	1	坐 (动)	n.s.	手指	3	Sen: 89 ± 10% ACCC: 83 ± 11% Spe: 77 ± 19%
塞尔瓦拉, 给你 2011	24名健康成人 (未注明)	5–20	仰卧 (非自愿) movement运动, 10 受试者), 坐 (志愿者手指) movement运动, 14 科目)	MLT1020 (ADI 仪器, CO, 美国), PPG 100 (Biopac, CA, (美国)	手指耳朵, 额头	2	在非自愿的 运动, 累积: 99.0% (耳) 准确度: 94.8% (手指) 加速度: 93.3% (额头) 自愿 移动 (手指) , 森: 85.0% Spe: 99.4%
Elgendi, 2016	40名健康成人 (34.7± 6.6)	80 s	行使 (动)	Salus APG (鹿岛 Mediabind公司, 大坂, 日本) 的	手指	3	F1分数 优秀: 86% 可接受: 87.2% 不合格: 79.1%
孤儿 例如, 2014	19名健康成人 (未注明)	5	n.s.	EQ-02生命监测仪 (Hidalgo, Swavesey, 英国), 手腕 Ox2 3150 (Nonin 医疗公司, 普利茅斯, 美国明尼苏达州)	手指	2	森: 91% Spe: 95%
李和克利福德, 2012	104例患者 MIMIC II数据库 (未注明)	n.s.	n.s.	n.s.	n.s.	3	加速度: 88.1% (培训) 加速度: 91.8% (测试)
Papini等人, 2018	16个健康的成年人, 16例心律失常 患者 (n.s.)	过夜或 24 h	仰卧	n.s.	手指	2	PPV: 97% (健康) PPV: 95% (心律失常)
Karlen等人, 2012	未指明 患者 二氧化碳碱和 复杂系统 实验室 数据库 (1–74)	2–8	n.s.	n.s.	n.s.	0–100	PPV: 99.2% 森: 96.2%
Liu等人, 2020b	10名健康成人 (23.5± 1.7)	3	n.s.	CS2000 (medis, 伊尔梅瑙, 德国)	颈部 (颈动脉 动脉)	3	在“高”年级, Sen: 81% Spe: 90%在等级“低”, 森: 84% Spe: 93%
Liu等人, 2020a	14名健康成人 (22.7± 2.1)	3	n.s.	CS2000 (medis, 伊尔梅瑙, 德国)	颈部 (颈动脉 动脉)	3	加速度: 89.5% (VGG-19) 加速度: 92.5% (ResNet-50)
Naeini等人, 2019	N.S. (未注明)	5天	平凡生活	E4 (Empatica, MA, 美国), PulseOn (pulseon, 埃斯波, 芬兰)	手腕	2	年级 “不可靠”, PPV: 76.74% 森: 83.54% 在“可靠”一级, PPV: 88.50% 美分: 83.33%
Pradhan等人, 2019	26名健康成人 (约 (第六十五条)	24 h	平凡生活	E4 (Empatica, MA, 美国)	手腕	5	累积: 74.5%

PPV, 阳性预测值; Sen, 灵敏度; Acc, 准确度; Spe, 特异性; n.s., 未具体说明。

Machine Learning- and Deep Learning-Based Signal Quality Assessment

Liu et al. (2020b) evaluated PPG SQI using a five-layer fuzzy neural network. In their study, the quality of the signal was classified into three grades from the error of stroke volume measured with a commercial device. Stroke volume was calculated from PPG, and SQI evaluation performance was evaluated by inputting parameters extracted from PPG to the developed model. As a result, sensitivity of 0.81 and specificity 0.9 were shown for high-quality PPG, while sensitivity of 0.84 and specificity of 0.93 were shown for low-quality PPG. In another study by Liu et al. (2020a), PPG and derivative PPG were segmented for each beat and merged into a two-dimensional image to be used as input, and a machine learning model, a deep convolutional neural network (DCNN), VGG-19, or a residual DCNN (ResNet-50) was used to classify PPG segments into three grades of high, middle, and low. As a result, the study showed that the machine learning method using two-dimensional (2D) residual DCNN (ResNet-50) could more accurately evaluate signal quality than the method using general DCNN. Naeini et al. (2019) introduced a CNN-based method to evaluate the quality of PPG in an Internet-of-things-based health monitoring system. Their study performed binary classification of “reliable or unreliable” for PPG quality using an entire 60-s PPG signal as a CNN input, not extracted features, showing a precision of 0.89, and a recall of 0.83. Pradhan et al. (2019) conducted a study comparing the performance of five machine learning classifiers (k-nearest neighbor, multi-class support vector machine, naive Bayes, decision tree, and random forest) to evaluate the SQI of PPG using a wrist-wearable device. In their study, PPG quality was classified into five grades; it was found that the random forest SQI evaluation algorithm had the highest classification accuracy, with an accuracy of 74.5%. In a recent study, Guo et al. (2021) detected wearable PPG artifacts with a DICE score of 0.87–0.91 through a combination of active-contour-based loss and an adapted U-Net architecture; compared to the existing general research methods, this method shows superior performance. However, to sufficiently verify the performance of the deep-learning model, verification using more abundant data is required.

DISCUSSION

As seen in previous studies, most PPG pre-processing techniques rely on frequency domain filtering, which is effective in removing noise in a range that does not overlap with the core frequency of PPG. However, frequency domain filtering has limitations in handling non-stationary noise, making it possible to predict limitations that existing popular pre-processing technologies face when presuming increase in the use of PPG in future mobile environment. In the mobile environment, various types of non-stationary noise representing MAs can be introduced. This is expected to provide a completely different experience from measurement in an existing well-controlled environment. EMD or wavelet-based pre-processing technology can be a good alternative for dealing with frequency noise that does not overlap

with the frequency component of PPG or non-stationary signals. However, it is also difficult to cope with severe distortion of the signal, such as saturation due to MAs and poor contact. Therefore, an innovative countermeasure against severe signal distortion and non-stationary dynamics is needed in the future by pursuing PPG pre-processing.

In relation to heartbeat, since PPG has a relatively simple waveform, the complexity of the pulsatile feature detection algorithm is relatively low for PPG signals compared to other physiological signals. The pulsatile feature point detection accuracy PPG may depend on the pre-processing algorithm with superior noise removal or waveform recovery performance rather than a pulsatile feature point detection algorithm. On the other hand, while the use of PPG intrapulse waveform feature continues to increase, there is no clearly verified detection algorithm. Nor is related research active. From this point of view, future PPG feature detection can be performed by focusing on an intrapulse feature detection algorithm related to differential pulse waves or dicrotic features rather than an algorithm that detects pulsatile features such as pulse onset and systolic peak.

Spatiotemporal features of PPG have already been analyzed in great detail for all inflection points of the waveform (Charlton et al., 2018; Yang et al., 2018; Mousavi et al., 2019). Therefore, rather than finding completely new morphological features from the PPG waveform, it may be more effective to find the clinical significance of existing features or discover a combination feature. However, as features become more sophisticated, more effort is required to detect a feature that might increase false detection rate. Therefore, when discovering and selecting features, it is important to keep in mind that the minimum number of features should always be used to obtain maximum effect. From this point of view, a machine learning-based analysis method that can estimate a specific result by inputting a raw signal without a special feature extraction process can have the potential for a new breakthrough for research on a PPG feature with increasing complexity.

For the representative noise of PPG, such as MAs, baseline wandering, and low perfusion, it has been reported that the baseline wandering noise of PPG can be effectively reduced with improved PPG detection performance through a relatively simple and easy-to-implement algorithm, such as a frequency filter or interpolation method. In addition, there have been attempts to decrease noise caused by low perfusion through hardware improvement, as well as software methods, such as adaptive filtering. However, a method that can completely remove the distortion of PPG waveform due to low perfusion remains unknown. Therefore, further research is needed to improve PPG distortion due to low perfusion. An approach from the viewpoint of noise removal technology and waveform reconstruction can be considered. MA as the most important topic of PPG signal processing can lead to the complete loss of PPG. Due to increased PPG measurement in a mobile environment, most in-depth research has been conducted for MA, compared to other noise factors. Despite various sophisticated algorithms that have been proposed for reducing MAs, a standard method for removing motion noise has yet to be introduced. Reviewing published studies on the removal of MAs revealed that an ICA method

基于机器学习和深度学习的信号质量评估

Liu等人 (2020 b) 使用五层模糊神经网络评价PPG SQI。在他们的研究中, 信号的质量被分为三个等级, 从商业设备测量的每搏输出量的误差。从PPG计算每搏输出量, 并通过将从PPG提取的参数输入到开发的模型来评价SQI评价性能。结果, 高质量PPG的灵敏度为0.81, 特异性为0.9, 而低质量PPG的灵敏度为0.84, 特异性为0.93。在Liu等人 (2020 a) 的另一项研究中, PPG和衍生PPG针对每个搏动进行分割, 并合并到二维图像中用作输入, 并使用机器学习模型、深度卷积神经网络 (DCNN)、VGG-19或残差DCNN (ResNet-50) 将PPG分段分为高、中、低三个等级。因此, 研究表明, 使用二维 (2D) 残差DCNN (ResNet-50) 的机器学习方法可以比使用一般DCNN的方法更准确地评估信号质量。Naeini等人

(2019) 介绍了一种基于CNN的方法, 用于评估基于物联网的健康监测系统中PPG的质量。他们的研究使用整个60秒PPG信号作为CNN输入, 对PPG质量进行了“可靠或不可靠”的二进制分类, 未提取特征, 显示精度为0.89, 召回率为0.83。Pradhan等人 (2019) 进行了一项研究, 比较了五种机器学习分类器 (k -最近邻、多类支持向量机、朴素贝叶斯、决策树和随机森林) 的性能, 以使用腕戴式设备评价PPG的SQI。在他们的研究中, PPG质量被分为五个等级;发现随机森林SQI评估算法的分类准确率最高, 准确率为74.5个百分点。在最近的一项研究中, Guo等人 (2021) 通过结合基于活动轮廓的损失和自适应U-Net架构检测可穿戴PPG伪影, DICE评分为0.87–0.91;与现有的一般研究方法相比, 该方法显示出上级性能。然而, 为了充分验证深度学习模型的性能, 需要使用更丰富的数据进行验证。

EMD或基于小波的预处理技术可以是用于处理与PPG或非平稳信号的频率分量不重叠的频率噪声的良好替代方案。然而, 它也很难科普严重的信号失真, 如饱和由于MA和接触不良。因此, 未来需要通过追求PPG预处理来对抗严重信号失真和非平稳动态的创新对策。

关于心跳, 由于PPG具有相对简单的波形, 因此与其他生理信号相比, PPG信号的脉动特征检测算法的复杂度相对较低。脉动特征点检测准确度PPG可以取决于具有上级噪声去除或波形恢复性能的预处理算法, 而不是脉动特征点检测算法。另一方面, 虽然PPG脉内波形特征的使用持续增加, 但没有明确验证的检测算法。相关研究也不活跃。从这个角度来看, 未来的PPG特征检测可以通过关注与差分脉搏波或重搏特征相关的脉搏内特征检测算法而不是检测诸如脉搏开始和收缩峰值的脉动特征的算法来执行。

已经针对波形的所有拐点非常详细地分析了PPG的时空特征 (查尔顿等人, 2018年; Yang等人, 2018; Mousavi等人, 2019年)。因此, 与其从PPG波形中找到全新的形态学特征, 不如找到现有特征的临床意义或发现组合特征可能更有效。然而, 随着特征变得越来越复杂, 需要更多的努力来检测可能增加误检率的特征。因此, 在发现和选择特征时, 重要的是要记住, 应始终使用最少数量的特征以获得最大效果。从这一点来看, 基于机器学习的分析方法可以通过输入原始信号来估计特定结果, 而无需特殊的特征提取过程, 这可能会为复杂性增加的PPG特征的研究带来新的突破。

对于PPG的代表性噪声, 例如MA、基线漂移和低灌注, 已经报道了通过相对简单且易于实现的算法, 例如频率滤波器或插值方法, 可以有效地降低PPG的基线漂移噪声, 同时提高PPG检测性能。此外, 已经尝试通过硬件改进以及软件方法 (诸如自适应滤波) 来减少由低灌注引起的噪声。然而, 能够完全消除由于低灌注引起的PPG波形失真的方法仍然未知。因此, 需要进一步的研究来改善由于低灌注引起的PPG失真。可以考虑从噪声去除技术和波形重构的观点来看的方法。MA作为PPG信号处理中最重要的课题, 可能导致PPG的完全丢失。由于在移动的环境中增加的PPG测量, 与其他噪声因素相比, 已经针对MA进行了最深入的研究。尽管已经提出了各种复杂的算法来减少MA, 但是还没有引入用于去除运动噪声的标准方法。回顾已发表的关于去除MA的研究, 发现伊卡方法

讨论

如在先前的研究中所见, 大多数PPG预处理技术依赖于频域滤波, 其在去除与PPG的核心频率不重叠的范围中的噪声方面是有效的。然而, 频域滤波在处理非平稳噪声方面具有局限性, 使得能够预测现有流行的预处理技术在假定未来移动的环境中PPG的使用增加时所面临的局限性。在移动的环境中, 可以引入表示MA的各种类型的非平稳噪声。预计这将提供与现有良好控制环境中的测量完全不同的体验

(Kim and Yoo, 2006), an acceleration sensor-based (Gibbs and Asada, 2005), and an adaptive filtering method using a Kalman filter (Seyedtabaii and Seyedtabaii, 2008) could be used. In the case of removing motion noise through simple frequency domain filtering using a high-pass filter, motion noise cannot be removed sensitively according to the intensity or type of motion. The ICA method and the adaptive filtering method can relatively improve the performance of motion noise removal. However, when the degree of motion noise is severe, they cannot be applied; for example, when the signal is saturated and completely lost because of motion. In such a case, a method of dividing the measured PPG into sections in which a signal exists, and a section in which the signal is lost, and analyzing selectively according to the classified section, has been proposed. In this method, the section in which motion noise can be removed is analyzed by applying motion noise removal technology, while the section in which motion noise could not be removed is excluded from analysis. Recently, research studies on SQI as an index for evaluating signal quality to distinguish between an analyzable section and an unanalyzable section have significantly increased. By evaluating the quality of a signal using SQI, false alarms in a patient monitoring device can be prevented, and the accuracy of clinical analysis can be improved by excluding error sections when interpreting signals. SQI is expected to be used in parallel with signal processing technology in the pre-processing stage. As mobile healthcare or wearable technology develops, its utilization will increase further. Machine learning technology is being applied in all areas of PPG signal processing, such as noise reduction, feature detection, and result analysis.

Machine learning in physiological analysis can omit complex and high error probability processing stages, such as feature detection, and derive results through end-to-end learning. This is expected to improve accuracy in analysis. For example, if a machine learning technique is applied, heart rate may be derived from the PPG signal itself, without other procedures, such as frequency domain transform, and peak detection or peak detection and feature detection can be excluded when deriving analytical results, such as SQI. In addition, since machine learning can be used to remove noise or generate new waveforms, its application to PPG processing is expected to increase in the future. Although machine learning is a promising method for analyzing PPG signals to be used in various applications, it is necessary to secure a highly relevant large data set and develop specialized models for each subdivided application. In particular, attempts to find meaningful information from PPG using various deep learning models are continuously increasing. Representative applications of PPG analysis using deep learning include heart rate estimation (Biswas et al., 2019;

Reiss et al., 2019; Panwar et al., 2020; Chang et al., 2021; Mehrgardt et al., 2021), cuff-less blood pressure estimation (Panwar et al., 2020; El-Hajj and Kyriacou, 2021a,b; Schrumpf et al., 2021a,b; Tazarv and Levorato, 2021), and arterial fibrillation prediction (Poh et al., 2018; Kwon et al., 2019; Aschbacher et al., 2020; Cheng et al., 2020; Pereira et al., 2020). In addition, PPG-based deep learning models are being used for respiratory rate estimation (Ravichandran et al., 2019), sleep monitoring (Korkalainen et al., 2020), diabetes (Avram et al., 2019), vascular aging estimation (Dall'Olio et al., 2020), and peripheral arterial disease classification (Allen et al., 2021). In addition, to explain the causal relationship between input data and output results, an in-depth approach using technologies such as explainable AI, which has been recently studied, needs to be conducted. With respect to bio-signals, although explainable AI has been mainly applied to ECG (Sanjana et al., 2020; Ganeshkumar et al., 2021; Jo et al., 2021; Maweu et al., 2021; Raza et al., 2021; Taniguchi et al., 2021), it is difficult to find a clear application case for medical purposes in PPG. Although it is difficult to say that the application of explainable AI to PPG has been generalized yet, it seems clear that explainable AI will be introduced into PPG analysis given the tendency for the development of machine learning to be introduced into other fields. Machine learning is currently being continuously researched and developed. Finding and utilizing recent techniques and new methods, including explainable AI, will help in the analysis of PPG signals.

AUTHOR CONTRIBUTIONS

HSh contributed to the conception and design of the manuscript, and drafting, writing, and critical review of the final document. JP, HSe, and S-SK contributed to the literature search, data collection and analysis, drafting and writing, and figure design and drawing. All authors contributed to the article and approved the submitted version.

FUNDING

This research was supported by the Basic Science Research Program through the National Research Foundation of Korea (NRF), funded by the Ministry of Education (NRF-2018R1D1A3B07046442), Republic of Korea, and supported by the Korea Health Technology R&D Project through the Korea Health Industry Development Institute (KHIDI), funded by the Ministry of Health and Welfare, South Korea, (HI21C0011).

REFERENCES

- Adler, J. N., Hughes, L. A., Vtvilecchia, R., and Camargo, A. C. Jr. (1998). Effect of skin pigmentation on pulse oximetry accuracy in the emergency department. *Acad. Emergency Med.* 5, 965–970. doi: 10.1111/j.1553-2712.1998.tb02772.x
- Ahonen, J., Jokela, R., Uutela, K., and Huiku, M. (2007). Surgical stress index reflects surgical stress in gynaecological laparoscopic day-case surgery. *Br. J. Anaesthesia* 98, 456–461. doi: 10.1093/bja/aem035
- Aiba, Y., Ohshima, S., Horiguchi, S. I., Morioka, I., Miyashita, K., Kiyota, I., et al. (1999). Peripheral hemodynamics evaluated by acceleration plethysmography in workers exposed to lead. *Industrial Health* 37, 3–8. doi: 10.2486/indhealth.37.3
- Alian, A. A., and Shelley, K. H. (2014). Photoplethysmography. *Best Pract. Res. Clin. Anaesthesiol.* 28, 395–406.
- Allen, J. (2007). Photoplethysmography and its application in clinical physiological measurement. *Physiol. Meas.* 28:R1. doi: 10.1088/0967-3334/28/3/R01

(Kim和Yoo, 2006)、基于加速度传感器的方法 (Gibbs和Asada, 2005) 以及使用卡尔曼滤波器的自适应滤波方法 (Seyedtabaii和Seyedtabaii, 2008)。在通过使用高通滤波器的简单频域滤波来去除运动噪声的情况下, 不能根据运动的强度或类型灵敏地去除运动噪声。伊卡方法和自适应滤波方法可以相对提高运动噪声去除的性能。然而, 当运动噪声的程度严重时, 它们不能被应用;例如, 当信号饱和并且由于运动而完全丢失时。在这种情况下, 已经提出了将测量的PPG划分为信号存在的部分和信号丢失的部分, 并且根据分类的部分选择性地进行分析的方法。该方法利用运动噪声去除技术对能够去除运动噪声的部分进行分析, 而对不能去除运动噪声的部分则不进行分析。近来, 关于SQI作为用于评估信号质量以区分可分析部分和不可分析部分的指标的研究已经显著增加。通过使用SQI评估信号的质量, 可以防止患者监测装置中的误报警, 并且可以通过在解释信号时排除错误部分来提高临床分析的准确性。SQI预计将与信号处理技术在预处理阶段并行使用。随着移动的医疗保健或可穿戴技术的发展, 其利用率将进一步增加。机器学习技术正被应用于PPG信号处理的所有领域, 如降噪、特征检测和结果分析。

生理分析中的机器学习可以省略复杂和高错误概率的处理阶段, 例如特征检测, 并通过端到端学习获得结果。预计这将提高分析的准确性。例如, 如果应用机器学习技术, 则可以从PPG信号本身导出心率, 而不需要其他过程, 诸如频域变换, 并且当导出分析结果(诸如SQI)时, 可以排除峰值检测或峰值检测和特征检测。此外, 由于机器学习可用于去除噪声或生成新波形, 因此预计未来其在PPG处理中的应用将增加。虽然机器学习是一种很有前途的分析PPG信号的方法, 可用于各种应用, 但有必要确保高度相关的大型数据集, 并为每个细分应用开发专门的模型。特别是, 使用各种深度学习模型从PPG中找到有意义信息的尝试正在不断增加。使用深度学习的PPG分析的代表性应用包括心率估计 (Biswas et al.

2019; Reiss等人, 2019; Panwar等人, 2020; Chang等人, 2021; Mehrgardt等人, 2021)、无袖带血压估计 (Panwar等人, 2020; El-Hajj和Kyriacou, 2021 a, B; Schrumpf等人, 2021 a, B; Tazarv和Levorato, 2021) 和动脉纤维性颤动预测 (Poh等人, 2018; Kwon等人, 2019; Aschbacher等人, 2020年; Cheng等人, 2020; 佩雷拉等人, 2020年)。此外, 基于PPG的深度学习模型正在用于呼吸率估计 (Ravichandran等人, 2019), 睡眠监测 (Korkalainen等人, 2020)、糖尿病 (Avram等人, 2019)、血管老化估计 (Dall'Olio等人, 2020) 和外周动脉疾病分类 (艾伦等人, 2021年)。此外, 为了解释输入数据和输出结果之间的因果关系, 需要使用最近研究的可解释AI等技术进行深入研究。关于生物信号, 尽管可解释的AI主要应用于ECG (Sanjana et al., 2020; Ganeshkumar等人, 2021; Jo等人, 2021; Maweu等人, 2021; Raza等人, 2021; Taniguchi等人, 2021), 很难在PPG中找到明确的医疗用途应用案例。虽然很难说可解释AI在PPG中的应用已经推广, 但考虑到机器学习的发展趋势将被引入其他领域, 似乎很明显, 可解释AI将被引入PPG分析。机器学习目前正在不断研究和开发。发现和利用最新的技术和新方法, 包括可解释的人工智能, 将有助于分析PPG信号。

作者贡献

HSh对手稿的概念和设计以及最终文件的起草、撰写和批判性审查做出了贡献。JP、HSe和S-SK参与了文献检索、数据收集和分析、起草和撰写以及图形设计和绘制。所有作者均对文章做出了贡献, 并批准了提交的版本。

资金

本研究由韩国教育部资助的韩国国家研究基金会 (NRF) 的基础科学计划提供支持 (NRF 2018 R1 D1 A3 B 07046442), 大韩民国, 并通过韩国健康产业发展研究所 (KHIDI) 得到韩国健康技术研发项目的支持, 由韩国卫生福利部资助, (HI21C0011)。

引用

- Adler, J. N., 休斯湖一、Vtvileccchia河, 和Camargo, A. C. Jr. (1998年)。急诊科皮肤色素沉着对脉搏血氧测定准确性的影响。
Acad.急诊医学5, 965–970。doi: 10.1111/j.1553-2712.1998.tb02772.x
Ahonen, J., 约凯拉河, Uutela, K., 和Huiku, M. (2007年)。手术应激指数反映妇科腹腔镜日间手术患者的手术应激。Br. J. Anaesthesia麻醉98, 456–461。doi: 10.1093/bja/aem035

- Aiba, Y., Ohshima, S., Horiguchi, S.一、盛冈岛Miyashita, K., 清田岛等人 (1999年)。加速度体积描记法评价铅作业工人外周血流动力学。工业健康37, 3–8。doi: 10.2486/indhealth.37.3
Alian, A.一、和Shelley, K. H. (2014年)。光电体积描记法。最佳实践研究临床麻醉剂。28, 395–406.
艾伦, J. (2007年)。光电容积描记法及其在临床生理测量中的应用。生理学测量28: R1。doi: 10.1088/0967-3334/28/3/R01

- Allen, J., Liu, H., Iqbal, S., Zheng, D., and Stansby, G. (2021). Deep learning-based photoplethysmography classification for peripheral arterial disease detection: a proof-of-concept study. *Physiol. Meas.* 42:054002. doi: 10.1088/1361-6579/abf9f3
- Allen, J., and Murray, A. (1993). Development of a neural network screening aid for diagnosing lower limb peripheral vascular disease from photoelectric plethysmography pulse waveforms. *Physiol. Meas.* 14:13. doi: 10.1088/0967-3334/14/1/003
- Allen, J., and Murray, A. (2000a). Similarity in bilateral photoplethysmographic peripheral pulse wave characteristics at the ears, thumbs and toes. *Physiol. Meas.* 21:369. doi: 10.1088/0967-3334/21/3/303
- Allen, J., and Murray, A. (2000b). Variability of photoplethysmography peripheral pulse measurements at the ears, thumbs and toes. *IEEE Proc.-Sci. Meas. Technol.* 147, 403–407.
- Allen, J., and Murray, A. (2002). Age-related changes in peripheral pulse timing characteristics at the ears, fingers and toes. *J. Hum. Hypertens.* 16, 711–717. doi: 10.1038/sj.jhh.1001478
- Allen, J., and Murray, A. (2004). “Effects of filtering on multisite photoplethysmography pulse waveform characteristics,” in *Proceeding of the Computers in Cardiology, 2004*, (IEEE), 485–488.
- Alnæb, M. E., Alobaid, N., Seifalian, A. M., Mikhailidis, D. P., and Hamilton, G. (2007). Optical techniques in the assessment of peripheral arterial disease. *Curr. Vasc. Pharmacol.* 5, 53–59. doi: 10.2174/157016107779317242
- Alty, S. R., Angarita-Jaimes, N., Millasseau, S. C., and Chowienczyk, P. J. (2007). Predicting arterial stiffness from the digital volume pulse waveform. *IEEE Trans. Biomed. Eng.* 54, 2268–2275. doi: 10.1109/tbme.2007.897805
- Asada, H. H., Shaltis, P., Reisner, A., Rhee, S., and Hutchinson, R. C. (2003). Mobile monitoring with wearable photoplethysmographic biosensors. *IEEE Eng. Med. Biol. Magazine* 22, 28–40. doi: 10.1109/memb.2003.1213624
- Aschbacher, K., Yilmaz, D., Kerem, Y., Crawford, S., Benaron, D., Liu, J., et al. (2020). Atrial fibrillation detection from raw photoplethysmography waveforms: a deep learning application. *Heart Rhythm O2* 1, 3–9. doi: 10.1016/j.hroo.2020.02.002
- Avram, R., Tison, G., Kuhar, P., Marcus, G., Pletcher, M., Olgin, J. E., et al. (2019). Predicting diabetes from photoplethysmography using deep learning. *J. Am. Coll. Cardiol.* 73, 16–16. doi: 10.3349/jmc.2022.63.S93
- Awad, A. A., Haddadin, A. S., Tantawy, H., Badr, T. M., Stout, R. G., Silverman, D. G., et al. (2007). The relationship between the photoplethysmographic waveform and systemic vascular resistance. *J. Clin. Monit. Comput.* 21, 365–372. doi: 10.1007/s10877-007-9097-5
- Ayata, D., Yaslan, Y., and Kamasak, M. E. (2018). Emotion based music recommendation system using wearable physiological sensors. *IEEE Trans. Consumer Electron.* 64, 196–203. doi: 10.1109/tce.2018.2844736
- Baek, H. J., Kim, J. S., Kim, Y. S., Lee, H. B., and Park, K. S. (2007). “Second derivative of photoplethysmography for estimating vascular aging,” in *Proceeding of the 6th International Special Topic Conference on Information Technology Applications in Biomedicine*, (IEEE), 70–72. doi: 10.1371/journal.pone.0135659
- Baek, H. J., Kim, K. K., Kim, J. S., Lee, B., and Park, K. S. (2009). Enhancing the estimation of blood pressure using pulse arrival time and two confounding factors. *Physiol. Meas.* 31:145. doi: 10.1088/0967-3334/31/2/002
- Baghia, S., and Shaw, L. (2011). A real time analysis of PPG signal for measurement of SpO₂ and pulse rate. *Int. J. Comput. Appl.* 36, 45–50.
- Baker, W. B., Parthasarathy, A. B., Busch, D. R., Mesquita, R. C., Greenberg, J. H., and Yodh, A. (2014). Modified Beer-Lambert law for blood flow. *Biomed. Optics Express* 5, 4053–4075. doi: 10.1364/BOE.5.004053
- Barnes, R. W., Clayton, J. M., Bone, G. E., Slaymaker, E. E., and Reinertson, J. (1977). Supraorbital photoplethysmography. Simple, accurate screening for carotid occlusive disease. *J. Surgical Res.* 22, 319–327. doi: 10.1016/0022-4804(77)90150-0
- Beer, A. (1851). Versuch der absorptions-verhältnisse des cordierites für rothes licht zu bestimmen. *Ann. Physik Chem.* 84, 37–52. doi: 10.1002/andp.18511600904
- Behar, J., Roebuck, A., Shahid, M., Daly, J., Hallack, A., Palmius, N., et al. (2014). SleepAp: an automated obstructive sleep apnoea screening application for smartphones. *IEEE J. Biomed. Health Inform.* 19, 325–331. doi: 10.1109/JBHI.2014.2307913
- Bentham, M., Stansby, G., and Allen, J. (2018). Innovative multi-site photoplethysmography analysis for quantifying pulse amplitude and timing variability characteristics in peripheral arterial disease. *Diseases* 6:81. doi: 10.3390/diseases6030081
- Biswas, D., Everson, L., Liu, M., Panwar, M., Verhoef, B.-E., Patki, S., et al. (2019). CorNET: deep learning framework for PPG-based heart rate estimation and biometric identification in ambulant environment. *IEEE Trans. Biomed. Circuits Syst.* 13, 282–291. doi: 10.1109/TBCAS.2019.2892297
- Bohusch, T., Miller, T., Kreamer, W., Eisenhardt, J. R., and Foehl, H. C. (1994). Correlation of photoplethysmography, doppler velocimetry, digital blood pressure and skin temperature in the hand under conditions of warming. *Cardiopulmonary Phys. Ther.* 5, 15–18.
- Bortolotto, L. A., Blacher, J., Kondo, T., Takazawa, K., and Safar, M. E. (2000). Assessment of vascular aging and atherosclerosis in hypertensive subjects: second derivative of photoplethysmogram versus pulse wave velocity. *Am. J. Hypertens.* 13, 165–171. doi: 10.1016/s0895-7061(99)00192-2
- Brillante, D. G., O’sullivan, A. J., and Howes, L. G. (2008). Arterial stiffness indices in healthy volunteers using non-invasive digital photoplethysmography. *Blood Pressure* 17, 116–123. doi: 10.1080/08037050802059225
- Canac, N., Ranjbaran, M., O’Brien, M. J., Asgari, S., Scalzo, F., Thorpe, S. G., et al. (2019). Algorithm for reliable detection of pulse onsets in cerebral blood flow velocity signals. *Front. Neurol.* 10:1072. doi: 10.3389/fneur.2019.01072
- Cannesson, M., Besnard, C., Durand, P. G., Bohé, J., and Jacques, D. (2005). Relation between respiratory variations in pulse oximetry plethysmographic waveform amplitude and arterial pulse pressure in ventilated patients. *Crit. Care* 9:R562. doi: 10.1186/cc3799
- Cannesson, M., Desebbe, O., Rosamel, P., Delannoy, B., Robin, J., Bastien, O., et al. (2008b). Pleth variability index to monitor the respiratory variations in the pulse oximeter plethysmographic waveform amplitude and predict fluid responsiveness in the operating theatre. *Br. J. Anaesthesia* 101, 200–206. doi: 10.1093/bja/aen133
- Cannesson, M., Delannoy, B., Morand, A., Rosamel, P., Attof, Y., Bastien, O., et al. (2008a). Does the pleth variability index indicate the respiratory-induced variation in the plethysmogram and arterial pressure waveforms? *Anesthesia Analgesia* 106, 1189–1194. doi: 10.1213/ane.0b013e318167ab1f
- Challoner, A. (1979). Photoelectric plethysmography for estimating cutaneous blood flow. *Non-Invasive Physiol. Meas.* 1, 125–151.
- Chang, X., Li, G., Xing, G., Zhu, K., and Tu, L. (2021). DeepHeart: a deep learning approach for accurate heart rate estimation from PPG signals. *ACM Trans. Sensor Netw. (TOSN)* 17, 1–18.
- Charlton, P. H., Celka, P., Farukh, B., Chowienczyk, P., and Alastrauey, J. (2018). Assessing mental stress from the photoplethysmogram: a numerical study. *Physiol. Meas.* 39:054001. doi: 10.1088/1361-6579/aafe6a
- Chen, W., Kobayashi, T., Ichikawa, S., Takeuchi, Y., and Togawa, T. (2000). Continuous estimation of systolic blood pressure using the pulse arrival time and intermittent calibration. *Med. Biol. Eng. Comput.* 38, 569–574. doi: 10.1007/BF02345755
- Cheng, P., Chen, Z., Li, Q., Gong, Q., Zhu, J., and Liang, Y. (2020). Atrial fibrillation identification with PPG signals using a combination of time-frequency analysis and deep learning. *IEEE Access* 8, 172692–172706.
- Choi, B., Park, C., Lee, Y., Shin, H., Lee, S., Jeong, S., et al. (2018). Development of a new analgesic index using nasal photoplethysmography. *Anaesthesia* 73, 1123–1130. doi: 10.1111/anae.14327
- Choi, J., Ahmed, B., and Gutierrez-Osuna, R. (2011). Development and evaluation of an ambulatory stress monitor based on wearable sensors. *IEEE Trans. Inform. Technol. Biomed.* 16, 279–286. doi: 10.1109/TITB.2011.2169804
- Chu, C. L., Huang, Y. Y., Chen, Y. H., Lai, L. P., and Yeh, H. M. (2018). An observational study: the utility of perfusion index as a discharge criterion for pain assessment in the postanesthesia care unit. *PLoS One* 13:e0197630. doi: 10.1371/journal.pone.0197630
- Chua, C., and Heneghan, C. (2006). “Continuous blood pressure monitoring using ECG and finger photoplethysmogram,” in *Proceeding of the International Conference of the IEEE Engineering in Medicine and Biology Society*, (IEEE), 5117–5120. doi: 10.1109/IEMBS.2006.259612
- Dahlgren, G., Veintemilla, F., Settergren, G., and Liska, J. (1991). Left ventricular end-systolic pressure estimated from measurements in a peripheral artery. *J. Cardiothor. Vasc. Anesthesia* 5, 551–553. doi: 10.1016/1053-0770(91)90004-d

- 艾伦, J., 刘洪, Iqbal, S., Zheng, D., Stansby, G. (2021年)。基于深度学习的外周动脉疾病检测的光电容积描记法分类: 概念验证研究。生理学测量42: 054002. doi: 10.1088/1361-6579/ abf9f3
- 艾伦, J., Murray, A. (1993年)。光电容积脉搏波诊断下肢周围血管疾病之神经网路筛选辅助工具之开发。生理学测量十四点十三分doi: 10.1088/09673334/14/1/003
- 艾伦, J., Murray, A. (2000a)。双侧光体积描记外周脉搏特征在耳、拇指和脚趾处的相似性。生理学测量21点369分。doi: 10.1088/0967-3334/21/3/303
- 艾伦, J., Murray, A. (2000年b)。光体积描记术在耳、拇指和脚趾处的外周脉搏测量的变异性。IEEE Proc. – Sci. Meas. Technol. 147, 403–407
- 艾伦, J., Murray, A. (2002年) 的报告。耳朵、手指和脚趾的外周脉搏计时特征中的与耳鸣相关的变化。J.哈姆。高血压。16, 711–717。
- doi: 10.1038/sj.jhh.1001478
- 艾伦, J., Murray, A. (2004年)。“滤波对多部位光电容积脉搏波形特征的影响”, 《心脏病学计算机进展》, 2004年, (IEEE), 485–488。
- Alnaeb, M. E., Aloabaid, N., Seifalian, A. M., Mikhailstan, D. P., 和汉密尔顿, G. (2007年)。光学技术在外周动脉疾病评估中的应用。Curr. Vasc. Pharmacol. 5, 53–59. 手机: 157016107779317242
- Alty, S. R., Angarita-Jaimes, N., Millasseau, S. C.的方法, Chowienczyk, P. J. (2007)。从数字容积脉搏波形预测动脉硬度。IEEE生物医学学报Eng.54, 2268–2275中所述。doi: 10.1109/tbme.2007.897805
- Asada, H. H., Shaltis, P., Reisner, A., Rhee, S., 和哈钦森, R. C. (2003年) 的报告。使用可穿戴光电容积描记生物传感器的移动的监测。IEEE工程医学学杂志22, 28–40。doi: 10.1109/memb.2003.1213624
- Aschbacher, K., Yilmaz, D., 凯雷姆, Y., 克劳福德, S., Benaron, D., 刘杰, 等 (2020年)。从原始光电容积描记波形检测房颤: 深度学习应用。心律氧分压1, 3–9。doi: 10.1016/j.hroo.2020.02.002
- Avram, R., Tison, G., Kuhar, P., 马库斯, G., Fletcher, M., 奥尔金, J.E., 等 (2019)。
- 使用深度学习从光电容积描记术预测糖尿病。J. Am.胶原心脏73, 16–16。doi: 10.3349/ymj.2022.63.S93
- Awad, A.一、Haddadin, A.美国, 坦塔维, H., Badr, T. M., 斯托特河G., 西尔弗曼, D. G., 等 (2007年)。光电容积脉搏波形与体循环血管阻力的关系。临床监测杂志。Comput. 21, 365–372。
- doi: 10.1007/s10877-007-9097-5
- Ayata, D., Yaslan, Y., Kamasak, M. E. (2018年)。使用可穿戴生理传感器的基于情感的音乐推荐系统。IEEE Trans. Consumer Electronics. 64, 196–203. doi: 10.1109/tce.2018.2844736
- Baek, H. J., 金, K. K., Kim, J.S., Lee, B., Park, K. S. (2009年)。利用脉搏波到达时间和两个混杂因素增强血压估计。生理学测量31分145秒。doi: 10.1088/0967-3334/31/2/002
- Bagha, S., 和Shaw, L. (2011年)。用于测量SpO₂和脉率的PPG信号的真实的时间分析。国际计算机Appl.36, 45–50.
- Baker, W. B., Parthasarathy, A. B., Busch, D. R., 梅斯基塔河C.的方法, Greenberg, J.H., 和Yodh, A. (2014年)。修正的Beer-Lambert血流定律。BioMed. Optics Express 5, 4053–4075.
- 巴恩斯, R. W., 克莱顿, J. M., Bone, G. E., Slaymaker, E. E., Reinertson, J. (1977) .眶上光电容积描记术。颈动脉闭塞性疾病的简单、准确筛查。J. Surgical Res.22, 319–327。doi: 10.1016/00224804 (77) 90150-0
- Beer, A. (1851年)。Versuch der absorptions-verhältnisse des cordierites für Roßes Licht zu bestimmten. Ann. Physik Chem.84, 37–52. doi: 10.1002/andp.18511600904
- Behar, J., Roebuck, A., Shahid, M., Daly, J., Hallack, A., Palmius, N., 等 (2014年)。
- SleepAp: 智能手机的阻塞性睡眠呼吸暂停自动筛查应用程序。IEEE J. Biomed.健康信息。19, 325–331. doi: 10.1109/JBHI.2014.2307913
- Bentham, M., 斯坦斯比, G., 和艾伦, J. (2018)。创新的多部位光电容积描记分析, 用于量化外周动脉疾病的脉搏幅度和时间变异性特征。疾病6: 81 doi: 10.3390/diseases6030081
- Biswas, D., 艾弗森湖刘, M., Panwar, M., Verhoef, B.–E., Patki, S., 等人
- (2019年)。CorNET: 用于移动环境中基于PPG的心率估计和生物识别的深度学习框架。IEEE生物医学学报Circuits Syst. 13, 282–291. doi: 10.1109/TBCAS.2019.2892297
- 对不起, T. 米勒, T. Kreamer, W. Eisenhardt, J. R., ”愚蠢的, H. C. (1994年)。加温条件下手部光电容积描记、多普勒测速、指端血压和皮肤温度的相关性。
- 心脏病物理治疗J. 5, 15–18.
- 博尔托洛托湖一、Blacher, J., Kondo, T., Takazawa, K., 和Safar, M. E. (2000年) 的第10/2000号决议。高血压患者血管老化和动脉粥样硬化的评估: 光电容积描记图与脉搏波速度的二阶导数。Am. J. Hypertens.超级计算机13, 165–171. doi: 10.1016/s0895-7061 (99) 00192-2
- Brillante, D. G., O'sulphur, A. J., 和Howes, L. G. (2008年)。使用非侵入性数字光电容积描记法测量健康志愿者的动脉硬度指数。血压17, 116–123. doi: 10.1080/08037050802059225
- Canac, N., Ranjbaran, M., 奥布莱恩, M. J., Asgari, S., Scalzo, F., Thorpe, S. G., 等人
- (2019年)。脑血流速度信号中脉搏起始点的可靠检测算法。前面Neurol. 10点1072分。版权所有© 2019 – 2019 www.fneur.com
- Cannesson, M., 贝斯纳德角, Durand, P.G., Bohé, J., Jacques, D. (2005年)。机械通气患者脉搏血氧饱和度呼吸变化、体积描记波形振幅与动脉脉压的关系。关键护理9: R562. doi: 10.1186/cc3799
- Cannesson, M., Desebbe, O., Rosamel, P., Delannoy, B., 罗宾, J., Bastien, O., 等 (2008 b)。Pleth变异指数监测呼吸脉搏血氧仪体积描记波形振幅变化并预测液体
- 在手术室的反应。Br. J. Anaesthesia 101, 200–206. doi: 10.1093/bja/aen133
- Cannesson, M., Delannoy, B., Morand, A., Rosamel, P., Attof, Y., Bastien, O., 等 (2008 a)。体积描记图变异性指数是否指示了血管造影引起的体积描记图和动脉压波形的变化? Anesthesia Analgesia 106, 1189–1194. doi: 10.1213/ane.0b013e318167ab1f
- Challoner, A. (1979年)。光电容积描记法用于估计皮肤血流量。无创生理学测量1, 125–151.
- 张, X., Li, G., Xing, G., Zhu, K., 和Tu, L. (2021年)。DeepHeart: 一种深度学习方法, 用于从PPG信号中准确估计心率。ACM Trans.
- 传感器网络 (TOSN) 17, 1–18.
- 查尔顿, P. H., Celka, P., Farukh, B., Chowienczyk, P., Alastruey, J. (2018) .从光电容积描记图评估精神压力: 数值研究。生理学测量39: 054001. doi: 10.1088/1361-6579/aa8e6a
- 陈伟, 小林, Ichikawa, S., Takeuchi, Y., 和Togawa, T. (2000年) 的第10/2000号决议。使用脉搏到达时间和间歇校准连续估计收缩压。医学生物工程部38, 569–574。doi: 10.1007/BF02345755
- Cheng, P., 陈志, 李, Q., Gong, Q., Zhu, J., 和Liang, Y. (2020年)。使用时频分析和深度学习相结合的PPG信号识别房颤。IEEE Access 8, 172692–172706.
- Choi, B., 帕克, C., 李, Y., 申, H., 李, S., Jeong, S., 等 (2018) 。应用鼻腔光电容积描记法建立新的镇痛指标。Anaesthesia 73, 1123–1130. doi: 10.1111/anae.14327
- Choi, J., Ahmed, B., 和Gutierrez-Osuna, R. (2011年)。基于可穿戴传感器的动态压力监测仪的开发与评价。IEEE Trans. Inform. Technol. BioMed. 16, 279–286. doi: 10.1109/TITB.2011.2169804
- Chu, C. L., Huang, Y. 黄氏Y.是的, Chen, Y. H., 莱湖, 澳–地P., 和Yeh, H. M. (2018年)。一项观察性研究: 灌注指数作为急性心肌梗死患者出院标准的实用性
- 在麻醉后监护室进行疼痛评估。PLoS One 13: e0197630. doi: 10.1371/journal.pone.0197630
- Chua, C., 和Heneghan, C. (2006年)。“使用ECG和手指光电容积描记图进行连续血压监测”, 国际会议论文集
- IEEE医学与生物工程学会 (IEEE) 会议, 5117–5120. doi: 10.1109/IEMBS.2006.259612
- Dahlgren, G., Veintemilla, F., Settergren, G., Liska, J. (1991) .通过外周动脉测量值估算左心室收缩末期压。
- J·卡迪托Vasc.麻醉5, 551–553. doi: 10.1016/1053-0770 (91) 90004-d

- Dall'Olio, L., Curti, N., Remondini, D., Harb, Y. S., Asselbergs, F. W., Castellani, G., et al. (2020). Prediction of vascular aging based on smartphone acquired PPG signals. *Sci. Rep.* 10:19756. doi: 10.1038/s41598-020-76816-6
- De Trafford, J., and Lafferty, K. (1984). What does photoplethysmography measure? *Med. Biol. Eng. Comput.* 22, 479–480. doi: 10.1007/BF02447713
- Dillon, J. B., and Hertzman, A. B. (1941). The form of the volume pulse in the finger pad in health, arteriosclerosis, and hypertension. *Am. Heart J.* 21, 172–190. doi: 10.1016/s0002-8703(41)90966-3
- Ding, X., Yan, B. P., Zhang, Y.-T., Liu, J., Zhao, N., and Tsang, H. K. (2017). Pulse transit time based continuous cuffless blood pressure estimation: a new extension and a comprehensive evaluation. *Sci. Rep.* 7:11554. doi: 10.1038/s41598-017-11507-3
- Ding, X.-R., and Zhang, Y.-T. (2015). “Photoplethysmogram intensity ratio: a potential indicator for improving the accuracy of PTT-based cuffless blood pressure estimation,” in *Proceeding of the 37th Annual International Conference of the IEEE Engineering in Medicine and Biology Society (EMBC)*, (IEEE), 398–401. doi: 10.1109/EMBC.2015.7318383
- Dorlas, J., and Nijboer, J. (1985). Photo-electric plethysmography as a monitoring device in anaesthesia: application and interpretation. *Br. J. Anaesthesia* 57, 524–530. doi: 10.1093/bja/57.5.524
- Dresher, R. P., and Mendelson, Y. (2006b). “Reflectance forehead pulse oximetry: effects of contact pressure during walking,” in *Proceeding of the International Conference of the IEEE Engineering in Medicine and Biology Society*, (IEEE), 3529–3532. doi: 10.1109/IEMBS.2006.260136
- Dresher, R. P., and Mendelson, Y. (2006a). “A new reflectance pulse oximeter housing to reduce contact pressure effects,” in *Proceedings of the IEEE 32nd Annual Northeast Bioengineering Conference*, (IEEE), 49–50.
- Erikäinen, L. M., Bonomi, A. G., Schipper, F., Dekker, L. R., De Morree, H. M., Vullings, R., et al. (2019). Detecting atrial fibrillation and atrial flutter in daily life using photoplethysmography data. *IEEE J. Biomed. Health Inform.* 24, 1610–1618. doi: 10.1109/JBHI.2019.2950574
- El Hajj, C., and Kyriacou, P. A. (2020). “Cuffless and continuous blood pressure estimation from ppg signals using recurrent neural networks,” in *Proceeding of the 42nd Annual International Conference of the IEEE Engineering in Medicine & Biology Society (EMBC)*, (IEEE), 4269–4272. doi: 10.1109/EMBC44109.2020.9175699
- Elgendi, M. (2016). Optimal signal quality index for photoplethysmogram signals. *Bioengineering* 3:21. doi: 10.3390/bioengineering3040021
- El-Hajj, C., and Kyriacou, P.A. (2021a). Cuffless blood pressure estimation from PPG signals and its derivatives using deep learning models. *Biomed. Signal Process. Control* 70:102984.
- El-Hajj, C., and Kyriacou, P. A. (2021b). Deep learning models for cuffless blood pressure monitoring from PPG signals using attention mechanism. *Biomed. Signal Process. Control* 65:102301.
- Fallow, B. A., Tarumi, T., and Tanaka, H. (2013). Influence of skin type and wavelength on light wave reflection. *J. Clin. Monit. Comput.* 27, 313–317. doi: 10.1007/s10877-013-9436-7
- Ferro, B. R., Aguilera, A. R., and De La Vara Prieto, R. F. (2015). Automated detection of the onset and systolic peak in the pulse wave using Hilbert transform. *Biomed. Signal Process. Control* 20, 78–84. doi: 10.1016/j.bspc.2015.04.009
- Fischer, C., Glos, M., Penzel, T., and Fietze, I. (2017). Extended algorithm for real-time pulse waveform segmentation and artifact detection in photoplethysmograms. *Somnologie* 21, 110–120. doi: 10.1109/JBHI.2016.2518202
- Foo, J. Y. A. (2007). Development of a temperature-controlled miniature enclosure for monitoring poor perfusion photoplethysmographic signals. *Physiol. Meas.* 28:N67. doi: 10.1088/0967-3334/28/9/N01
- Foo, J. Y. A., Lim, C. S., and Wang, P. (2006). Evaluation of blood pressure changes using vascular transit time. *Physiol. Meas.* 27:685. doi: 10.1088/0967-3334/27/8/003
- Foo, J. Y. A., and Wilson, S. J. (2006). A computational system to optimise noise rejection in photoplethysmography signals during motion or poor perfusion states. *Med. Biol. Eng. Comput.* 44, 140–145. doi: 10.1007/s11517-005-0008-y
- Freckmann, G., Pleus, S., Haug, C., Bitton, G., and Nagar, R. (2012). Increasing local blood flow by warming the application site: beneficial effects on postprandial glycemic excursions. *J. Diabetes Sci. Technol.* 6, 780–785. doi: 10.1177/193229681200600407
- Fu, T.-H., Liu, S.-H., and Tang, K.-T. (2008). Heart rate extraction from photoplethysmogram waveform using wavelet multi-resolution analysis. *J. Med. Biol. Eng.* 28, 229–232.
- Fung, P., Dumont, G., Ries, C., Mott, C., and Ansermino, M. (2004). “Continuous noninvasive blood pressure measurement by pulse transit time,” in *Proceeding of the 26th Annual International Conference of the IEEE Engineering in Medicine and Biology Society*, (IEEE), 738–741.
- Ganeshkumar, M., Ravi, V., Sowmya, V., Gopalakrishnan, E., and Soman, K. K. (2021). “Explainable deep learning-based approach for multilabel classification of electrocardiogram,” in *Proceeding of the IEEE Transactions on Engineering Management*, (IEEE).
- Gibbs, P., and Asada, H. H. (2005). “Reducing motion artifact in wearable bio-sensors using MEMS accelerometers for active noise cancellation,” in *Proceedings of the 2005, American Control Conference*, 2005, (IEEE), 1581–1586.
- Gil, E., Orini, M., Bailón, R., Vergara, J. M., Mainardi, L., and Laguna, P. (2010). Photoplethysmography pulse rate variability as a surrogate measurement of heart rate variability during non-stationary conditions. *Physiol. Meas.* 31, 1271–1290. doi: 10.1088/0967-3334/31/9/015
- Goshvarpour, A., and Goshvarpour, A. (2018). Poincaré's section analysis for PPG-based automatic emotion recognition. *Chaos Solitons Fractals* 114, 400–407. doi: 10.1016/j.chaos.2018.07.035
- Goshvarpour, A., and Goshvarpour, A. (2020). Evaluation of novel entropy-based complex wavelet sub-bands measures of PPG in an emotion recognition system. *J. Med. Biol. Eng.* 40, 451–461.
- Guo, Y., Wang, H., Zhang, H., Liu, T., Liang, Z., Xia, Y., et al. (2019). Mobile photoplethysmographic technology to detect atrial fibrillation. *J. Am. College Cardiol.* 74, 2365–2375. doi: 10.1016/j.jacc.2019.08.019
- Guo, Z., Ding, C., Hu, X., and Rudin, C. (2021). A supervised machine learning semantic segmentation approach for detecting artifacts in plethysmography signals from wearables. *Physiol. Meas.* 42:125003. doi: 10.1088/1361-6579/ac3b3d
- Han, H., Kim, M.-J., and Kim, J. (2007). “Development of real-time motion artifact reduction algorithm for a wearable photoplethysmography,” in *Proceeding of the 29th Annual International Conference of the IEEE Engineering in Medicine and Biology Society*, (IEEE), 1538–1541. doi: 10.1109/IEMBS.2007.4352596
- Hartmut Gehring, M., Me, H. M., and Schmucker, P. (2002). The effects of motion artifact and low perfusion on the performance of a new generation of pulse oximeters in volunteers undergoing hypoxemia. *Respiratory Care* 47, 48–60. doi: 10.1097/00132586-199802000-00051
- Hasanin, A., Mohamed, S. A. R., and El-Adawy, A. (2017). Evaluation of perfusion index as a tool for pain assessment in critically ill patients. *J. Clin. Monit. Comput.* 31, 961–965. doi: 10.1007/s10877-016-9936-3
- He, J.-L., Lecarpentier, Y., Zamani, K., Coirault, C., Daccache, G., Chemla, D., et al. (1995). Relation between aortic diastolic notch pressure and mean aortic pressure in adults. *Am. J. Cardiol.* 76, 301–306. doi: 10.1016/s0002-9149(99)80086-1
- He, X., Goubran, R. A., and Liu, X. P. (2014). Secondary peak detection of PPG signal for continuous cuffless arterial blood pressure measurement. *IEEE Trans. Instrument. Meas.* 63, 1431–1439. doi: 10.1109/tim.2014.2299524
- Hertzman, A. B. (1937). Observations on the finger volume pulse recorded photoelectrically. *Am. J. Physiol.* 119, 334–335.
- Hertzman, A. B. (1938). The blood supply of various skin areas as estimated by the photoelectric plethysmograph. *Am. J. Physiol.-Legacy Content* 124, 328–340.
- Hertzman, A. B., and Dillon, J. B. (1940). Applications of photoelectric plethysmography in peripheral vascular disease. *Am. Heart J.* 20, 750–761. doi: 10.1016/s0002-8703(40)90534-8
- Hertzman, A. B., and Roth, L. W. (1942). The absence of vasoconstrictor reflexes in the forehead circulation. Effects of cold. *Am. J. Physiol.-Legacy Content* 136, 692–697.
- Hilmisson, H., Berman, S., and Magnusdottir, S. (2020). Sleep apnea diagnosis in children using software-generated apnea-hypopnea index (AHI) derived from data recorded with a single photoplethysmogram sensor (PPG). *Sleep Breath.* 24, 1739–1749. doi: 10.1007/s11325-020-02049-6
- Hummler, H. D., Engelmann, A., Pohlandt, F., Högel, J., and Franz, A. R. (2006). Decreased accuracy of pulse oximetry measurements during low perfusion

- 达利奥湖Curti, N., Remondini, D., Harb, Y. 美国, Asselbergs, F. W., Castellani, G., 等 (2020年)。基于智能手机采集的PPG信号预测血管老化。Sci. 代表表10: 19756. doi: 10.1038/s41598-020-76816-6 De特拉福德, J., 和Lafford, K. (1984年)。光电容积描记法测量什么? 医学生物工程部22, 479–480. doi: 10.1007/BF02447713 Dillon, J.B., 和Hertzman, A. B. (1941年)。健康、动脉硬化、高血压时指腹容积脉搏的形态。Am. Heart J. 21, 172–190. doi: 10.1016/s 0002 -8703 (41) 90966-3丁, X., Yan, B. P., 张玉-T., 刘杰, 赵, N., 和Tsang, H. K. (2017年)。
- 基于脉搏传导时间的连续无袖带血压估计: 一种新的扩展和综合评价。Sci. Rep. 7: 11554. doi: 10.1038/s 41598-017-11507-3
- 叮, X. – R., Zhang, Y.- T. (2015年)。“Photoplethysmogram intensity ratio: a potential indicator for improving the accuracy of PTT based cuffless blood pressure estimation”, 在IEEE医学和生物学工程学会(EMBC)第37届年度国际会议论文集(IEEE), 398–401中。doi: 10.1109/EMBC.2015.7318383
- Dorlas, J., Nijboer, J. (1985) .光电体积描记术作为麻醉监测设备: 应用和解释。Br. J. Anaesthesia 57, 524–530. doi: 10.1093/bja/57.5.524 德雷舍, R. P., 和 Mendelson, Y. (2006年b)。“反射前额脉搏血氧仪: 行走过程中接触压力的影响”, 国际会议论文集
- IEEE医学与生物工程学会(IEEE)会议, 3529–3532. doi: 10.1109/EMBS.2006.260136 德雷舍, R. P., 和Mendelson, Y. (2006年a)。“一种新的反射式脉搏血氧仪外壳, 以减少接触压力效应”, IEEE第32届东北生物工程年会论文集, (IEEE), 49–50。埃里凯宁湖M., Bonomi, A. G., Schipper, F., 德克尔湖R., De Morree, H. M., Vullings河, 等 (2019)。利用光电容积描记数据检测日常生活中的心房颤动和心房扑动。IEEE J. Biomed. Health Inform. 24, 1610–1618. doi: 10.1109/JBHI.2019.2950574 El Hajj, C., 和Kyriacou, P. A. (2020年)。“使用递归神经网络从ppg信号进行无袖带和连续血压估计”,
- 第42届IEEE医学与生物学工程学会(EMBC)国际年会, (IEEE), 4269–4272. doi: 10.1109/EMBC.2020.9175699
- Elgendi, M. (2016年)。光电容积描记图信号的最佳信号质量指标。生物工程3: 21. doi: 10.3390/bioengineering3040021 El-Hajj, C., 和Kyriacou, P. A. (2021年a)。使用深度学习模型从PPG信号及其导数进行无袖带血压估计。BioMed.信号处理。控制70: 102984。
- El-Hajj, C., 和Kyriacou, P. A. (2021 b年版)。使用注意力机制从PPG信号进行无袖带血压监测的深度学习模型。BioMed.
- 信号处理。控制中心65: 102301。
- 休耕, B. 一、Tarumi, T., 和Tanaka, H. (2013年)。皮肤类型和波长对光波反射率的影响。临床监测杂志。Comput. 27, 313–317. doi: 10.1007/s10877-013-9436-7 Ferro, B. R., 阿奎莱拉A. R., 和De La Vara Prieto, R. F. (2015年)。使用希尔斯变换自动检测脉搏波中的起始和收缩峰。BioMed.信号处理。控制20, 78–84. doi: 10.1016/j.bspc.2015.
- 04.009 Fischer, C., 格洛斯先生, Penzel, T., 和Fietze, I. (2017年)。用于光电容积脉搏波图中实时脉搏波形分割和伪影检测的扩展算法。Sommologie 21, 110–120. doi: 10.1109/JBHI.2016.
- 2518202 Foo, J. Y. A. (2007年)。用于监测灌注不良光电容积描记信号的温度控制微型外壳的开发。生理学测量 28: N67. doi: 10.1088/0967-3334/28/9/N01 Foo, J. Y. A. 一、林角, 澳-地美国, Wang, P. (2006) .使用血管通过时间评估血压变化。生理学测量27: 685. doi: 10.1088/0967-3334/27/8/003 Foo, J. Y. A., Wilson, S. J. (2006年)。一种计算系统, 用于在运动或不良灌注状态期间优化光电容积描记信号中的噪声抑制。医学生物工程部44, 140–145. doi: 10.1007/s11517-005-0008-y Freckmann, G., Pleus, S., Haug, C., Bitton, G., 和Nagar, R. (2012年)。通过加热给药部位增加局部血流量: 对餐后血糖波动的有益影响。糖尿病科学杂志Technol. 6, 780–785. doi: 10.1177/
- 傅, T.- H. 刘氏H. 和唐, K. T. (2008年)。基于小波多分辨率分析的光电容积脉搏波心率提取。J. Med. 生物工程28, 229–232。
- Fung, P., Dumont, G., 里斯角, 莫特角, 和Ansermino, M. (2004年)。“通过脉搏传导时间进行连续无创血压测量”, 在Proceeding中 第26届IEEE医学和生物学工程学会国际年会(IEEE), 738–741。
- Ganeshkumar, M., 拉维, V., Sowmya, V., Gopalakrishnan, E., 和Soman, K. (2021年)。“可解释的基于深度学习的心电图多标签分类方法”, IEEE工程管理学报(IEEE)。
- 吉布斯, P., Asada, H. H. (2005年)。“使用MEMS加速度计减少可穿戴生物传感器中的运动伪影, 以实现主动噪声消除,” 在Proceedings of the 2005, American Control Conference, 2005, (IEEE), 1581–1586中。
- 吉尔, E. Orini, M., 拜伦, R., 维加拉, J.M. Mainardi, L. 和拉古纳, P. (2010)。光电容积描记法脉搏率变异性作为非平稳条件下心率变异性替代测量。生理学测量 31, 1271–1290. doi: 10.1088/0967-3334/31/9/015
- Goshvarpour, A., 和Goshvarpour, A. (2018年)。基于PPG的自动情感识别的庞加莱截面分析。Chaos Solitons Fractals 114, 400–407. doi: 10.1016/j.chaos.2018.07.035 Goshvarpour, A., 和Goshvarpour, A. (2020年)。在情感识别系统中评估PPG的新基于熵的复小波子带测量。J. Med. Biol. Eng. 40, 451–461.
- Guo, Y., 中国科学院, 王, H., 张洪, Liu, T., 梁志, 夏, Y., 等 (2019)。移动的光电容积描记技术检测房颤。J. Am.心脏病. 74, 2365–2375. doi: 10.1016/j.jacc.2019.08.019 Guo, Z., 丁氏角, Hu, X., 和Rudin, C. (2021年)。一种用于检测可穿戴设备体积描记信号中伪影的监督机器学习语义分割方法。生理学测量 42: 125003. doi: 10.1088/1361-6579/ac3b3d Han, H., 金, M.- J., Kim, J. (2007) .“可穿戴式光电容积描记器的实时运动伪影减少算法的开发,”
- 在第29届IEEE医学和生物学工程学会(IEEE)年度国际会议论文集, 1538–1541. doi: 10.1109/EMBS.2007.4352596
- Hartmut Gehring, M., 我H M., Schmucker, P. (2002) .在经历低氧血症的志愿者中运动伪影和低灌注对新一代脉搏血氧仪性能的影响。呼吸护理47, 48–60。 doi: 10.1097/00132586-199802000-00051 Hasarin, A., 穆罕默德, S. A. R., 和El-Adawy, A. (2017年)。评价灌注指数作为危重患者疼痛评估的工具。临床监测杂志。Comput. 31, 961–965. doi: 10.1007/s10877-016-9936-3 He, J.- L., Lecarpentier, Y., Zamani, K., Coirault角, Daccache, G., Chemla, D., 等 (1995) 。成人主动脉重搏切迹压与平均主动脉压的关系。Am.心脏病学杂志。76, 301–306. doi: 10.1016/s0002-9149(99) 80086-1 He, X., 古布兰河一, 和Liu, X. P. (2014) 。用于连续无袖带动脉血压测量的PPG信号的次级峰值检测。IEEE Trans. 仪器Meas. 63, 1431–1439. doi: 10.1109/tim.2014.2299524 Hertzman, A. B. (1937年)。光电记录手指容积脉搏的观察。Am. J. Physiol. 119, 334–335. Hertzman, A. B. (1938年)。由光电容积描记器估计的各个皮肤区域的血液供应。Am. J. Physiol.– Legacy Content 124, 328–340. Hertzman, A. B., 和Dillon, J. B. (1940年)。光电容积描记术在周围血管疾病中的应用。Am. Heart J. 20, 750–761. doi: 10.1016/s 0002-8703 (40) 90534-8 Hertzman, A. B., 和Roth, L. W. (1942年)。前额循环中血管收缩反射的缺失。寒冷的影响。Am. J. Physiol.– Legacy Content 136, 692–697. Hilmissen, H., Berman, S., 和Magnusdottir, S. (2020年)。使用软件生成的呼吸暂停低通气指数(AHI)诊断儿童睡眠呼吸暂停, 该指数来自单个光电容积描记图传感器(PPG)记录的数据。睡眠呼吸。24, 1739–1749作者: s11325-020-02049 D, 英曼, A. 对不起, F. 对不起, J. 弗兰兹, A. R. (2006)。

- caused by sepsis: is the perfusion index of any value? *Intensive Care Med.* 32, 1428–1431. doi: 10.1007/s00134-006-0254-y
- Imanaga, I., Hara, H., Koyanagi, S., and Tanaka, K. (1998). Correlation between wave components of the second derivative of plethysmogram and arterial distensibility. *Japanese Heart J.* 39, 775–784. doi: 10.1536/ihj.39.775
- Jang, D.-G., Farooq, U., Park, S.-H., and Hahn, M. (2014). A robust method for pulse peak determination in a digital volume pulse waveform with a wandering baseline. *IEEE Trans. Biomed. Circuits Syst.* 8, 729–737. doi: 10.1109/TBCAS.2013.2295102
- Jo, Y.-Y., Cho, Y., Lee, S. Y., Kwon, J.-M., Kim, K.-H., Jeon, K.-H., et al. (2021). Explainable artificial intelligence to detect atrial fibrillation using electrocardiogram. *Int. J. Cardiol.* 328, 104–110. doi: 10.1016/j.ijcard.2020.11.053
- Jones, D. P. (1987). Medical electro-optics: measurements in the human microcirculation. *Phys. Technol.* 18:79. doi: 10.1515/jbcp.1992.3.3.193
- Joseph, G., Joseph, A., Titus, G., Thomas, R. M., and Jose, D. (2014). “Photoplethysmogram (PPG) signal analysis and wavelet de-noising,” in *Proceeding of the Annual International Conference on Emerging Research Areas: Magnetics, Machines and Drives (AICERA/iCMMD)*, (IEEE), 1–5.
- Jubadi, W. M., and Sahak, S. F. A. M. (2009). “Heartbeat monitoring alert via SMS,” in *Proceeding of the IEEE Symposium on Industrial Electronics & Applications*, (IEEE), 1–5. doi: 10.9734/bjast/2016/28453
- Kallio, H., Lindberg, L., Majander, A., Utela, K., Niskanen, M., and Paloheimo, M. (2008). Measurement of surgical stress in anaesthetized children. *Br. J. Anaesthesia* 101, 383–389. doi: 10.1093/bja/aen204
- Kamal, A., Harness, J., Irving, G., and Mearns, A. (1989). Skin photoplethysmography—a review. *Comput. Methods Programs Biomed.* 28, 257–269. doi: 10.1016/0169-2607(89)90159-4
- Karlen, W., Kobayashi, K., Ansermino, J. M., and Dumont, G. (2012). Photoplethysmogram signal quality estimation using repeated Gaussian filters and cross-correlation. *Physiol. Meas.* 33:1617. doi: 10.1088/0967-3334/33/10/1617
- Karlen, W., Raman, S., Ansermino, J. M., and Dumont, G. A. (2013). Multiparameter respiratory rate estimation from the photoplethysmogram. *IEEE Trans. Biomed. Eng.* 60, 1946–1953. doi: 10.1109/TBME.2013.2246160
- Kavsaoglu, A. R., Polat, K., and Bozkurt, M. R. (2016). An innovative peak detection algorithm for photoplethysmography signals: an adaptive segmentation method. *Turkish J. Electrical Eng. Comput. Sci.* 24, 1782–1796. doi: 10.3906/elk-1310-177
- Khan, M., Pretty, C. G., Amies, A. C., Elliott, R., Chiew, Y. S., Shaw, G. M., et al. (2016). Analysing the effects of cold, normal, and warm digits on transmittance pulse oximetry. *Biomed. Signal Process. Control* 26, 34–41. doi: 10.1016/j.bspc.2015.12.006
- Kim, B. S., and Yoo, S. K. (2006). Motion artifact reduction in photoplethysmography using independent component analysis. *IEEE Trans. Biomed. Eng.* 53, 566–568. doi: 10.1109/TBME.2005.869784
- Kim, J., Kim, J., and Ko, H. (2016). Low-power photoplethysmogram acquisition integrated circuit with robust light interference compensation. *Sensors* 16:46. doi: 10.3390/s16010046
- Kim, J., Lee, J.-W., and Shin, H. (2019). Pre-processing of photoplethysmographic waveform for amplitude regularization. *J. Electrical Eng. Technol.* 14, 1741–1748.
- Kim, J., Lee, T., Kim, J., and Ko, H. (2015). “Ambient light cancellation in photoplethysmogram application using alternating sampling and charge redistribution technique,” in *Proceeding of the 37th Annual International Conference of the IEEE Engineering in Medicine and Biology Society (EMBC)*, (IEEE), 6441–6444. doi: 10.1109/EMBC.2015.7319867
- Korhonen, I., and Yli-Hankala, A. (2009). Photoplethysmography and nociception. *Acta Anaesthesiol. Scandinavica* 53, 975–985. doi: 10.1111/j.1399-6576.2009.02026.x
- Korkkalainen, H., Aakkko, J., Duce, B., Kainulainen, S., Leino, A., Nikkinen, S., et al. (2020). Deep learning enables sleep staging from photoplethysmogram for patients with suspected sleep apnea. *Sleep* 43:zsaa098. doi: 10.1093/sleep/zsaa098
- Krishnan, R., Natarajan, B., and Warren, S. (2008). “Motion artifact reduction in photoplethysmography using magnitude-based frequency domain independent component analysis,” in *Proceedings of the 17th International Conference on Computer Communications and Networks*, (IEEE), 1–5.
- Krishnaswamy, A., and Baranoski, G. V. (2004). A biophysically-based spectral model of light interaction with human skin. *Comput. Graphics Forum* 23, 331–340. doi: 10.1111/j.1467-8659.2004.00764.x
- Kwon, S., Hong, J., Choi, E.-K., Lee, E., Hostallero, D. E., Kang, W. J., et al. (2019). Deep learning approaches to detect atrial fibrillation using photoplethysmographic signals: algorithms development study. *JMIR mHealth uHealth* 7:e12770. doi: 10.2196/12770
- Kyriacou, P., Powell, S., Langford, R., and Jones, D. (2002). Investigation of oesophageal photoplethysmographic signals and blood oxygen saturation measurements in cardiothoracic surgery patients. *Physiol. Meas.* 23:533. doi: 10.1088/0967-3334/23/3/305
- Lakshmanan, S., Chatterjee, D., and Muniyandi, M. (2018). “Noninvasive assistive method to diagnose arterial disease-takayasu’s arteritis,” in *Computational Vision and Bio Inspired Computing*, eds D. J. Hemant and S. Smys (Berlin: Springer), 384–398. doi: 10.1007/978-3-319-71767-8_32
- Landsverk, S. A., Hoiseth, L. O., Kvandal, P., Hisdal, J., Skare, O., and Kirkeboen, K. A. (2008). Poor agreement between respiratory variations in pulse oximetry photoplethysmographic waveform amplitude and pulse pressure in intensive care unit patients. *Anesthesiol.: J. Am. Soc. Anesthesiol.* 109, 849–855. doi: 10.1097/ALN.0b013e318195f9f
- Lazazzera, R., Deviaene, M., Varon, C., Buyse, B., Testelmans, D., Laguna, P., et al. (2020). Detection and classification of sleep apnea and hypopnea using PPG and SpO $\%_2$ signals. *IEEE Trans. Biomed. Eng.* 68, 1496–1506. doi: 10.1109/tbme.2020.3028041
- Lee, C., Shin, H. S., and Lee, M. (2011a). Relations between ac-dc components and optical path length in photoplethysmography. *J. Biomed. Optics* 16:077012. doi: 10.1117/1.3600769
- Lee, C., Shin, H. S., Park, J., and Lee, M. (2011b). The optimal attachment position for a fingertip photoplethysmographic sensor with low DC. *IEEE Sensors J.* 12, 1253–1254.
- Lee, Q. Y., Chan, G. S., Redmond, S. J., Middleton, P. M., Steel, E., Malouf, P., et al. (2011c). Multivariate classification of systemic vascular resistance using photoplethysmography. *Physiol. Meas.* 32:1117. doi: 10.1088/0967-3334/32/8/008
- Lee, J., Kim, M., Park, H.-K., and Kim, I. Y. (2020). Motion artifact reduction in wearable photoplethysmography based on multi-channel sensors with multiple wavelengths. *Sensors* 20:1493. doi: 10.3390/s20051493
- Lee, M. S., Lee, Y. K., Pae, D. S., Lim, M. T., Kim, D. W., and Kang, T. K. (2019). Fast emotion recognition based on single pulse PPG signal with convolutional neural network. *Appl. Sci.* 9:3355. doi: 10.3390/app9163355
- Lee, Q. Y., Redmond, S. J., Chan, G. S., Middleton, P. M., Steel, E., Malouf, P., et al. (2013). Estimation of cardiac output and systemic vascular resistance using a multivariate regression model with features selected from the finger photoplethysmogram and routine cardiovascular measurements. *Biomed. Eng. Online* 12:19. doi: 10.1186/1475-925X-12-19
- Li, Q., and Clifford, G. D. (2012). Dynamic time warping and machine learning for signal quality assessment of pulsatile signals. *Physiol. Meas.* 33:1491. doi: 10.1088/0967-3334/33/9/1491
- Li, S., Liu, L., Wu, J., Tang, B., and Li, D. (2018). Comparison and noise suppression of the transmitted and reflected photoplethysmography signals. *BioMed. Res. Int.* 2018:4523593. doi: 10.1155/2018/4523593
- Li, X., Chen, J., Zhao, G., and Pietikainen, M. (2014). “Remote heart rate measurement from face videos under realistic situations,” in *Proceedings of the IEEE Conference on Computer Vision and Pattern Recognition*, (IEEE), 4264–4271.
- Lima, A., and Bakker, J. (2006). “Noninvasive monitoring of peripheral perfusion,” in *Applied Physiology in Intensive Care Medicine*, eds M. R. Pinsky, L. Brochard, and J. Mancebo (Berlin: Springer), 131–141. doi: 10.1007/3-540-37363-2_26
- Lin, Y.-H., Lin, C.-F., and You, H.-Z. (2011). “A driver’s physiological monitoring system based on a wearable PPG sensor and a smartphone,” in *Proceeding of the International Conference on Security-Enriched Urban Computing and Smart Grid*, (Springer), 326–335. doi: 10.1007/978-3-642-23948-9_36
- Lindberg, L.-G., and Oberg, P. A. (1993). Optical properties of blood in motion. *Optical Eng.* 32, 253–258. doi: 10.1117/12.60688
- Linder, S. P., Wendelken, S. M., Wei, E., and McGrath, S. P. (2006). Using the morphology of photoplethysmogram peaks to detect changes in posture. *J. Clin. Monitor. Comput.* 20, 151–158. doi: 10.1007/s10877-006-9015-2

- 脓毒症引起的：灌注指数有价值吗？重症监护医学32, 1428–1431。doi: 10.1007/s00134-006-0254-y
- 伊马纳加岛哈拉, H., Koyanagi, S., 和Tanaka, K. (1998年)。体积描记图二阶导数波形分量与动脉扩张性的相关性。《日本心脏杂志》, 39, 775–784。doi: 10.1536/jihj.39.775 Jang, D.- G., 法鲁克大学, 公园, S.- H. 和Hahn, M. (2014年)。一种用于在具有漂移基线的数字容积脉搏波形中确定脉搏峰值的稳健方法。IEEE生物医学学报系统8, 729–737。doi: 10.1109/TBCAS.2013.2295102 Jo, Y.-是的, Cho, Y., 李, S. 是的, 权, J. - M., 金, K.- H., Jeon, K.- H. 等人
- (2021年)。可解释的人工智能使用心电图检测心房颤动。国际心脏病学杂志。328, 104–110. doi: 10.1016/j.ijcard.2020.11.053
- Jones, D. P. (1987)。医用光电学：人体微循环测量。物理技术18: 79。doi: 10.1515/jbcp.1992.3.3.193 Joseph, G., Joseph, A., Titus, G., 托马斯河M., 和Jose, D. (2014年)。
- “光电容积描记图 (PPG) 信号分析和小波去噪”，在年度国际会议上的新兴研究领域：磁性，机器和驱动器 (AICERA/ICMMD) , (IEEE) , 1–5。
- Jubadi, W. M., 和Sahak, S. F. A. M. (2009年)。“心跳监测短信提醒”在IEEE工业电子和应用研讨会上的论文集中,(IEEE) , 1–5. doi: 10.9734/bjast/2016/28453 Kallio, H., 林德伯格湖, Majander, A., Uutela, K., Niskanen, M., 和Paloheimo, M. (2008年)。麻醉儿童手术应激的测量。Br. J. 麻醉101, 383–389。doi: 10.1093/bja/aen204 Kamal, A., J., 欧文, G., 和Mearns, A. (1989年)。皮肤光电容积描记术综述。Comput.方法程序生物医学。28, 257–269。doi: 10.1016/0169-2607 (89) 90159-4卡伦, W., 小林, K., 安瑟米诺, J.M.和杜蒙, G. (2012年)。
- 使用重复高斯滤波器和互相关的光电容积描记图信号质量估计。生理学测量33: 1617。doi: 10.1088/0967-3334/33/10/ 1617
- 凯文, W., Raman, S., Ansermino, J. M., 作者: Dumont, G. A. A. (2013)。从光电容积描记图估计多参数呼吸率。IEEE生物医学学报Eng. 60, 1946–1953. doi: 10.1109/TBME.2013.2246160
- Kavasao Zagglu, A. R., Polat, K., 和博兹库尔特, M. R. (2016年)。光电容积脉搏波信号的一种创新峰值检测算法：一种自适应分割方法。土耳其电气工程计算杂志。Sci. 24, 1782–1796. doi: 10.3906/elk1310-177 Khan, M., 很漂亮, C. G., Amies, A. C.的方法, 埃利奥特河, Chiew, Y.美国, 肖, G. M., 等人
- (2016年)。冷指、正常指和暖指对透射式脉搏血氧饱和度的影响分析。BioMed.信号处理。控制26, 34–41. doi: 10.1016/j.bspc.2015.12.006
- 金, B. 美国, 和Yoo, S. K. (2006年)。使用独立分量分析减少光电容积描记术中的运动伪影。IEEE Trans. BioMed. Eng. 53, 566–568. 2005.869784 Kim, J., 金, J., 和Ko, H. (2016年)。具有鲁棒光干扰补偿的低功耗光电容积描记图采集集成电路。传感器16: 46。doi: 10.3390/s16010046 Kim, J., 李, J. – W., 和Shin, H. (2019年)。用于振幅正则化的光电容积脉搏波预处理。J. Electrical Eng. Technol. 14, 1741– 1748.金, J., Lee, T., 金, J., 和Ko, H. (2015年)。“使用交替采样和充电的光电容积描记图应用中的环境光消除
- 重新分配技术”，在IEEE医学和生物学工程学会 (EMBC) 第37届年度国际会议论文集 (IEEE) , 6441–6444中。doi: 10.1109/EMBC.2015.7319867
- 科尔霍宁岛和Yli-Hankala, A. (2009年)。光体积描记术和伤害感受。麻醉学学报Scandinavica 53, 975–985. doi: 10.1111/j.1399-6576.2009.02026.x
- Korkkalainen, H., Aakko, J., 领袖, B., Kainulainen, S., Leino, A., Nikkinen, S., 等 (2020年)。深度学习可以根据光电容积描记图对疑似睡眠呼吸暂停患者进行睡眠分期。第43章：你是谁? doi: 10.1093/sleep/ zsa098 Krishnan, R., Natarajan, B., 和Warren, S. (2008年)。“使用基于幅度的频域的光电脉搏波描记术中的运动伪影减少
- 独立分量分析”，第17届计算机通信和网络国际会议论文集, (IEEE) , 1–5。
- Krishnaswamy, A., Baranowski, G. (2004年)。光与人体皮肤相互作用的基于生物药理学的光谱模型。Comput. Graphics Forum 23, 331–340. doi: 10.1111/j.1467-8659.2004.00764.x Kwon, S., Hong, J., Choi, E. K., 李, E., Hostallero, D. E、康, W. J., 等 (2019)。使用光电体积描记信号检测房颤的深度学习方法：算法开发研究。JMIR mHealth uHealth 7: e12770. doi: 10.2196/12770 Kyriacou, P., 鲍威尔, S., 兰福德河, 和Jones, D. (2002年) 的报告。食管光电容积脉搏波信号与血氧饱和度的研究
- 胸心外科患者的测量。生理学测量23: 533。doi: 10.1088/0967-3334/23/3/305
- Lakshmanan, S., Chatterjee, D., 和Muniyandi, M. (2018年)。“诊断动脉疾病—大动脉炎的非侵入性辅助方法”，Vision and Bio Inspired Computing, eds D. J. Hemanth和S. Smys (柏林: Springer) , 384–398.电话: +86–10 – 8888888传真: +86–10 – 88888888
- Landsverk, S.一、霍伊塞斯湖O., Kvandal, P., Hisdal, J., 斯卡雷, O., 和Kirkeboen, K. A. (2008年)。重症监护病房患者脉搏血氧饱和度光电容积描记波形振幅和脉压的呼吸变化之间的一致性较差。麻醉剂: J. Am.麻醉学会109, 849–855. doi: 10.1097/ALN.0b013e3181895f9f Lazazzera, R., Deviaene, M., Varon角, Buyse, B., Testelmans, D., 拉古纳角, 等 (2020年)。睡眠呼吸暂停和低通气的检测和分类
- PPG和SpO信号。IEEE生物医学学报Eng.68, 1496–1506. doi: 10.1109/tbme.2020.3028041
- 李, C., 申, H.美国, 和Lee, M. (2011年a)。光电容积脉搏波中交直流分量与光程长度的关系。J.生物医学。光学16: 077012.
- doi: 10.1117/1.3600769 Lee, C., 申, H.美国, 帕克, J., 和Lee, M. (2011年b)。具有低DC的指尖光电体积描记传感器的最佳附着位置。IEEE Sensors J. 12, 1253–1254。李角, 澳-地是的, 陈, G.美国, 雷德蒙, S. J., 米德尔顿, 下午, Steel, E., Malouf, P., 等 (2011 c)。使用光电容积描记术对全身血管阻力进行多变量分类。生理学测量32: 1117. doi: 10.1088/0967-3334/32/8/ 008 Lee, J., Kim, M., 帕克, H. – K., 金, 我, Y. (2020年)。基于具有多个波长的多通道传感器的可穿戴光电体积描记中的运动伪影减少。传感器20: 1493. doi: 10.3390/s20051493 Lee, M.美国, 李, Y. K., Pae, D.美国, 林, M. T., Kim, D. W., Kang, T. K. (2019年)。
- 基于卷积神经网络的单脉冲PPG信号快速情感识别。应用科学九点三千三百五十五分。doi: 10.3390/app9163355
- 李角, 澳-地是的, 雷德蒙, S. J., 陈, G.美国, 米德尔顿, 下午, Steel, E., Malouf, P., 等 (2013年)。使用多变量回归模型估计心输出量和全身血管阻力, 该模型具有选自手指光电容积描记图和常规心血管测量的特征。BioMed. Eng. 在线时间12点19分。doi: 10.1186/1475-925X-12-19 Li, Q., Clifford, G. D. (2012年)。动态时间规整和机器学习
- 用于脉动信号的信号质量评估。生理学测量33: 1491。doi: 10.1088/0967-3334/33/9/1491
- Li, S., 刘, L., 吴, J., Tang, B., 和Li, D. (2018年)。透射和反射光电体积描记信号的比较和噪声抑制。BioMed. Res.
- 国际2018年: 4523593. doi: 10.1155/2018/4523593 Li, X., 陈杰, 赵, G., 和Pietikainen, M. (2014年)。“在现实情况下从面部视频进行远程心率测量”，
- IEEE计算机视觉和模式识别会议 (IEEE) , 4264–4271。
- Lima, A., Bakker, J. (2006) .“外周灌注的无创监测,” 在重症监护医学中的应用生理学, 编辑M. R.平斯基湖布洛查德,
- 和J. Mancebo (柏林: Springer) , 131–141. doi: 10.1007/3-540-37363-2_26 Lin, Y. – H., 林角, 英-地F.、你, H. Z. (2011年)。“基于可穿戴PPG传感器和智能手机的驾驶员生理监测系统”，
- 加强安全的城市计算和智能
- Grid, (Springer) , 326–335. doi: 10.1007/978-3-642-23948-9_36
- Lindberg, L. – G., 和Oberg, P. A. (1993年)。运动中血液的光学特性。
- 光学工程32, 253–258。doi: 10.1117/12.60688 Linder, S. P., Wendelken, S. M., Wei, E., 和麦格拉思, S. P. (2006) 。
- 使用光电容积描记图峰的形态学来检测姿势的变化。J. Clin. Monitor. Comput. 20, 151–158. doi: 10.1007/s10877-006-9015-2

- Liu, J., Li, Y., Ding, X.-R., Dai, W.-X., and Zhang, Y.-T. (2015). "Effects of cuff inflation and deflation on pulse transit time measured from ECG and multi-wavelength PPG," in *Proceeding of the 37th Annual International Conference of the IEEE Engineering in Medicine and Biology Society (EMBC)*, (IEEE), 5973–5976. doi: 10.1109/EMBC.2015.7319752
- Liu, J., Yan, B. P., Zhang, Y.-T., Ding, X.-R., Su, P., and Zhao, N. (2018). Multi-wavelength photoplethysmography enabling continuous blood pressure measurement with compact wearable electronics. *IEEE Trans. Biomed. Eng.* 66, 1514–1525. doi: 10.1109/TBME.2018.2874957
- Liu, J., Yan, B. P.-Y., Dai, W.-X., Ding, X.-R., Zhang, Y.-T., and Zhao, N. (2016a). Multi-wavelength photoplethysmography method for skin arterial pulse extraction. *Biomed. Optics Express* 7, 4313–4326. doi: 10.1364/BOE.7.004313
- Liu, J., Zhang, Y.-T., Ding, X.-R., Dai, W.-X., and Zhao, N. (2016b). "A preliminary study on multi-wavelength PPG based pulse transit time detection for cuffless blood pressure measurement," in *Proceeding of the 38th Annual International Conference of the IEEE Engineering in Medicine and Biology Society (EMBC)*, (IEEE), 615–618. doi: 10.1109/EMBC.2016.759077
- Liu, S.-H., Li, R.-X., Wang, J.-J., Chen, W., and Su, C.-H. (2020a). Classification of photoplethysmographic signal quality with deep convolution neural networks for accurate measurement of cardiac stroke volume. *Appl. Sci.* 10:4612.
- Liu, S.-H., Wang, J.-J., Chen, W., Pan, K.-L., and Su, C.-H. (2020b). Classification of photoplethysmographic signal quality with fuzzy neural network for improvement of stroke volume measurement. *Appl. Sci.* 10:1476. doi: 10.3390/app10041476
- Lu, S., Zhao, H., Ju, K., Shin, K., Lee, M., Shelley, K., et al. (2008). Can photoplethysmography variability serve as an alternative approach to obtain heart rate variability information? *J. Clin. Monit. Comput.* 22, 23–29. doi: 10.1007/s10877-007-9103-y
- Ma, H. T. (2014). A blood pressure monitoring method for stroke management. *BioMed Res. Int.* 2014:571623. doi: 10.1155/2014/571623
- Madhav, K. V., Ram, M. R., Krishna, E. H., Komalla, N. R., and Reddy, K. A. (2011). "Estimation of respiration rate from ECG, BP and PPG signals using empirical mode decomposition," in *Proceeding of the IEEE International Instrumentation and Measurement Technology Conference*, (IEEE), 1–4.
- Mase, M., Mattei, W., Cucino, R., Faes, L., and Nollo, G. (2011). Feasibility of cuff-free measurement of systolic and diastolic arterial blood pressure. *J. Electrocardiol.* 44, 201–207. doi: 10.1016/j.jelectrocard.2010.11.019
- Matsumura, K., Toda, S., and Kato, Y. (2020). RGB and near-infrared light reflectance/transmittance photoplethysmography for measuring heart rate during motion. *IEEE Access* 8, 80233–80242. doi: 10.1109/access.2020.2990438
- Maweu, B. M., Dakshit, S., Shamsuddin, R., and Prabhakaran, B. (2021). CEFEs: a CNN explainable framework for ECG signals. *Artif. Intell. Med.* 115:102059. doi: 10.1016/j.artmed.2021.102059
- McCombie, D., Asada, H., and Reisner, A. (2005). "Identification of vascular dynamics and estimation of the cardiac output waveform from wearable PPG sensors," in *Proceedings of the 2005 IEEE Engineering in Medicine and Biology 27th Annual Conference* (Piscataway, NJ: IEEE), 3490–3493. doi: 10.1109/EMBS.2005.1617231
- McKay, N. D., Griffiths, B., Di Maria, C., Hedley, S., Murray, A., and Allen, J. (2014). Novel photoplethysmography cardiovascular assessments in patients with Raynaud's phenomenon and systemic sclerosis: a pilot study. *Rheumatology* 53, 1855–1863. doi: 10.1093/rheumatology/keu196
- Mehrgardt, P., Khushi, M., Poon, S., and Withana, A. (2021). Deep learning fused wearable pressure and PPG data for accurate heart rate monitoring. *IEEE Sens. J.* 21, 27106–27115.
- Mejía-Mejía, E., Budidha, K., Abay, T. Y., May, J. M., and Kyriacou, P. A. (2020). Heart rate variability (HRV) and pulse rate variability (PRV) for the assessment of autonomic responses. *Front. Physiol.* 11:779. doi: 10.3389/fphys.2020.00779
- Millasseau, S. C., Kelly, R., Ritter, J., and Chowienczyk, P. (2002). Determination of age-related increases in large artery stiffness by digital pulse contour analysis. *Clin. Sci.* 103, 371–377. doi: 10.1042/cs1030371
- Millasseau, S. C., Kelly, R. P., Ritter, J. M., and Chowienczyk, P. J. (2003). The vascular impact of aging and vasoactive drugs: comparison of two digital volume pulse measurements. *Am. J. Hypertens.* 16, 467–472. doi: 10.1016/s0895-7061(03)00569-7
- Millasseau, S. C., Ritter, J. M., Takazawa, K., and Chowienczyk, P. J. (2006). Contour analysis of the photoplethysmographic pulse measured at the finger. *J. Hypertens.* 24, 1449–1456. doi: 10.1097/01.hjh.0000239277.05068.87
- Monnet, X., Lamia, B., and Teboul, J.-L. (2005). Pulse oximeter as a sensor of fluid responsiveness: do we have our finger on the best solution? *Crit. Care* 9:429. doi: 10.1186/cc3876
- Mousavi, S. S., Firouzmand, M., Charmi, M., Hemmati, M., Moghadam, M., and Ghorbani, Y. (2019). Blood pressure estimation from appropriate and inappropriate PPG signals using A whole-based method. *Biomed. Signal Process. Control* 47, 196–206. doi: 10.1016/j.bspc.2018.08.022
- Mowafi, H. A., Arab, S. A., Ismail, S. A., Al-Ghamdi, A. A., and Al-Metwalli, R. R. (2008). Plethysmographic pulse wave amplitude is an effective indicator for intravascular injection of epinephrine-containing epidural test dose in sevoflurane-anesthetized pediatric patients. *Anesthesia Analgesia* 107, 1536–1541. doi: 10.1213/ane.0b013e3181844d08
- Mowafi, H. A., Ismail, S. A., Shafi, M. A., and Al-Ghamdi, A. A. (2009). The efficacy of perfusion index as an indicator for intravascular injection of epinephrine-containing epidural test dose in propofol-anesthetized adults. *Anesthesia Analgesia* 108, 549–553. doi: 10.1213/ane.0b013e31818fc35b
- Muehlsteff, J., Aubert, X., and Schuett, M. (2006). "Cuffless estimation of systolic blood pressure for short effort bicycle tests: the prominent role of the pre-ejection period," in *International Conference of the IEEE Engineering in Medicine and Biology Society*, (IEEE), 5088–5092. doi: 10.1109/IEMBS.2006.260275
- Murray, W. B., and Foster, P. A. (1996). The peripheral pulse wave: information overlooked. *J. Clin. Monit.* 12, 365–377. doi: 10.1007/BF02077634
- Nabeel, P., Jayaraj, J., and Mohanasankar, S. (2017). Single-source PPG-based local pulse wave velocity measurement: a potential cuffless blood pressure estimation technique. *Physiol. Meas.* 38:2122. doi: 10.1088/1361-6579/aa9550
- Naeini, E. K., Azimi, I., Rahmani, A. M., Liljeberg, P., and Dutt, N. (2019). A Real-time PPG quality assessment approach for healthcare internet-of-things. *Procedia Comput. Sci.* 151, 551–558. doi: 10.1016/j.procs.2019.04.074
- Nilsson, L., Johansson, A., and Kalman, S. (2003a). Macrocirculation is not the sole determinant of respiratory induced variations in the reflection mode photoplethysmographic signal. *Physiol. Meas.* 24:925. doi: 10.1088/0967-3334/24/4/009
- Nilsson, L., Johansson, A., and Kalman, S. (2003b). Respiratory variations in the reflection mode photoplethysmographic signal. Relationships to peripheral venous pressure. *Med. Biol. Eng. Comput.* 41, 249–254. doi: 10.1007/BF02348428
- Nitzan, M., Babchenko, A., Faib, I., Davidson, E., and Adler, D. (2000). "Assessment of changes in arterial compliance by photoplethysmography," in *Proceeding of the 21st IEEE Convention of the Electrical and Electronic Engineers in Israel. Proceedings (Cat. No. 00EX377)*, (IEEE), 351–354.
- Nitzan, M., Faib, I., and Friedman, H. (2006). Respiration-induced changes in tissue blood volume distal to occluded artery, measured by photoplethysmography. *J. Biomed. Optics* 11:040506. doi: 10.1117/1.2236285
- Nitzan, M., Romem, A., and Koppel, R. (2014). Pulse oximetry: fundamentals and technology update. *Med. Devices (Auckland, NZ)* 7:231. doi: 10.2147/MDER.S47319
- Orjuela-Cañón, A. D., Delisle-Rodríguez, D., López-Delis, A., De La Vara-Prieto, R. F., and Cuadra-Sanz, M. B. (2013). "Onset and peak pattern recognition on photoplethysmographic signals using neural networks," in *Proceeding of the Iberoamerican Congress on Pattern Recognition*, (Springer), 543–550.
- Orphanidou, C., Bonnici, T., Charlton, P., Clifton, D., Vallance, D., and Tarassenko, L. (2014). Signal-quality indices for the electrocardiogram and photoplethysmogram: derivation and applications to wireless monitoring. *IEEE J. Biomed. Health Inform.* 19, 832–838. doi: 10.1109/JBHI.2014.233851
- Otsuka, T., Kawada, T., Katsumata, M., and Ibuki, C. (2006). Utility of second derivative of the finger photoplethysmogram for the estimation of the risk of coronary heart disease in the general population. *Circulation J.* 70, 304–310. doi: 10.1253/circj.70.304
- Panwar, M., Gautam, A., Biswas, D., and Acharyya, A. (2020). PP-Net: a deep learning framework for PPG-based blood pressure and heart rate estimation. *IEEE Sens. J.* 20, 10000–10011. doi: 10.1109/jsen.2020.2990864
- Papini, G. B., Fonseca, P., Eerikäinen, L. M., Overeem, S., Bergmans, J. W., and Vullings, R. (2018). Sinus or not: a new beat detection algorithm based on a pulse morphology quality index to extract normal sinus rhythm beats from

- 刘杰, 李, Y., 叮, X. - R., 戴, W.- X., Zhang, Y.- T. (2015年)。“袖带充气和放气对从ECG和多通道测量的脉搏传导时间的影响”。第37届IEEE医学和生物学工程学会(EMBC)国际年会论文集, (IEEE), 5973-5976. doi: 10.1109/EMBC.2015.7319752
- 刘杰, Yan, B. P., 张玉-T., 叮, X. - R., 苏, P., 和Zhao, N. (2018年)。多波长光电容积描记术, 可通过紧凑型可穿戴电子设备实现连续血压测量。IEEE生物医学学报Eng.66, 1514-1525. doi: 10.1109/TBME.2018.2874957
- 刘杰, Yan, B. P. -是的, 戴, W.- X., 叮, X. - R., 张玉-T., 和Zhao, N. (2016a)。皮肤动脉脉搏提取的多波长光电容积描记法。BioMed.光学快报7, 4313-4326. doi: 10.1364/BOE.7. 004313
- 刘杰, 张玉-T., 叮, X. - R., 戴, W.- X., 和Zhao, N. (2016b)。“A preliminary study on multi-wavelength PPG based pulse transmission time detection for cuffless blood pressure measurement”, in Proceeding of the 第38届IEEE医学和生物学工程学会(EMBC)国际年会, (IEEE), 615-618. doi: 10.1109/EMBC.2016.759 0777
- 刘氏H、利河, 巴西-地X., 王建-J., 陈伟, 和Su, C.- H. (2020 a年版)。使用深度卷积神经网络对光电容积脉搏波信号质量进行分类, 以准确测量心脏每搏输出量。应 用科学10: 4612. 刘氏H、王建-J., 陈伟, 潘, K.- L., 和Su, C.- H. (2020 b 年)。用模糊神经网络对光电容积脉搏波信号质量进行分类以改进每搏输出量测量。应 用科学10:1476分。doi: 10.3390/app10041476 Lu, S., 赵, H., Ju, K., Shin, K., 李, M., Shelley, K., 等 (2008年)。光电容积描记术变异性能否作为获取心率 变异性信息的替代方法? 临床监测杂志。Comput. 22, 23-29. doi: 10.1007/s10877-007-9103-y Ma, H. T. (2014年)。用于中风管理的血压监测方法。 BioMed Res. Int. 2014: 571623. doi: 10.1155/2014/571623 Madhav, K. V. Ram, M. R., 克里希纳, E. H. Komalla, N. R., 和Reddy, K. A. (2011年)。
- “使用经验模式分解从ECG、BP和PPG信号估计呼吸率”, IEEE国际仪器和测量技术 会议论文集, (IEEE), 1-4。
- Mase, M., Mattei, W., 库西诺河费斯湖, 和Nollo, G. (2011年)。无袖带测量收 缩压和舒张压的可行性。J. Electrocardiol. 44, 201-207. doi: 10.1016/j.jelectrocard.2010.
- 11.019 Matsumura, K., 户田, 和Kato, Y. (2020年)。RGB和近红外光反射/透射 光电容积描记法, 用于测量运动期间的心率。IEEE Access 8, 80233-80242. doi: 10.1109/access.2020.2990438 Maweu, B. M., Dakshit, S., Shamsuddin, R., 和Prabhakaran, B. (2021年)。CEFEs: ECG信号的CNN可解释框架。第内特尔 115: 102059. doi: 10.1016/j.artmed.2021.102059 McCombie, D., Asada, H., 和Reisner, A. (2005年)。“从可穿戴PPG识别血管动力学和估计心输出量波形
- 传感器”, 在2005年IEEE医学和生物学工程第27届年会论文集(皮斯卡特维, NJ: IEEE), 3490-3493中。doi: 10.1109/IEMBS.2005.1617231
- McKay, N. D., Griffiths, B., 迪玛丽亚角, 赫德利, S., Murray, A., 和艾伦, J. (2014)。雷诺现象和系统性硬化症患者的新型光电容积描记心血管评估: 一项初步 研究。流变学53, 1855-1863. doi: 10.1093/rheumatology/keu196 Mehrgardt, P., Khushi, M., 潘, S., 和Withana, A. (2021年)。深度学习融合可穿戴压力和PPG数 据, 实现准确的心率监测。IEEE传感器 J. 21, 27106-27115.
- 梅希亚-梅希亚, E., Budidha, K., Abay, T.是的, May, J.M., 和Kyriacou, P. A. (2020年)。心率变异性(HRV)和脉率变异性(PRV)用于评估自主神经反应。前面生理学11: 779. doi: 10.3389/fphys.2020.00779
- Millasseau, S. C.的方法, 凯利, R., Ritter, J., Chowienczyk, P. (2002)。通过数 字脉搏轮廓分析确定年龄相关的大动脉僵硬度增加。临床科学103, 371-377. doi: 10.1042/cs1030371 Millasseau, S. C.的方法, 凯利, R., 巴西-地P., Ritter, J.M., Chowienczyk, P. J. (2003)。衰老和血管活性药物对血管的影响: 两种数字容积脉搏测量的比较。Am. J. Hypertens.超级计算机16, 467-472. doi: 10.1016/s0895-7061(03)00569-7
- Millasseau, S. C.的方法, Ritter, J.M., Takazawa, K., Chowienczyk, P. J. (2006)。在手指处测量的光电容积描记脉搏的轮廓分析。J. Hypertens.超级计算机24, 1449-1456. doi: 10.1097/hjh.0000239277.05068.77
- Monnet, X., 拉米亚, B., 和Teboul, J. - L. (2005年)。脉搏血氧仪作为液体反应 性的传感器: 我们是否有最佳解决方案? 关键护理9: 429. doi: 10.1186/cc3876 Mousavi, S.美国, Firouzmand, M., Charmi, M., Hemmati, M., Moghadam, M., 和Ghorbani, Y. (2019年)。使用基于整体的方法从适当和不适当的PPG信号估计血压。BioMed.信号处理。
- 对照47, 196-206. doi: 10.1016/j.bspc.2018.08.022 Mowleman, H. - Arab, S. - Ismail, S. - Al-Ghamdi, A. - 和Al-Metwalli, R. R. (2008年)。体积描记 脉搏波振幅是七氟烷麻醉儿科患者血管内注射含肾上腺素硬膜外试验剂量的有效指 标。Anesthesia Analgesia 107, 1536-1541. doi: 10.1213/ane.0b013e3181844d08 Mowleman, H. - Ismail, S. - Shafi, M. - 和Al-Ghamdi, A. A. (2009年)。
- 灌注指数作为丙泊酚麻醉成人血管内注射含肾上腺素硬膜外试验剂量的有效性指标。 Anesthesia Analgesia 108, 549-553. doi: 10.1213/ane.0b013e31818fc35b
- Muehlsteff, J., Aubert, X., 和Schuett, M. (2006年)。“短用力自行车试验中收缩压的无袖带估计: 在IEEE医学工程国际会议上, 和Biology Society, (IEEE), 5088-5092. doi: 10.1109/IEMBS.2006.260275 Murray, W. B., 和福斯特, P.A. (1996年)。外周脉搏波: 被忽视的信息。临床监测 杂志。12, 365-377. doi: 10.1007/BF02077634 Nabeel, P., Jayaraj, J., 和 Mohanansankar, S. (2017年)。基于单源PPG的局部脉搏波速度测量: 潜在的无袖带 血压估计技术。生理学测量38: 2122. doi: 10.1088/1361-6579/aa9550 Naeini, E. K., 阿兹米岛Rahmani, A. M., Liljeberg, P., 和Dutt, N. (2019年)。用于医疗 物联网的实时PPG质量评估方法。Procedia计算Sci. 151, 551-558. doi: 10.1016/j.procs.2019.04.074 Nilsson, L., Johansson, A., 和Kalman, S. (2003a)。大循环不是呼吸引起的反射模式光体 积描记信号变化的唯一决定因素。生理学测量二十四点九百二十五分。doi: 10.1088/0967-3334/24/4/009 Nilsson, L., Johansson, A., 和Kalman, S. (2003b)。反射模式光体体积描记信号中的呼吸变化。与外周静脉压的关系。医学 生物工程部41, 249-254. doi: 10.1007/BF 02348428 Nitzan, M., Babchenko, A., 法伊卜岛, Davidson, E., 和Adler, D. (2000年)。第10/2000号决议。“通过 光电容积描记术评估动脉顺应性的变化”, 以色列电气和电子工程师第21届IEEE会议文 集。
- Proceedings (Cat. No. 00EX377), (IEEE), 351-354. Nitzan, M., 法伊卜岛, Friedman, H. (2006年)。通过光体体积描记术测量的闭塞 动脉远端组织血容量的呼吸诱导变化。J. BioMed.光学11: 040506. doi: 10.1117/1.2236285 Nitzan, M., Ambassador, A. 和Koppel, R. (2014年)。脉搏血氧仪: 基础与技术更新。医学器械(奥克兰, 新 西兰) 7: 231. doi: 10.2147/MDER.
- S47319 Orjuela-Cañón, A. D., Delisle-Rodríguez, D., López-Delis, A., 德拉瓦 拉-普列托F. 和Cuadra-Sanz, M. B. (2013年)。“使用神经网络对光体容积描 记信号的起始和峰值模式识别”, 载于《伊比利亚美洲模式识别大会论文集》, (施普林格), 543-550. Orphanidou角, Bonnici, T., 查尔顿, P., 克利夫顿博士, Vallance, D., 和Tarassenko, L. (2014年)。心电图和光体容积描记图的信号质 量指数: 推导和在无线监测中的应用。
- IEEE J. Biomed.健康信息。19, 832-838. doi: 10.1109/JBHI.2014.23 38351
- 梅希亚-梅希亚, T., Kawada, T., Katsumata, M., 和Ibuki, C. (2006年)。手指光体容 积描记图二阶导数在估计普通人群冠心病风险中的应用Circulation J. 70, 304-310. doi: 10.1253/circj.70.304 Panwar, M., Gautam, A., Biswas, D., 和Acharyya, A. (2020年)。PP-Net: 基于PPG的血压和心率估计的深度学习框架。IEEE Sens. J. 20, 10000-10011. doi: 10.1109/jsen.2020.2990864 Papini, G. B., Fonseca, P., 埃里凯宁湖M., Overeem, S., Bergmans, J.W., 和Vullings, R. (2018年)。窦性或非窦性: 一种基于脉搏形态质量指数的新搏动检测算法,

- wrist-worn photoplethysmography recordings. *Physiol. Meas.* 39:115007. doi: 10.1088/1361-6579/aae7f8
- Parak, J., and Korhonen, I. (2014). "Evaluation of wearable consumer heart rate monitors based on photoplethysmography," in *Proceeding of the 36th Annual International Conference of the IEEE Engineering in Medicine and Biology Society*, (IEEE), 3670–3673. doi: 10.1109/EMBC.2014.6944419
- Park, K. S., and Choi, S. H. (2019). Smart technologies toward sleep monitoring at home. *Biomed. Eng. Lett.* 9, 73–85. doi: 10.1007/s13534-018-0091-2
- Patterson, J. A., and Yang, G.-Z. (2011). Ratiometric artifact reduction in low power reflective photoplethysmography. *IEEE Trans. Biomed. Circuits Syst.* 5, 330–338. doi: 10.1109/TBCAS.2011.2161304
- Pereira, T., Tran, N., Gadhouni, K., Pelter, M. M., Do, D. H., Lee, R. J., et al. (2020). Photoplethysmography based atrial fibrillation detection: a review. *NPJ Digital Med.* 3, 1–12. doi: 10.1038/s41746-019-0207-9
- Pimentel, M. A., Charlton, P. H., and Clifton, D. A. (2015). "Probabilistic estimation of respiratory rate from wearable sensors," in *Wearable Electronics Sensors*, ed. S. C. Mukhopadhyay (Berlin: Springer), 241–262. doi: 10.1007/s41669-021-00290-7
- Pintavirooj, C., Ni, B., Chatkobkool, C., and Pinijkij, K. (2021). Noninvasive portable hemoglobin concentration monitoring system using optical sensor for anemia disease. *Healthcare* 9:647. doi: 10.3390/healthcare9060647
- Poh, M.-Z., Poh, Y. C., Chan, P.-H., Wong, C.-K., Pun, L., Leung, W. W.-C., et al. (2018). Diagnostic assessment of a deep learning system for detecting atrial fibrillation in pulse waveforms. *Heart* 104, 1921–1928. doi: 10.1136/heartjnl-2018-313147
- Poh, M.-Z., Swenson, N. C., and Picard, R. W. (2010). Motion-tolerant magnetic earring sensor and wireless earpiece for wearable photoplethysmography. *IEEE Trans. Inform. Technol. Biomed.* 14, 786–794. doi: 10.1109/TITB.2010.2042607
- Poon, C., and Zhang, Y. (2005). "Cuff-less and noninvasive measurements of arterial blood pressure by pulse transit time," in *Proceeding of the IEEE Engineering in Medicine and Biology 27th Annual Conference*, (IEEE), 5877–5880. doi: 10.1109/IEMBS.2005.1615827
- Poon, C. C. Y., Teng, X. F., Wong, Y. M., Zhang, C., and Zhang, Y. T. (2004). "Changes in the photoplethysmogram waveform after exercise," in *Proceeding of the 2nd IEEE/EMBS International Summer School on Medical Devices and Biosensors*, (IEEE), 115–118.
- Pradhan, N., Rajan, S., and Adler, A. (2019). Evaluation of the signal quality of wrist-based photoplethysmography. *Physiol. Meas.* 40:065008. doi: 10.1088/1361-6579/ab225a
- Proesmans, T., Mortelmans, C., Van Haelst, R., Verbrugge, F., Vandervoort, P., and Vaes, B. (2019). Mobile phone-based use of the photoplethysmography technique to detect atrial fibrillation in primary care: diagnostic accuracy study of the FibrCheck app. *JMIR mHealth uHealth* 7:e12284. doi: 10.2196/12284
- Rakshit, R., Reddy, V. R., and Deshpande, P. (2016). "Emotion detection and recognition using HRV features derived from photoplethysmogram signals," in *Proceedings of the 2nd workshop on Emotion Representations and Modelling for Companion Systems* (New York, NY: Association for Computing Machinery), 1–6.
- Ravichandran, V., Murugesan, B., Balakarthykeyan, V., Ram, K., Preejith, S., Joseph, J., et al. (2019). "RespNet: a deep learning model for extraction of respiration from photoplethysmogram," in *Proceeding of the 41st Annual International Conference of the IEEE Engineering in Medicine and Biology Society (EMBC)*, (IEEE), 5556–5559. doi: 10.1109/EMBC.2019.8856301
- Raza, A., Tran, K. P., Koehl, L., and Li, S. (2021). Designing ECG monitoring healthcare system with federated transfer learning and explainable AI. *arXiv Preprint*
- Reddy, K. A., George, B., and Kumar, V. J. (2008). Use of fourier series analysis for motion artifact reduction and data compression of photoplethysmographic signals. *IEEE Trans. Instrument. Meas.* 58, 1706–1711.
- Reisner, A., Shaltis, P. A., Mccombie, D., and Asada, H. H. (2008). Utility of the photoplethysmogram in circulatory monitoring. *Anesthesiol. J. Am. Soc. Anesthesiol.* 108, 950–958. doi: 10.1097/ALN.0b013e31816c89e1
- Reiss, A., Indlekofer, I., Schmidt, P., and Van Laerhoven, K. (2019). Deep PPG: large-scale heart rate estimation with convolutional neural networks. *Sensors* 19:3079. doi: 10.3390/s19143079
- Reynolds, K., De Kock, J., Tarassenko, L., and Moyle, J. (1991). Temperature dependence of LED and its theoretical effect on pulse oximetry. *Br. J. Anaesthesia* 67, 638–643. doi: 10.1093/bja/67.5.638
- Rojano, J. F., and Isaza, C. V. (2016). Singular value decomposition of the time-frequency distribution of PPG signals for motion artifact reduction. *Int. J. Signal Process. Syst.* 4, 475–482. doi: 10.18178/ijspes.4.6.475-482
- Roy, M. S., Bag, P., and Gupta, R. (2019). "Reconstruction of corrupted and lost segments from photoplethysmographic data using recurrent neural network," in *Proceeding of the IEEE Region 10 Symposium (TENSYMP)*, (IEEE), 214–219.
- Rubins, U., Grabovskis, A., Grube, J., and Kukulis, I. (2008). "Photoplethysmography Analysis of Artery Properties in Patients with Cardiovascular Diseases," in *Proceeding of the 14th Nordic-Baltic Conference on Biomedical Engineering and Medical Physics*, (Berlin: Springer), 319–322. doi: 10.1007/978-3-540-69367-3_85
- Ruggiero, E., Alonso-De Castro, S., Habtemariam, A., and Salassa, L. (2016). Upconverting nanoparticles for the near infrared photoactivation of transition metal complexes: new opportunities and challenges in medicinal inorganic photochemistry. *Dalton Trans.* 45, 13012–13020. doi: 10.1039/c6dt01428c
- Rybynok, V., and Kyriacou, P. (2010). "Beer-lambert law along non-linear mean light pathways for the rational analysis of photoplethysmography," in *Proceeding of the Journal of Physics: Conference Series*, (IOP Publishing), 012061. doi: 10.1088/1742-6596/238/1/012061
- Saganowski, S., Kazienko, P., Dziezyc, M., Jakimow, P., Komoszyńska, J., Michalska, W., et al. (2020). Review of consumer wearables in emotion, stress, meditation, sleep, and activity detection and analysis. *arXiv preprint*
- Salehzadeh, S., Dao, D. K., Chong, J. W., Mcmanus, D., Darling, C., Mendelson, Y., et al. (2014). Photoplethysmograph signal reconstruction based on a novel motion artifact detection-reduction approach. Part II: motion and noise artifact removal. *Ann. Biomed. Eng.* 42, 2251–2263. doi: 10.1007/s10439-014-1030-8
- Sanjana, K., Sowmya, V., Gopalakrishnan, E., and Soman, K. (2020). Explainable artificial intelligence for heart rate variability in ECG signal. *Healthcare Technol. Lett.* 7:146. doi: 10.1049/htl.2020.0033
- Sañudo, B., De Hoyos, M., Muñoz-López, A., Perry, J., and Abt, G. (2019). Pilot study assessing the influence of skin type on the heart rate measurements obtained by photoplethysmography with the apple watch. *J. Med. Syst.* 43, 1–8. doi: 10.1007/s10916-019-1325-2
- Schäfer, A., and Vagedes, J. (2013). How accurate is pulse rate variability as an estimate of heart rate variability?: a review on studies comparing photoplethysmographic technology with an electrocardiogram. *Int. J. Cardiol.* 166, 15–29. doi: 10.1016/j.ijcard.2012.03.119
- Scholkmann, F., Boss, J., and Wolf, M. (2012). An efficient algorithm for automatic peak detection in noisy periodic and quasi-periodic signals. *Algorithms* 5, 588–603.
- Schrumpf, F., Frenzel, P., Aust, C., Osterhoff, G., and Fuchs, M. (2021a). "Assessment of deep learning based blood pressure prediction from PPG and rPPG signals," in *Proceedings of the IEEE/CVF Conference on Computer Vision and Pattern Recognition*, (IEEE), 3820–3830.
- Schrumpf, F., Frenzel, P., Aust, C., Osterhoff, G., and Fuchs, M. (2021b). Assessment of non-invasive blood pressure prediction from PPG and rPPG Signals Using Deep Learning. *Sensors* 21:6022. doi: 10.3390/s21186022
- Seitsonen, E. R. J., Korhonen, I. K. J., Van Gils, M. J., Huiku, M., Lötjönen, J. M. P., Korttila, K. T., et al. (2005). EEG spectral entropy, heart rate, photoplethysmography and motor responses to skin incision during sevoflurane anaesthesia. *Acta Anaesthesiol. Scandinavica* 49, 284–292. doi: 10.1111/j.1399-6576.2005.00654.x
- Selvaraj, N., Mendelson, Y., Shelley, K. H., Silverman, D. G., and Chon, K. H. (2011). "Statistical approach for the detection of motion/noise artifacts in Photoplethysmogram," in *Proceeding of the Annual International Conference of the IEEE Engineering in Medicine and Biology Society*, (IEEE), 4972–4975. doi: 10.1109/IEMBS.2011.6091232
- Senay, L. C. Jr., Prokop, L. D., Cronau, L., and Hertzman, A. B. (1963). Relation of local skin temperature and local sweating to cutaneous blood flow. *J. Appl. Physiol.* 18, 781–785. doi: 10.1152/jappl.1963.18.4.781
- Seok, H. S., Choi, B.-M., Noh, G.-J., and Shin, H. (2019). Postoperative pain assessment model based on pulse contour characteristics analysis. *IEEE J. Biomed. Health Inform.* 23, 2317–2324. doi: 10.1109/JBHI.2018.2890482
- Seyedtabaii, S., and Seyedtabaii, L. (2008). Kalman filter based adaptive reduction of motion artifact from photoplethysmographic signal. *World Acad. Sci. Eng. Technol.* 37, 173–176.

- 腕戴式光电容积描记记录。生理学测量39: 115007。doi: 10.1088/1361-6579/aae7f8
- Parak, J., 和Korhonen, I. (2014年)。“基于光电脉搏波的可穿戴消费者心率监测器的评估”, 第36届年度会议论文集
IEEE医学与生物工程国际会议
社会, (IEEE), 3670–3673, doi: 10.1109/EMBC.2014.6944419 Park, K.美国, 和Choi, S. H. (2019年)。智能技术在家中监测睡眠。BioMed.英国快报9, 73–85. doi: 10.1007/s13534-018-0091-2 Patterson, J.A., 杨, G. Z. (2011年)。低功率反射式光电容积描记术中比例伪影的减少。IEEE生物医学学报电路系统5, 330–338. doi: 10.1109/TBCAS.2011.2161304佩雷拉, T., Tran, N., Gadhoumi, K., Peltier, M. M., 多, D. H. 利河, 巴西–地J., 等 (2020年)。
- 基于光电容积描记术的心房颤动检测: 综述。NPJ Digital Med. 3, 1–12. doi: 10.1038/s41746-019-0207-9
- Pimentel, M.一、查尔顿, P. H., 和克利夫顿, D. A. (2015年)。“Probably estimation of respiratory rate from wearable sensors”, Wearable Electronics Sensors, ed.S. C. Mukhopadhyay (柏林: 施普林格), 241–262. doi: 10.1007/s41669-021-00290-7 Pintavirooj, C., Ni, B., Chatkobkool, C., 和Pinijkij, K. (2021年)。用于贫血疾病的使用光学传感器的无创便携式血红蛋白浓度监测系统。卫生保健9: 647. doi: 10.3390/healthcare9060647 Poh, M.– Z., Poh, Y. C.的方法, Chan, P.– H. 黄角K., 潘湖, 梁, W. W.– C.的方法, 等人
(2018年)。深度学习系统用于检测脉搏波形中的房颤的诊断评估。104, 1921–1928年。doi: 10.1136/heartjnl/2018–313147
- Poh, M. Z., Swenson, N. C.的方法, 和Picard, R. W. (2010年)。可穿戴式光电容积脉搏波仪的运动容限磁性耳环传感器和无线耳机。IEEE Trans. Inform. 生物医学技术。14, 786–794. doi: 10.1109/TITB.2010.2042607 Poon, C., 和Zhang, Y. (2005年)。“通过脉搏传导时间进行无袖带和无创动脉血压测量”, IEEE会议录
医学与生物工程第27届年会, (IEEE), 5877–5880. doi: 10.1109/EMBS.2005.1615827 C.是的, Teng, X. F.、黄, Y. M., 张, C., 和Zhang, Y. T. (2004年)。
“运动后光电容积描记图波形的变化”, 第二届IEEE/EMBS国际医疗器械和生物传感器暑期学校会议录, (IEEE), 115–118。
- Pradhan, N., Rajan, S., 和Adler, A. (2019年)。腕部光电容积脉搏波信号质量的评价。生理学测量40: 065008, doi: 10.1088/1361-6579/ab225a Proesmans, T., Mortelmans, C., 货车Haelst, R., Verbrugge, F., Vandervoort, P., 和Vaes, B. (2019年)。基于移动的手机使用光电容积描记技术检测初级保健中的房颤:
FibriCheck应用程序的诊断准确性研究。JMIR mHealth uHealth 7: e12284. doi: 10.2196/12284 Rakshit, R., 雷迪, V. R., Deshpande, P. (2016)。“使用从光电容积描记图信号导出的HRV特征进行情感检测和识别”,
第二次研讨会上的情感表示和建模的同伴系统 (纽约, 纽约: 协会计算机械), 1–6。
- 拉维钱德兰, 诉, 木鲁格桑、B.、Balakarthyen, V., 拉姆, K., Preejith, S., 约瑟夫, J., 等。 (2019)。《RespNet: 从光电容积图提取呼吸的深度学习模型》, 在第41届年度的过程中
国际IEEE医学与生物工程国际会议
学会 (EMBC), (IEEE), 5556–5559. doi: 10.1109/EMBC.2019.8856301 Raza, A., 特兰, K. P., Koehl, L., 和李, S. (2021年)。设计了一个心电监测医疗系统, 该系统具有联合迁移学习和可解释的AI。阿尔克西夫
预印本
雷迪, 澳–地一、乔治, B., Kumar, V. J. (2008) .傅立叶级数分析用于光电容积描记信号的运动伪影减少和数据压缩。IEEE Trans. Instrument. Meas. 58, 1706–1711。
Reisner, A., Shaltis, P. A., Mccombie, D., Asada, H. H. (2008年)。光电容积描记图在循环监测中的应用。麻醉剂: J. Am. Soc. 麻醉剂。108, 950–958. doi: 10.1097/ALN.0b013e31816c89e1 Reiss, A., 因德勒克夫岛, 施密特, P., 和货车Laerhoven, K. (2019年)。深度PPG: 使用卷积神经网络进行大规模心率估计。传感器19: 3079. doi: 10.3390/s19143079 Reynolds, K., De科克, J., 塔拉先科湖Moyle, J. (1991) .LED的温度依赖性及其对脉搏血氧仪的理论影响。Br. J. Anaesthesia麻醉67, 638–643. doi: 10.1093/bja/67.5.638
- Rojano, J.F., 和Isaza, C. (2016年)。PPG信号时频分布的奇异值分解, 用于减少运动伪影。信号处理国际期刊。系统4, 475–482. doi: 10.18178/ijsp.4.6.475–482 Roy, M.美国, 包, P., 和Gupta, R. (2019年)。“使用递归神经网络从光电容积描记数据重建损坏和丢失的片段
网络,”在IEEE区域10研讨会 (TENSYMP) 的论文集, (IEEE), 214–219中。
鲁宾斯大学, Grabovskis, A., Grube, J., 和库库利斯岛 (2008年)。
“心血管疾病患者动脉特性的光电容积描记分析”, 第14届北欧–波罗的海生物医学工程和医学物理会议论文集, (柏林: Springer), 319–322。电话: +86–10 – 88888888传真: +86–10 – 88888888
Ruggiero, E., Alonso–De Castro, S., Habtemariam, A., 和Salassa, L. (2016年)。过渡金属配合物近红外光活化的上转换纳米粒子: 医药无机光化学的新机遇与挑战。《道尔顿》, 第45卷, 第13012–13020页。doi: 10.1039/c6dt01428c
Rybynok, V., Kyriacou, P. (2010) .“用于光电容积描记法的理性分析的沿着非线性平均光路的比尔–朗伯定律”, 《物理学期刊论文集: 会议系列》, (IOP出版社), 012061.
doi: 10.1088/1742-6596/238/1/012061 Saganowski, S., Kazienko, P., Dziesteczyc, M., Jakimów, P., Komosy'nska, J., Michalska, W., 等 (2020年)。消费者可穿戴设备在情绪、压力、冥想、睡眠和活动检测与分析方面的综述。204. Salehizadeh, S., Dao, D. K., Chong, J.W., Mcmanus, D., 亲爱的C Mendelson, Y., 等 (2014年)。光电容积脉搏波信号重建
基于新颖的运动伪影检测–减少方法。第二部分: 运动和噪声伪影去除。安。生物医学。Eng.42, 2251–2263中所述。doi: 10.1007/s10439-014-1030-8
Sanjana, K., Sowmya, V., Gopalakrishnan, E., 和Soman, K. (2020年)。ECG信号中心率变异性可解释人工智能。医疗技术
Lett.七点一百四十六分。doi: 10.1049/htl.2020.0033 Sañudo, B., De Hoyos, M., Muñoz–López, A., 佩里, J., 和Abt, G. (2019年)。评估皮肤类型对使用Apple Watch通过光电容积描记法获得的心率测量值的影响的初步研究。J. Med. Syst. 43, 1–8.
doi: 10.1007/s10916-019-1325-2 Schäfer, A., Vagedes, J. (2013) .脉率变异性作为心率变异性估算值的准确性如何? : 光电容积描记技术与心电图的比较研究综述。国际心脏病学杂志。
166, 15–29. doi: 10.1016/j.ijcard.2012.03.119 Scholkmann, F., 头儿, 杰, 沃尔夫, M. (2012年)。含噪周期和准周期信号自动峰值检测的一种有效算法。算法5, 588–603。
Schumpf, F. 所以, P., P., 在你看来, C Osterhoff, G. 福克斯, M. (201 a) ?
“Assessment of deep learning based blood pressure prediction from PPG and rPPG signals, ”in Proceedings of the IEEE/CVF Conference on Computer Vision and Pattern Recognition, (IEEE), 3820–3830.
Schumpf, F. 所以, P., P., 在你看来, C Osterhoff, G. 福克斯, M. (2021 b) ? 使用深度学习评估PPG和rPPG信号的无创血压预测。传感器21: 6022. doi: 10.3390/s21186022
Seitsonen, E. R. J., 科尔霍宁岛K. J., 货车Gils, M. J., Huiku, M., Löötönen, J. M. P., Korttila, K. T., 等 (2005)。七氟醚麻醉期间对皮肤切口的EEG谱熵、心率、光电容积描记和运动反应。麻醉学报Scandinavica 49, 284–292. doi: 10.1111/j.1399-6576.2005.00654.x Mendelson, Y., Shelley, K. H. 西尔弗曼, D. G., 和Chon, K. H.
(2011年)。“光电容积描记图中运动/噪声伪影检测的统计方法”, IEEE医学和生物工程学会 (IEEE) 年度国际会议论文集, 4972–4975. doi: 10.1109/EMBS.2011.6091232
塞奈湖C.小的, 普罗科普湖D、克罗瑙湖和Hertzman, A. B. (1963年出版)。局部皮肤温度和局部出汗与皮肤血流量的关系。J. Appl. Physiol. 18, 781–785. doi: 10.1152/jappl.1963.18.4.781 Seok, H.美国, 崔, B.–M., 诺, G. J., 和Shin, H. (2019年)。基于脉搏轮廓特征分析的术后疼痛评估模型。IEEE J. BioMed. Health Informatics. 23, 2317–2324. doi: 10.1109/JBHI.2018.2890482
Seyedtabaii, S., 和Seyedtabaii, L. (2008年)。基于卡尔曼滤波的光电容积脉搏波运动伪影自适应消除。世界科学院Sci. Eng.

技术支持37, 173–176。

- Shafique, M., Kyriacou, P. A., and Pal, S. (2012). Investigation of photoplethysmographic signals and blood oxygen saturation values on healthy volunteers during cuff-induced hypoperfusion using a multimode PPG/SpO₂ sensor. *Med. Biol. Eng. Comput.* 50, 575–583. doi: 10.1007/s11517-012-0910-z
- Shan, S.-M., Tang, S.-C., Huang, P.-W., Lin, Y.-M., Huang, W.-H., Lai, D.-M., et al. (2016). “Reliable PPG-based algorithm in atrial fibrillation detection,” in *Proceeding of the IEEE Biomedical Circuits and Systems Conference (BioCAS)*, (IEEE), 340–343.
- Shelley, K. H. (2007). Photoplethysmography: beyond the calculation of arterial oxygen saturation and heart rate. *Anesthesia Analgesia* 105, S31–S36. doi: 10.1213/01.ane.0000269512.82836.c9
- Shelley, K. H., Jablonka, D. H., Awad, A. A., Stout, R. G., Rezkanna, H., and Silverman, D. G. (2006). What is the best site for measuring the effect of ventilation on the pulse oximeter waveform? *Anesthesia Analgesia* 103, 372–377. doi: 10.1213/01.ane.0000222477.67637.17
- Shelley, K. H., Murray, W. B., and Chang, D. (1997). Arterial-pulse oximetry loops: a new method of monitoring vascular tone. *J. Clin. Monit.* 13, 223–228. doi: 10.1023/a:1007361020825
- Shelley, K. H., Silverman, D. G., and Shelley, A. J. (2014). *Volume Status Monitor: Peripheral Venous Pressure, Hypervolemia and Coherence Analysis*. U.S. Patent No. 8,727,997. Washington, DC: U.S. Patent and Trademark Office.
- Shi, P., Hu, S., Zhu, Y., Zheng, J., Qiu, Y., and Cheang, P. (2009). Insight into the dicrotic notch in photoplethysmographic pulses from the finger tip of young adults. *J. Med. Eng. Technol.* 33, 628–633. doi: 10.3109/03091900903150980
- Shin, H., and Min, S. D. (2017). Feasibility study for the non-invasive blood pressure estimation based on ppg morphology: normotensive subject study. *Biomed. Eng. Online* 16:10. doi: 10.1186/s12938-016-0302-y
- Shin, H. S., Lee, C., and Lee, M. (2009). Adaptive threshold method for the peak detection of photoplethysmographic waveform. *Comput. Biol. Med.* 39, 1145–1152. doi: 10.1016/j.combiomed.2009.10.006
- Shin, H. S., Lee, C., and Lee, M. (2010). Ideal filtering approach on DCT domain for biomedical signals: index blocked DCT filtering method (IB-DCTFM). *J. Med. Syst.* 34, 741–753. doi: 10.1007/s10916-009-9289-2
- Sim, J. K., Ahn, B., and Doh, I. (2018). A contact-force regulated photoplethysmography (PPG) platform. *AIP Adv.* 8:045210. doi: 10.1063/1.5020914
- Simek, J., Wichterle, D., Melenovsky, V., Malik, J., Svacina, S., and Widimsky, J. (2005). Second derivative of the finger arterial pressure waveform: an insight into dynamics of the peripheral arterial pressure pulse. *Physiol. Res.* 54:505.
- Sinex, J. E. (1999). Pulse oximetry: principles and limitations. *Am. J. Emergency Med.* 17, 59–66.
- Song, J., Li, D., Ma, X., Teng, G., and Wei, J. (2019). PQR signal quality indexes: a method for real-time photoplethysmogram signal quality estimation based on noise interferences. *Biomed. Signal Process. Control* 47, 88–95. doi: 10.1016/j.bspc.2018.05.020
- Spigulis, J., Gailite, L., and Lihachev, A. (2007a). “Multi-wavelength photoplethysmography for simultaneous recording of skin blood pulsations at different vascular depths,” in *Proceedings of the Advanced Biomedical and Clinical Diagnostic Systems V*, eds R. Raghavachari, T. Vo-Dinh, W. S. Grundfest, D. A. Benaron, and G. E. Cohn (Bellingham, WA: International Society for Optics and Photonics), 64301.
- Spigulis, J., Gailite, L., Lihachev, A., and Erts, R. (2007b). Simultaneous recording of skin blood pulsations at different vascular depths by multiwavelength photoplethysmography. *Appl. Optics* 46, 1754–1759. doi: 10.1364/ao.46.001754
- Stern, R. M. (1974). Ear lobe photoplethysmography. *Psychophysiology* 11, 73–75.
- Struys, M., Vanpeteghem, C., Huiku, M., Uutela, K., Blyaert, N., and Mortier, E. (2007). Changes in a surgical stress index in response to standardized pain stimuli during propofol-remifentanil infusion. *Br. J. Anaesthesia* 99, 359–367. doi: 10.1093/bja/aem173
- Sukor, J. A., Redmond, S., and Lovell, N. (2011). Signal quality measures for pulse oximetry through waveform morphology analysis. *Physiol. Meas.* 32:369. doi: 10.1088/0967-3334/32/3/008
- Takazawa, K. (1993). Clinical usefulness of the second derivative of a plethysmogram (acceleration plethysmogram). *J. Cardiol.* 23, 207–217.
- Takazawa, K., Tanaka, N., Fujita, M., Matsuoka, O., Saiki, T., Aikawa, M., et al. (1998). Assessment of vasoactive agents and vascular aging by the second derivative of photoplethysmogram waveform. *Hypertension* 32, 365–370. doi: 10.1161/01.hyp.32.2.365
- Tang, S.-C., Huang, P.-W., Hung, C.-S., Shan, S.-M., Lin, Y.-H., Shieh, J.-S., et al. (2017). Identification of atrial fibrillation by quantitative analyses of fingertip photoplethysmogram. *Sci. Rep.* 7:45644. doi: 10.1038/srep45644
- Tang, S. D., Goh, Y. S., Wong, M. D., and Lew, Y. E. (2016). “PPG signal reconstruction using a combination of discrete wavelet transform and empirical mode decomposition,” in *Proceeding of the 6th International Conference on Intelligent and Advanced Systems (ICIAS)*, (IEEE), 1–4.
- Taniguchi, H., Takata, T., Takechi, M., Furukawa, A., Iwasawa, J., Kawamura, A., et al. (2021). Explainable artificial intelligence model for diagnosis of atrial fibrillation using holter electrocardiogram waveforms. *Int. Heart J.* 62, 534–539. doi: 10.1536/ihj.21-094
- Tarvirdizadeh, B., Golgouneh, A., Tajdari, F., and Khodabakhshi, E. (2018). A novel online method for identifying motion artifact and photoplethysmography signal reconstruction using artificial neural networks and adaptive neuro-fuzzy inference system. *Neural Comput. Appl.* 32, 3549–3566. doi: 10.1007/s00521-018-3767-8
- Tazarv, A., and Levorato, M. (2021). A deep learning approach to predict blood pressure from ppg signals. *arXiv Preprint* doi: 10.1109/EMBC46164.2021.9629687
- Temko, A. (2017). Accurate heart rate monitoring during physical exercises using PPG. *IEEE Trans. Biomed. Eng.* 64, 2016–2024. doi: 10.1109/TBME.2017.2676243
- Teng, X., and Zhang, Y.-T. (2006). The effect of applied sensor contact force on pulse transit time. *Physiol. Meas.* 27:675. doi: 10.1088/0967-3334/27/8/002
- Timimi, A. A., Ali, M. M., and Chellappan, K. (2017). A novel AMARS technique for baseline wander removal applied to photoplethysmogram. *IEEE Trans. Biomed. Circuits Syst.* 11, 627–639. doi: 10.1109/TBCAS.2017.2649940
- Uçar, M. K., Bozkurt, M. R., Polat, K., and Bilgin, C. (2015). “Investigation of effects of time domain features of the photoplethysmography (PPG) signal on sleep respiratory arrests,” in *Proceeding of the 23rd Signal Processing and Communications Applications Conference (STU)*, (IEEE), 124–127.
- Ushiroyama, T. (2005). Assessment of chilly sensation in Japanese women with laser Doppler fluxmetry and acceleration plethysmogram with respect to peripheral circulation. *Bull. Osaka Med. Coll.* 51, 76–84.
- Vadrevu, S., and Manikandan, M. S. (2018). A robust pulse onset and peak detection method for automated PPG signal analysis system. *IEEE Trans. Instrument. Meas.* 68, 807–817.
- Valencell, T. (2015). *Optical Heart Rate Monitoring: What You Need to Know*. Raleigh: Valencell. Diakesis Dari.
- Venema, B., Blanik, N., Blazek, V., Gehring, H., Opp, A., and Leonhardt, S. (2012). Advances in reflective oxygen saturation monitoring with a novel in-ear sensor system: results of a human hypoxia study. *IEEE Trans. Biomed. Eng.* 59, 2003–2010. doi: 10.1109/TBME.2012.2196276
- Wang, C., Huang, C., and Ye, S. (2014). “Noninvasive cardiac output monitoring system based on photoplethysmography,” in *Proceedings of the 2014 IEEE International Conference on Progress in Informatics and Computing* (Piscataway, NJ: IEEE), 669–673.
- Wang, L., Poon, C., and Zhang, Y. (2010). The non-invasive and continuous estimation of cardiac output using a photoplethysmogram and electrocardiogram during incremental exercise. *Physiol. Meas.* 31, 715–726. doi: 10.1088/0967-3334/31/5/008
- Wang, G., Atef, M., and Lian, Y. (2018). Towards a continuous non-invasive cuffless blood pressure monitoring system using PPG: systems and circuits review. *IEEE Circuits Syst. Magazine* 18, 6–26. doi: 10.1109/mcas.2018.2849261
- Wang, K., Xu, L., Wang, L., Li, Z., and Li, Y. (2003). “Pulse baseline wander removal using wavelet approximation,” in *Proceeding of the Computers in Cardiology*, (IEEE), 605–608.
- Wang, L., Pickwell-Macpherson, E., Liang, Y. P., and Zhang, Y. T. (2009). “Noninvasive cardiac output estimation using a novel photoplethysmogram index,” in *Proceeding of the Annual International Conference of the IEEE Engineering in Medicine and Biology Society*, (Piscataway, NJ: IEEE), 1746–1749. doi: 10.1109/IEMBS.2009.5333091
- Wannenburg, J., and Malekian, R. (2015). Body sensor network for mobile health monitoring, a diagnosis and anticipating system. *IEEE Sens. J.* 15, 6839–6852.

- Shafique, M., Kyriacou, P. A., 和 S. (2012年)。使用多模式PPG/SpO 2传感器对健康志愿者在袖带诱导的低灌注期间的光电容积描记信号和血氧饱和度值进行研究。医学生物工程部50, 575–583。
doi: 10.1007/s11517-012-0910-z Shan, S. – M.、钳子, S. – C.、黄, P. – W.、林, Y. – M.、黄, W. – H.、黎, D. – M. 等。 (2016年)。“可靠的基于PPG的算法在心房颤动检测,”在 IEEE生物医学电路与系统会议论文集 (BioCAS) , (IEEE) , 340–343。
- Shelley, K. H. (2007年)。光电容积描记法:超越动脉血氧饱和度和心率的计算。麻醉镇痛105, S31–S36。doi: 10.1213/01.ane.0000269512.82836.c9 Shelley, K. H., Jablonka, D. H., Awad, A. – 、斯托特河G., Rezkanna, H., 和 Silverman, D. G. (2006年)。测量通气对脉搏血氧仪波形影响的最佳部位是什么? Anesthesia Analgesia 103, 372–377。doi: 10.1213/01.ane.0000222477.67637.17 Shelley, K. H., Murray, W. B., 和 Chang, D. (1997年)。动脉脉搏血氧饱和度环:一种监测血管张力的新方法。临床监测杂志. 13, 223–228。
doi: 10.1023/a:1007361020825 Shelley, K. H.、西尔弗曼, D. G., 和 Shelley, A. J. (2014年)。卷状态监视器:
- 外周静脉压、高血容量及相关性分析。美国专利号8, 727, 997。华盛顿, DC: 美国专利商标局。
- 施, P., Hu, S., Zhu, Y., 中国科学院, 郑杰, Qiu, Y., 中国农业大学出版社, Cheang, P. (2009) .青年人指尖光电容积脉搏重搏切迹的研究。J. Med. Eng. Technol. 33, 628 – 633. doi: 10.3109/03091900903150980 Shin, H., 和Min, S. D. (2017年)。基于ppg形态学的无创血压估计的可行性研究:正常血压受试者研究。BioMed.英语在线16: 10. doi: 10.1186/s12938 – 016 – 0302-y Shin, H.美国, 李, C., 和Lee, M. (2009年)。光电容积脉搏波峰值检测的自适应阈值方法。Comput.生物医学39, 1145 – 1152. doi: 10.1016/j.combiomed.2009.10.006 Shin, H.美国, 李, C., 和Lee, M. (2010年)。生物医学信号DCT域理想滤波方法:索引分块DCT滤波方法 (IB-DCTFM) 。J. Med. 系统34, 741–753. doi: 10.1007/s10916-009-9289-2 Sim, J.K., Ahn, B., 和 Doh, I. (2018年)。接触力调节
- 光电容积描记 (PPG) 平台。AIP Adv. 8: 045210. doi: 10.1063/1.5020914
- 你好, J, 对不起, D. Melenovsky, V.马利克, J. 瑞士, S. Widimsky, J. (2005年)。手指动脉压波形的二阶导数:对外周动脉压脉搏动力学的洞察。生理学研究54: 505。
- Sinex, J. E. (1999年)。脉搏血氧仪:原理和局限性。Am. J. Emergency Med. 17, 59–66.宋杰Li, D., 姆, X., Teng, G., Wei, J. (2019) .PQR信号质量指数:一种基于噪声干扰的实时光电容积描记图信号质量估计方法。BioMed.信号处理。控制47, 88–95. doi: 10.1016/j.
- bspc.2018.05.020 Spigulis, J., 盖利特湖, 和Lihachev, A. (2007年a)。“多波长光电容积描记术用于同时记录皮肤血液脉动
- 在不同的血管深度”, 在Proceedings of the Advanced Biomedical and Clinical Diagnostic Systems V, eds R. RagHAVACHARI, T. Vo-Dinh, W. S. Grundfest, D. A. Benaron和G. E.科恩 (贝灵汉, 华盛顿州: 国际光学和光子学会) , 64301。
- Spigulis, J., 盖利特湖, Lihachev, A., 和Erts, R. (2007年b)。用多波长光电容积描记术同时记录不同血管深度的皮肤血液脉动。Appl. Optics 46, 1754–1759.
doi: 10.1364/ao.46.001754 Stern, R. M. (1974年)。耳垂光电容积描记法。Psychophysiology 11, 73–75.
- Stryuys, M., Vanpeteghem角, Huiku, M., Uutela, K., Blyaert, N., 和Mortier, E. (2007年)。丙泊酚-瑞芬太尼输注期间手术应激指数对标准化疼痛刺激的反应变化。Br. J. Anaesthesia 99, 359–367. doi: 10.1093/bja/aem173
- Sukor, J. A., 雷德蒙, S., 和Lovell, N. (2011年)。通过波形形态学分析测量脉搏血氧饱和度的信号质量。生理学测量三十二点三百六十九分。
doi: 10.1088/0967-3334/32/3/008 Takazawa, K. (1993年)。体积描记图二阶导数 (加速度体积描记图) 的临床应用。心脏病学杂志. 23, 207–217.
- 高泽, K. 、田中, N., 藤田, M.、松冈, O. 、斋木, T. 、相川, M. 等。
(1998年)。血管活性物质和血管老化的第二次评估
- 光电容积描记图波形的导数。Hypertension 32, 365–370. doi: 10.1161/01.hyp.32.2.365 Tang, S.– C.的方法, 黄, P. – W., 洪角, 澳–地美国, Shan, S.– M., 林, Y.– H., Shieh, J.– 美国, 等(7年)。指尖光电容积图定量分析鉴别心房颤动。Sci. Rep. 7: 45644. doi: 10.1038/srep45644 Tang, S. D. 和戈, Y. 美国, 黄, M. D., Lew, Y. E. (2016年)。“模式分解,”第六届智能与先进系统国际会议论文集, (IEEE) , 1–4。
- Taniguchi, H., Takata, T., Takechi, M., Furukawa, A., Iwasawa, J., Kawamura, A., 等 (2021年)。利用霍尔特心电图波形诊断心房颤动的可解释人工智能模型。Int. Heart J. 62, 534–539.
- Tarvirdizadeh, B., Golgouneh, A., Tajdari, F., 和Khodabakhshi, E. (2018年)。提出了一种基于人工神经网络和自适应神经模糊推理系统的运动伪影识别和光电容积脉搏波信号重建的新方法。神经元计算32, 3549–3566. doi: 10.1007/s00521018-3767-8 Tazarv, A., 和Levorato, M. (2021年)。从ppg信号预测血压的深度学习方法。arXiv预印本doi: 10.1109/EMBC.46164.2021.
- 9629687 Temko, A. (2017)。Accurate heart rate monitoring during physical exercises using PPG. IEEE Trans. Biomed. Eng. 64, 2016–2024. doi: 10.1109/TBME.2017.2762423 Teng, X., 和Zhang, Y.–T. (2006)。The effect of applied sensor contact force on pulse transit time. Physiol. Meas. 27:675. doi: 10.1088/0967-3334/27/8/002 Timimi, A. A., Ali, M. M., 和Chellappan, K. (2017)。A novel AMARS technique for baseline wander removal applied to photoplethysmogram. IEEE Trans. doi: 10.1109/TBME.2017.2649940 Uçar, M. K., Bozkurt, M. R., Polat, K., 和Bilgin, C. (2015)。“Investigation of effects of time domain features of the photoplethysmography (PPG) signal
- on sleep respiratory arrests,” in Proceeding of the 23nd Signal Processing and Communications Applications Conference (SIU), (IEEE), 124–127.
- Ushiroyama, T. (2005年)。用激光多普勒流量计和外周循环加速度体积描记图评估日本女性的冷冰冰的。Bull. Osaka Med. Coll. 51, 76–84. Vadrevu, S., Manikandan, M. S. (2018年)。用于自动PPG信号分析系统的鲁棒脉冲起始和峰值检测方法。IEEE Trans. doi: 10.1109/TBME.2012.2196276
- 仪器Meas. 68, 807–817.
- Valencell, T. (2015年)。光学心率监测:你需要知道的
罗利:瓦伦赛尔。Diakses Dari。
- Venema, B., Blanik, N., Blazek, V., Gehring, H., Opp, A., 和Leonhardt, S. (2012年)。用新型线性传感器系统进行反射式氧饱和度监测的进展:人体缺氧研究的结果。IEEE生物医学学报Eng. 59, 2003–2010. doi: 10.1109/TBME.2012.2196276
- Wang, C., 中国地质大学, Huang, C., 和Ye, S. (2014年)。“基于光电容积描记术的无创心输出量监测系统”, 2014年IEEE会议论文集
信息学和计算进展国际会议 (皮斯卡特维, 新泽西州: IEEE) , 669–673.
- Wang, L., 美国, 潘, C., 和Zhang, Y. (2010年)。递增负荷运动中使用光电容积描记图和心电图对心输出量的无创和连续估计。生理学测量31, 715–726.
doi: 10.1088/0967-3334/31/5/008 Wang, G., Atef, M., 和Lian, Y. (2018年)。使用PPG的连续无创袖带血压监测系统:系统和电路综述。IEEE电路系统杂志18, 6–26. doi: 10.1109/mcas.2018.2849261 Wang, K., 徐, L., Wang, L., 美国, Li, Z., 和Li, Y. (2003年) 的报告。“脉冲基线漂移消除
- 使用小波近似”, 在心脏病学计算机进展中, (IEEE) , 605–608.
- Wang, L., 美国, Pickwell-Macpherson, E., Liang, Y. P., 和Zhang, Y. T. (2009年)。“使用新型光电容积描记指数进行无创心输出量估计”, IEEE医学和生物学工程学会年度国际会议论文集, (皮斯卡特维, NJ: IEEE) , 1746–1749. doi: 10.1109/EMBS.2009.5333091
- Wannenburg, J., 和Malekian, R. (2015年)。用于移动的健康监测、诊断和预测系统的身体传感器网络。IEEE Sens.J.15, 6839–6852.

- Webster, J. G. (1997). *Design of Pulse Oximeters*. Boca Raton, FL: CRC Press.
- Widrow, B., Glover, J. R., Mccool, J. M., Kaunitz, J., Williams, C. S., Hearn, R. H., et al. (1975). Adaptive noise cancelling: principles and applications. *Proc. IEEE* 63, 1692–1716. doi: 10.1109/proc.1975.10036
- Wong, M. Y.-M., Poon, C. C.-Y., and Zhang, Y.-T. (2009). An evaluation of the cuffless blood pressure estimation based on pulse transit time technique: a half year study on normotensive subjects. *Cardiovasc. Eng.* 9, 32–38. doi: 10.1007/s10558-009-9070-7
- Xu, L., Cheng, J., and Chen, X. (2017). Illumination variation interference suppression in remote PPG using PLS and MEMD. *Electron. Lett.* 53, 216–218.
- Xu, L., Meng, M. Q.-H., Liu, R., and Wang, K. (2008). “Robust peak detection of pulse waveform using height ratio,” in *Proceeding of the 30th Annual International Conference of the IEEE Engineering in Medicine and Biology Society*, (IEEE), 3856–3859. doi: 10.1109/IEMBS.2008.4650051
- Yan, L., Hu, S., Alzahrani, A., Alharbi, S., and Blanos, P. (2017). A multi-wavelength opto-electronic patch sensor to effectively detect physiological changes against human skin types. *Biosensors* 7:22. doi: 10.3390/bios7020022
- Yang, C., Veiga, C., Rodriguez-Andina, J. J., Farina, J., Iniguez, A., and Yin, S. (2019). Using PPG signals and wearable devices for atrial fibrillation screening. *IEEE Trans. Industrial Electron.* 66, 8832–8842.
- Yang, Y. L., Seok, H. S., Noh, G.-J., Choi, B.-M., and Shin, H. (2018). Postoperative pain assessment indices based on photoplethysmography waveform analysis. *Front. Physiol.* 9:1199. doi: 10.3389/fphys.2018.01199
- Yousef, Q., Reaz, M., and Ali, M. A. M. (2012). The analysis of PPG morphology: investigating the effects of aging on arterial compliance. *Meas. Sci. Rev.* 12, 266–271.
- Yuan, H., Memon, S. F., Newe, T., Lewis, E., and Leen, G. (2018). Motion artefact minimization from photoplethysmography based non-invasive hemoglobin sensor based on an envelope filtering algorithm. *Measurement* 115, 288–298. doi: 10.1016/j.measurement.2017.10.060
- Zangróniz, R., Martínez-Rodrigo, A., López, M. T., Pastor, J. M., and Fernández-Caballero, A. (2018). Estimation of mental distress from photoplethysmography. *Appl. Sci.* 8:69. doi: 10.3390/app8010069
- Zhang, Q., Lindberg, L.-G., Kadefors, R., and Styf, J. (2001). A non-invasive measure of changes in blood flow in the human anterior tibial muscle. *Eur. J. Appl. Physiol.* 84, 448–452. doi: 10.1007/s004210100413
- Zhang, X.-Y., and Zhang, Y.-T. (2006). The effect of local mild cold exposure on pulse transit time. *Physiol. Meas.* 27:649. doi: 10.1088/0967-3334/27/7/008
- Zhu, Q., Tian, X., Wong, C.-W., and Wu, M. (2021). Learning your heart actions from pulse: ECG waveform reconstruction from PPG. *IEEE Internet Things J.* 8, 16734–16748.
- Zijlstra, W., Buursma, A., and Meeuwesen-Van Der Roest, W. (1991). Absorption spectra of human fetal and adult oxyhemoglobin, deoxyhemoglobin, carboxyhemoglobin, and methemoglobin. *Clin. Chem.* 37, 1633–1638. doi: 10.1093/clinchem/37.9.1633
- Zimmermann, M., Feibicke, T., Keyl, C., Prasser, C., Moritz, S., Graf, B. M., et al. (2010). Accuracy of stroke volume variation compared with pleth variability index to predict fluid responsiveness in mechanically ventilated patients undergoing major surgery. *Eur. J. Anaesthesiol. (EJA)* 27, 555–561. doi: 10.1097/EJA.0b013e328335fbfd1

Conflict of Interest: The authors declare that the research was conducted in the absence of any commercial or financial relationships that could be construed as a potential conflict of interest.

Publisher's Note: All claims expressed in this article are solely those of the authors and do not necessarily represent those of their affiliated organizations, or those of the publisher, the editors and the reviewers. Any product that may be evaluated in this article, or claim that may be made by its manufacturer, is not guaranteed or endorsed by the publisher.

Copyright © 2022 Park, Seok, Kim and Shin. This is an open-access article distributed under the terms of the Creative Commons Attribution License (CC BY). The use, distribution or reproduction in other forums is permitted, provided the original author(s) and the copyright owner(s) are credited and that the original publication in this journal is cited, in accordance with accepted academic practice. No use, distribution or reproduction is permitted which does not comply with these terms.

韦伯斯特（1997年）。脉搏血氧仪的设计。博卡拉顿，佛罗里达州：CRC出版社。
 Widrow, B., 格洛弗, J.R., 麦库尔, J.M., Kaunitz, J., 威廉姆斯, C.美国, 赫恩河 H. 等 (1975)。自适应噪声消除：原理与应用。Proc. IEEE 63, 1692–1716. doi: 10.1109/proc.1975.10036 Wong, M. Y.—M., 潘角, 澳—地C.—是的, Zhang, Y.—T. (2009年)。基于脉搏传导时间技术的无袖带血压估计的评价：正常血压受试者半年研究。Cardiovasc. Eng.9, 32–38. doi: 10.1007/s10558-009-9070-7 Xu, L., Cheng, J., 和Chen, X. (2017年)。使用PLS和MEMD的远程PPG中的照明变化干扰抑制。电子。53, 216–218。徐, L., 孟, M.问: H、刘, R., 和Wang, K. (2008年)。“使用高度比的脉搏波形的鲁棒峰值检测”，第30届会议论文集
 张, Q., 林德伯格湖G., Kadefors河, Styf, J. (2001) .人类胫前肌血流变化的非侵入性测量。EUR. J.
 Appl. Physiol.84, 448–452. doi: 10.1007/s004210100413 Zhang, X.—是的, Zhang, Y.—T. (2006年)。局部轻度冷暴露对脉搏传导时间的影响。生理学测量 27: 649.
 doi: 10.1088/0967-3334/27/7/008 Zhu, Q., Tian, X., 黄角W., 和Wu, M. (2021年)。从脉搏中学习心脏活动：从PPG重建ECG波形。IEEE Internet Things J. 8, 16734–16748. Zijlstra, W., Buursma, A., Meeuwsen—Van Der Roest, W. (1991年)。人胎儿和成人氧合血红蛋白、脱氧血红蛋白、碳氧血红蛋白和高铁血红蛋白的吸收光谱。临床化学37, 1633–1638. doi: 10.1007/BF00221638 Zimmermann, M., Feibicke, T., Keyl, C., Prasser, C., 莫里茨, S., 格拉夫, B. M., 等 (2010年)。每搏输出量变异性与容积描记变异性指数预测机械通气患者液体反应性的准确性比较

IEEE医学和生物学工程学会 (IEEE) 年度国际会议, 3856–3859。doi: 10.1109/IEMBS.2008.4650051

Yan, L., Hu, S., Alzahrani, A., Alharbi, S., Blanos, P. (2017) .多波长光电贴片传感器, 可有效检测人体皮肤类型的生理变化。生物传感器7: 22. doi: 10.3390/bios7020022 Yang, C., Veiga角, Rodriguez—Andina, J. J., Farina, J., Agueguez, A., 和Yin, S.

(2019年)。使用PPG信号和可穿戴设备进行房颤筛查。

IEEE Trans. Industrial Electron.66, 8832–8842.

Yang, Y. L., Seok, H.美国, 诺, G. J., 崔, B.—M., 和Shin, H. (2018年)。基于光电容积脉搏波形分析的术后疼痛评估指标。

前面生理学9: 1199。doi: 10.3389/fphys.2018.01199 Yousef, Q., Reaz, M., 和Ali, M. A. M. (2012年)。PPG形态学分析：研究年龄对动脉顺应性的影响。Meas. Sci. Rev. 12, 266–271.袁, H., Memon, S. F., Newe, T., 刘易斯, E., 和Leen, G. (2018年)。基于包络滤波算法的基于光电体积描记术的无创血红蛋白传感器的运动伪影最小化。测量115, 288–298。

doi: 10.1016/j.measurement.2017.10.060 Zangroniz, R., 马丁内斯—罗德里戈, A., 洛佩兹, M. T., 牧师, J.M., 和费尔南德斯—卡瓦列罗, A. (2018年)。从光体积描记术估计精神痛苦。应用科学。8点69分。doi: 10.3390/app8010069

接受大手术的病人EUR. J. Anaesthesiol. (EJA)27, 555–561。doi: 10.1097/EJA.0b013e328335fb1

利益冲突：作者声明，本研究是在不存在任何可能被视为潜在利益冲突的商业或财务关系的情况下进行的。

出版商备注：本文中表达的所有声明仅为作者的声明，不一定代表其附属组织或出版商、编辑和审稿人的声明。本文中可能评估的任何产品，或其制造商可能提出的任何声明，均不受出版商的担保或认可。

版权所有© 2022 Park, Seok, Kim and Shin.这是一篇开放获取的文章，根据知识共享署名许可证 (CC BY) 的条款分发。允许在其他论坛使用、分发或复制，前提是注明原作者和版权所有者，并根据公认的学术惯例引用本期刊的原始出版物。不允许在不遵守这些条款的情况下使用、分发或复制。